The Effect of Fragile X Mental Retardation Protein on Substantia Nigra Dopaminergic Neuronal Excitability

Pan Gao

Table of Contents

Abstract

Parkinson's disease (PD) is a neurodegenerative disease that results in the loss of dopaminergic (DA) neurons and characteristic motor impairments. α-Synuclein aggregation and Lewy bodies are considered to be neuropathological hallmarks of PD. The vulnerability of DA neurons is selective and related to their unique electrophysiological activity. Fragile X mental retardation protein (FMRP), a protein that controls the expression and function of numerous neuronal genes related to neuronal excitability and synaptic function, disappears from expression in animal and cell models of PD, and its expression decreases in substantia nigra pars compacta (SNc) DA neurons early in the disease process of PD patients and before the appearance of Lewy bodies. This study investigates the role of FMRP in the excitability of SNc DA neurons using electrophysiological patch clamp techniques and immunohistochemical techniques. The findings suggest that FMRP has an important role in the excitability of SNc DA neurons and that a decrease in its abundance has the potential to affect the nigrostriatal pathway.

List of figures

List of tables

List of symbols and abbreviations

$[Ca^{2+}]i$	Intracellular calcium concentration
AAV	Adenoassociated virus
aCSF	Artificial cerebrospinal fluid
AD	Alzheimer's disease
AHP	Afterhyperpolarization
ALS	Amyotrophic lateral sclerosis
AMPA	α-amino-3-hydroxy-5-methyl-4-isoxazolepropionic acid
AP	Action potential
ASD	Autism spectrum disorders
ATP	Adenosine triphosphate
CNS	Central nervous system
CP/CPT	Caudoputamen
CPC	Caudal CP
CPI	Intermediate CP
CPR	Rostral CP
CREB	cAMP response element-binding protein
DA	dopamine/dopaminergic
DaT	Dopamine transporter
DBS	Deep brain stimulation
DMS	Dorsomedial striatum
DMSO	Dimethyl sulfoxide
DMV	Dorsal motor nucleus of the vagus
DR1	Dopamine receptor 1
DR2	Dopamine receptor 2
e-phys	Electrophysiology
ER	Endoplasmic reticulum
FMRP	Fragile X mental retardation protein
FXS	Fragile X syndrome
FXTAS	Fragile X like Fragile X-associated tremor/ataxia syndrome
GABA	γ-Aminobutyric acid

GFP   Green fluorescent protein

GIRK   G-protein-gated inwardly rectifying potassium

GPCRs   G-protein-coupled receptors

GPi   Internal globus pallidus

GTP   Guanosine triphosphate

HCN   Hyperpolarization-Activated Cyclic Nucleotide-Gated

HET   Heterozygous

IF Immunofluorescence

INaP   Persistent sodium current

KO   Knock out

LB   Lewy's body

LC   Locus coeruleus

LC-MS/MS   Liquid chromatography-mass spectrometry

LJP   Liquid junction potential

LP   Lewy's body pathology

LUHMES   Lund Human Mesencephalic

MMP9   Matrix Metalloproteinase 9

MSN   Medium spiny neuron

NMDA   N-methyl-D-aspartate

NSC-1   Neuronal Calcium Sensor 1

OXPHOS   Mitochondrial oxidative phosphorylation

PBS   Phosphate-buffered saline

PCR   Polymerase chain reaction

PD   Parkinson's disease

PFA   Paraformaldehyde

PFC   Prefrontal cortex

PFF   Pre-formed fibrils

PKC   Protein Kinase C

PN   Postnatal

PPN   Pedunculopontine nucleus

pS6   Phosphorylated ribosomal protein S6

RMP   Rest membrane potential

ROS	Reactive oxygen species
SNc	Substantia nigra pars compacta
SNr	Substantia nigra pars reticular
STN	Subthalamic nucleus
STO	Subthreshold oscillation
TH	Tyrosine hydroxylase
TTX	Tetrodotoxin
VTA	Ventral tegmental area
WT	Wild-type
α-Syn	α-Synuclein

1. Introduction

1.1 Parkinson's disease

Parkinson's disease (PD) is the second most prevalent neurological movement disorder. It is characterized by the gradual and selective destruction of dopaminergic (DA) neurons in the substantia nigra par compacta (SNc). PD was initially coined by James Parkinson in his 1817 essay "Essay on the Shaking Palsy," which detailed the clinical aspects of involuntary tremulous motion (or tremulous paralysis) in a limited number of cases (Parkinson 2002).

After PD was originally conceptualized as a unique syndrome, neurologists and neurobiologists came to regard the characteristics of the symptoms and refined the definition of the disease. In 1865, William Sanders proposed the name "Parkinson's disease," and Charcot clarified the collection of clinical symptoms associated with it. Later in 1912, Friedrich H. Lewy extended disease characteristics acquired from clinical signs into the realm of pathological anatomy, first uncovering a lesion in the brains of Parkinson's disease patients labeled as Lewy's body (LB). By 1940, the concept that the DA neuronal degeneration in the SNc is crucial for motor symptoms was also largely acknowledged (Lees 2007). The breakthrough in therapy came in 1950, when Arvid Carlsson, the 2000 Nobel Prize in Physiology or Medicine awardee, discovered that dopamine depletion was the primary driver of motor symptoms in PD, thus successfully decelerating disease progression with the dopamine precursor, L-DOPA, as substitution therapy. While progress has been realized in the clinical management of locomotor symptoms since the official adoption of L-DOPA for clinical intervention in the mid-1960s, it has not been enough to halt the progress of the disease nor to restore the lost neuronal function (Fahn 2008). And in 2003, Braak's landmark study on sporadic PD cases suggested a critical role for the gut-brain axis, implying that PD may arise in the vagus nerve of the gastrointestinal system, and the course could often be traced back decades before motor symptoms appear (Braak, Del Tredici, *et al.* 2003).

Effective therapy for PD has yet to be discovered; conventional interventions such as L-DOPA replacement or surgical operations like deep brain stimulation (DBS) only manage to alleviate symptoms and slow down the process to a limited degree. To cope with the rising incidence of PD due to global aging, researchers are urgently searching for a safe and efficient therapy that is cost-effective at the same time. The current average incidence of PD in Han Chinese subjects is about 0.39% (> 50 years old), and a total of 4.94 million PD sufferers are estimated to appear in China by 2030, accounting for half of the PD cases worldwide (Dorsey *et al.* 2007; Li *et al.* 2019).

1.1.1 Clinical characteristics

Despite more than two centuries of research into the etiology of PD, little is known about the precise mechanisms underlying the disease. PD is found more frequently in the elderly and presents more often with late-onset symptoms, making age the most critical risk factor for occurrence (Collier, Kanaan, and Kordower 2011). The high chance of PD may result from an interplay of aging, genetic susceptibility, and environmental factors that culminate in the degeneration of nigrostriatal DA neurons.

Additional insights into the genome machinery of PD may be gained through genetic investigations of hereditary cases (*SNCA*, *PRKN*, *DJ-1*, *PINK1*, *LRRK2*). These include the A53T, A30P, E46K and G51D mutant variations of *SNCA*, which seem to be devoted to the early-onset cases, and H50Q, which is dedicated to the late-onset instances. Other genetic variants have also consolidated the importance of physiological processes such as mitochondria, oxidative stress, and synaptic/axonal dynamics in the pathogenesis of PD. For example, loss of function of the mitochondrial quality inspector, *PINK1*, results in the accumulation of reactive oxygen species (ROS), which leads to cell death (Barodia, Creed, and Goldberg 2017); Impaired function of *DJ-1* results in a reduced antioxidant capacity of neurons, making the cytosol more susceptible to α-Syn aggregation (Shendelman *et al.* 2004).

According to the latest research, PD may be traced back more than a decade before the onset of motor symptoms, inferring that environmental factors profoundly contribute to PD genesis. Some of the environmental factors thought to facilitate PD include exposure to pesticides, regular dairy intake, a history of melanoma or traumatic brain injury. As an interesting note, smoking and caffeine consumption are assumed to reduce the risk of PD, together with increased serum urate concentrations, ibuprofen application, and aerobic workout (Ascherio and Schwarzschild 2016).

The triad of motor symptoms that characterize PD are bradykinesia, resting tremor, and muscle rigor, which also serve as diagnostic criteria for the disease. Early non-motor symptoms like hyposmia, constipation, rapid eye movement sleep behavior disorder (RBD) are gaining attention and, therefore, can aid in the diagnosis of early PD to identify early high-risk patients for prompt intervention. However, the non-specificity and mildness of these symptoms are highly overlooked by patients and clinicians, making early diagnosis still challenging. To determine, or even quantify, the particular risk of PD for individuals, a combination of different PD hallmark events should be taken into consideration together with biochemical markers, radiographic features and the history of risk factor exposure. Technological advances in imaging such as single photon emission computed tomography (SPECT) based DaTscan, which visualizes dopamine transporters density in the striatum, are also getting approval for early clinical diagnosis (Gayed *et al.* 2015) albeit its cost-effectiveness has been called into doubt (de la Fuente-Fernandez 2012).

Both medical management and surgical procedures are used to treat PD. Pharmacological therapies primarily aim to restore dopamine levels by the administration of exogenous dopamine precursors (L-DOPA) or to increase dopamine activity through the administration of selective and irreversible monoamine oxidase B (MAO-B) inhibitor (Selegiline). Additionally, dopamine agonists (e.g., pramipexole, ropinirole) are sometimes used. Some substances that

target the non-dopaminergic system, such as the glutamate antagonist, amantadine, are used to treat PD via rebalancing the direct and indirect pathways of the nigrostriatal system. When medicinal therapy is not sufficient, either because the patient is unable to tolerate the medication owing to side effects or when the condition has deteriorated to the point of substantial motor symptoms, surgical intervention like deep brain stimulation (DBS) may also be employed. Microelectrodes are carefully positioned in specific nuclei by stereotactic surgery to regulate the excitability of neurons in the area, with the subthalamic nucleus (STN) and internal globus pallidus (GPi) as primary targets. Inhibition of the STN improves bradykinesia, rigidity, tremor, decreases end-of-dose effects, and may allow for a lessening in medication dosage, while electrode implantation into the GPi nucleus helps improve dyskinesia and mitigates cognitive decompensation or mood disturbances. The pedunculopontine nucleus (PPN) has also been a target for DBS. A favorable early report of improved gait and postural instability in patients has prompted clinical trials further to evaluate the effects of PPN-DBS on PD symptoms (Stefani *et al.* 2007). Substantia nigra pars reticulata (SNr) has been suggested as a target for improving refractory axial symptoms (RAS) with promising results (Valldeoriola *et al.* 2019). Numerous other DBS sites, including the zona incerta, posterior subthalamic region, and centromedian thalamus, have been found in succession. These targets need more research and analysis in order to develop protocols for common standardized operations (Anderson, Beecher, and Ba 2017).

1.1.2   α-Synuclein and Lewy body pathology

Two unique features characterize PD: the destruction of DA neurons in the SNc and the formation of Lewy bodies (LBs) in the cytoplasm of afflicted neurons. Fritz Heinrich Lewy originally reported inclusion bodies in a PD patients' dorsal vagal nucleus and basal Meynert's nucleus. Tretiakoff (1919) found the same sort of inclusion bodies in PD patients' SNc and dubbed it the "Lewy body". LBs are made mostly of a non-soluble misfolded protein aggregation that is deposited in the

cytoplasm. They are eosinophilic and primarily composed of α-Synuclein (α-Syn). Until recently, the precise role of α-Syn has remained unknown; however, it is known that the soluble monomer is involved in synaptic function, lipid metabolism, and epigenetic modification. Both in vitro and in vivo, α-Syn has a proclivity for self-assembly into organized insoluble amyloid fibrils. The misfolding and aggregation of α-Syn is a complicated process that begins with the recruitment of additional soluble monomers, which aggregate to form oligomers for deposition, and continues with the recruitment of organelles and related membrane structures (Trinkaus *et al.* 2021). Various factors, including but not limited to missense mutations in *SNCA* mutations (e.g., A53T, A30P, E46K, and H50Q), *SNCA* triploidy, S129 α-Syn hyperphosphorylation, generation of specific fragments and seeding, and the weakening of the α-Syn autophagy, are hypothesized to accelerate α-Syn aggregation, and abnormal liquid-liquid phase separation (LLPS) was proved involved as well. Protein condensation into a droplet state by LLPS is normally reversible, and is necessary for some cellular functions; α-Syn may be able to irreversibly trap cellular components via LLPS, maturing into gel-like deposits that irreversibly sequester essential cellular components, resulting in pathological processes (Ray *et al.* 2020; Hardenberg *et al.* 2021). This phenomenon can also be seen in other protein toxic related neurodegeneration disorders such as FUS protein in amyotrophic lateral sclerosis (ALS) and tau in Alzheimer's disease (AD) (Murakami *et al.* 2015; Kanaan *et al.* 2020).

Prion-like properties, i.e. the ability to spread between cells possessed for α-Syn make the spreading not only happen just within the central nervous system (CNS) but also start from peripheral sites such as nerve fibers in the gastrointestinal tract, salivary glands, and the nasal cavity to the CNS through the brain-gut axis or olfactory network, inducing further endogenous α-Syn misfolding (Braak, Rub, *et al.* 2003; Rietdijk *et al.* 2017). The distribution of LBs is therefore not random but develops over time in a staged fashion (from the lower brainstem to the rostral part of the brain) that is somewhat predictable and highly matched to the evolution of clinical symptoms. Braak *et al*. assessed the development of PD by studying the distribution of LBs in postmortem brain tissue, in conjunction with early non-motor

and motor symptoms that the implicated regions may prompt. LBs are mostly located in the olfactory bulb or lower brainstem during the first stage. Correspondingly, the initial stage of Braak is marked by modest and atypical non-motor symptoms such as RBD. LBs then advent to the locus coeruleus, medulla oblongata, and raphe nuclei in the second stage, while patients have a greater number of non-motor symptoms like excessive daytime sleepiness or anxiety. As LBs break into the nucleus basalis of Meynert or substantia nigra, the illness has accelerated to the third stage or even above, where motor symptoms become apparent and most patients are diagnosed clinically at this stage. In the fifth stage, LBs invade the temporal neocortex and sensory association premotor area, and significant DA neuron loss can be observed in SNc. Additionally, individuals at this stage can obtain substantial cognitive impairment. Ultimately, in the sixth stage, LBs scatter across the neocortex, eventually taking over the main sensory regions (*Figure 01.*) (Braak, Del Tredici, *et al.* 2003).
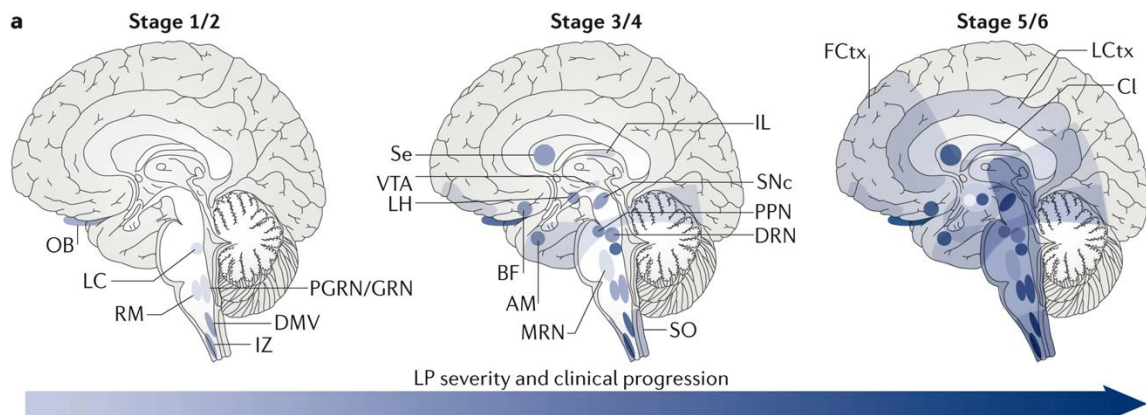
Figure 01. Lewy pathology severity and clinical progression (Surmeier, Obeso, and Halliday 2017).

Although LBs have been extensively shown to be a pathogenic sign of PD, they are not necessarily associated with neuron death. LBs were detected in many neurons in individuals who do not exhibit overt PD symptoms, and their distribution or quantity is unrelated to the degree of DA neuron loss, indicating that many cells may survive with LB for many years, exhibiting tolerance to LB (Parkkinen *et al.* 2011). Additional evidence suggests that neuronal dysfunction and destruction in PD-associated neurons precede the appearance of LB (Milber *et al.* 2012). The

development of LBs in PD does not correspond to the degeneration of the associated neurons; for example, whereas DA neurons in the SNc are implicated to death earlier than the locus coeruleus, the LBs appear only later than in the LC (Surmeier, Obeso, and Halliday 2017). Considering the mutant *SNCA* cases of PD and the recent experimental evidence of the pathogenic properties of misfolded α-Syn, a pathological role of α-Syn is very likely, whereas LB pathology might just be a bystander (Ishimoto and Yamakado 2021).

1.1.3 Selective vulnerability of DA neuron

The death of DA neurons in SNc is currently presumed to be predominantly apoptotic, owing to the slowly progressive nature of the disease (only a few neurons die at a time and are rapidly cleared), possibly as a result of an accumulation of stress events (mitochondrial dysfunction, ER stress, oxidative stress, and autophagy) (Venderova and Park 2012), although other types of cell death (e.g., ferroptosis) have also been mentioned (Shibu, Bharath, and Velmurugan 2021).

Axonal terminals in the dorsal striatum start to degenerate before the dendrite and cell bodies of DA neurons in SNc. The deficiency of DA release in the dorsal striatum is much greater than the corresponding loss of DA neurons in SNc (Betarbet *et al.* 2000), where DA neurons usually are decreased by 30-50% before the onset of motor symptoms, while dopamine levels in the striatum and putamen have been declined by 60% to 80% (Burke and O'Malley 2013). The dopamine transporter (DaT) in the striatum is significantly decreased in PD patients up to four years after a clinical diagnosis (Kordower *et al.* 2013). The remaining intact DA neurons work in an internal compensatory mechanism, release more dopamine and thus may significantly postpone the appearance of motor symptoms in patients for many years (Reetz *et al.* 2009). As soon as the DA neuronal loss exceeds 50%, the severity of motor symptoms is shown to be correlated with the cell counting in SNc rather than the dopamine levels in the striatum (Nandhagopal *et al.* 2011; Kordower *et al.* 2013). Another supportive result comes from a genome-wide association

study (GWAS), which examined numerous PD risk genes, finding that virtually all of them are involved in synapse activity, including, but not limited to, *SNCA, LRRK2, VPS35, PINK1, PRKN, DNAJC6, SYNJ1, VAMP4, and DJ1* (Goldberg *et al.* 2005; Kitada *et al.* 2007; Gcwensa *et al.* 2021). This retrograde direction of deterioration may be explained by α-Syn being absorbed and transferred in a retrograde way (or potentially antegrade). The neuronal vulnerability is not directly correlated with the propensity to acquire LP in some studies, and it was found that the retrograde spreading of LP does not follow simple connectivity rules. In other words, LP lesions do not constantly occur in the areas with direct and robust synaptic innervation, so the tendency for degeneration independent of LP generation supports a cell-autonomous mechanism of cell death (Surmeier, Obeso, and Halliday 2017).

Along with the gradual and selective degeneration of DA neurons in the SNc, other sensitive regions also suffer neuronal loss, including the cholinergic neurons in nucleus basalis and PPN, as well as glutamatergic neurons in the STN and basolateral amygdala nucleus (BL). Neurons in the dorsal medulla motor nucleus, the nucleus accumbens, and the anterior olfactory nucleus can be involved in LBs pathology. Notably, GABAergic neurons seem to be resistant to LB formation regardless of their location. Degeneration of these systems is heterogeneous across patients and is thought to contribute to the diversity of non-motor symptoms in PD (Surmeier, Obeso, and Halliday 2017).

On the structural level, vulnerable neurons often have long or thin axons that are densely branching, and the neurons either lack or are totally devoid of myelin sheathing (Surmeier, Obeso, and Halliday 2017; Pelzer *et al.* 2019). In terms of their role in the neuromodulatory control network (which modulates other neurons by releasing transmitters that activate slow G protein-coupled receptors), they are a key player. Another characteristic shared by vulnerable neurons in PD is their unique electrophysiology (e-phys) activity, which deserves to be discussed in full depth hereafter.

The autonomy of neuron degeneration is also seen in several subpopulations of midbrain DA neurons, and many studies have examined the possible molecular mechanism underlying the selective vulnerability of specific DA neuron subtypes spatially and temporally.

1. Spatial differences in neuronal vulnerability: DA neurons in the SNc are substantially more susceptible than their VTA counterparts; even within the SNc, DA neurons with distinct phenotypes and viability have been identified. For example, early studies found that DA neurons located in the ventral part of the SNc were more susceptible than those in the dorsal SNc, with a loss of up to 90% after 6-OHDA injection in the striatum, compared to the 25% loss of the population in the dorsal layer (Fearnley and Lees 1991). The primary cause for the difference is thought to be the abundance of calbindin, which is expressed at a higher level in dorsal DA neurons, making them much more capable of buffering calcium ions (Ca^{2+}) and so reducing the Ca^{2+} load during long-term firing (Liang *et al.* 1996; McRitchie and Halliday 1995); what is more, the PI3-kinase-Akt signaling pathway can be activated by calbindin, preventing DA neurons from undergoing apoptosis in a toxic environment(Sun *et al.* 2011). Other than that, the neurons in lateral SNc degenerate more rapidly and severely than the medial SNc(Okamura, Yokoyama, and Ibata 1995), which corresponds to the fact that DA depletion typically begins in the dorsolateral area of the rostral striatum into where ventrolateral SNc DA neurons cast (Betarbet *et al.* 2000; Mendez *et al.* 2005). This subtype of neuron (TH-positive A9 neurons) is the only neuron in the midbrain that expresses a G-protein-gated inwardly rectifying potassium channel (GIRK2/KCNJ6) (Karschin *et al.* 1996; Mendez *et al.* 2005). As omics (proteomics or genomes) precision has advanced to the single-cell level, numerous molecules expressed in a region-specific way were progressively uncovered through exploratory research based on single-cell mapping, including *Sox6, ALDH1A1, Ndnf, and Vglut2*.etc. ALDH1A1- and Sox6-positive neurons, which are mentioned located in the ventral part of SNc, decay predominantly in PD and project mostly to the dorsolateral striatum, with ALDH1A1-positive subtypes accounting for roughly 70% of total DA neurons in SNc (Cai *et al.* 2014; Liu *et al.* 2014; Pereira Luppi *et al.* 2021; Poulin *et al.*

2018; Wu *et al.* 2019). A recent study has revealed that Netrin-1 and its ligand DCC are exclusively expressed in SNc DA neurons, especially in the ventral part, and their receptors can trigger cell death in the absence of adequate ligand supply, introducing a new culprit for the selective vulnerability of DA neurons (Jasmin *et al.* 2021; Lo *et al.* 2022). Similarly, Netrin-1 expression has recently been found to be reduced in PD patients not only in the brain but also in the intestinal nervous system due to over-activation of the C/EBP-β signaling pathway (Ahn *et al.* 2021), which partially endorses the notion of the gut-brain axis as the onset of PD progression.

2. Temporal differences in neuronal vulnerability: DA neuron diversity formation in the midbrain is not only geographically ordered but also age-dependent. By using a genetic inducible fate mapping technique (GIFM) based on the dynamic expression of a key signaling molecule, the sonic hedgehog gene (SHH) (Blaess *et al.* 2011), during midbrain DA development, scientists have shown that the timing of the SHH expression is vital for the generation of distinct subclasses of DA neurons. Early Shh expression (embryonic day 8.5) in a progenitor group result in the formation of DA neurons expressing GIRK2/KCNJ6 primarily in the rostral SN, whereas the development of calbindin-positive DA neurons in the caudomedial VTA is preferentially related with later SHH expression (embryonic day 11.5) (Blaess *et al.* 2011). Notably, the DA neuron subpopulations in the rostral SN and caudomedial VTA, which define the starting and ending points of the DA neuron genesis timeframe, do also exhibit the most distinct functional properties that can clearly tell them apart in adulthood (Lammel *et al.* 2008). Different transcriptional pathways also contribute to the maintenance of developmental diversity among DA subpopulations in the adult brain (Andressoo and Saarma 2008). For instance, nuclear receptor-related 1 (NURR1) must be continuously expressed after maturity in order to retain subpopulations of DA neurons in the SNc, while VTA DA neurons survive in the absence of NURR1(Baydyuk, Nguyen, and Xu 2011; Kadkhodaei *et al.* 2009).

Additional genetic markers are required to research the function of distinct DA neuron subtypes in order to explore the heterogeneity of SNc DA neurons at the molecular level (*Figure 02.*). Genome-wide gene expression studies applying microarray and RNA sequencing (RNAseq) technologies, particularly the latest single-cell RNAseq (scRNAseq) technology, in combination with laser capture microdissection (LCM) and fluorescence-activated cell sorting (FACS), enable the systematic identification of genetic markers in distinct DA neuron subpopulations. Given that the pathology appears in the striatum prior to the SNc, another interesting theory for the reason of vulnerability was come up with. Kelvin C.Luk *et al.* established a novel PD model by using α-Syn pre-formed fibrils (PFF) injected into the striatum to induce pathological α-Syn aggregation. PFF successfully initiated the slowed progressive demise of the DA neurons with a gradual LBs invasion 180 days after PFF injection. The neuronal loss mainly occurs in the ventromedial SNc region, suggesting that connectivity between the striatum and SNc is also a determinant of such vulnerability (Luk *et al.* 2012).
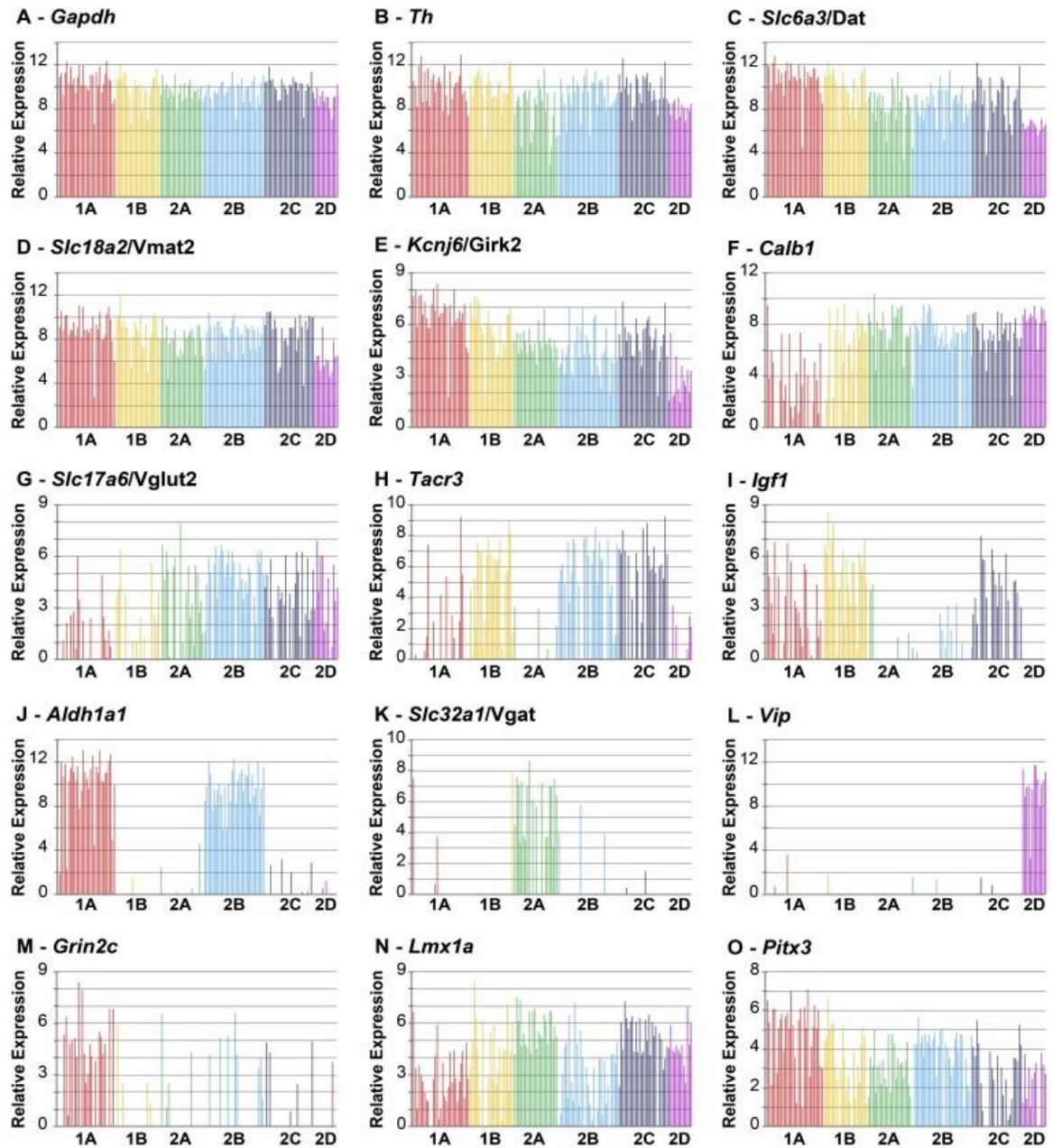
Figure 02. The differential expression of various genes in DA neuron subtypes at single-cell resolution (Anderegg, Poulin, and Awatramani 2015) *The relative expression levels of 96 genes were analyzed using qRT-PCR technique. Hierarchical clustering analysis was applied, and 153 neurons were assigned to one of six DA neuron subtypes. 1A (red), 1B (orange), 2A (green), 2B (light blue), 2C (dark blue), 2D (purple).*

1.1.4 Electrophysiology of DA neurons

The unique e-phys activity of SNc DA neurons is likely a major contributor to their vulnerability. They exhibit spontaneous slow activity with rhythms typically ranging from 1-10 Hz in vivo and approximately 0.5-3 Hz in vitro, with action potential (AP) duration reaching 2 ms and, in rare cases exceeding 4 ms (***Figure 03.***) (Bean 2007; Dragicevic, Schiemann, and Liss 2015; Grace and Onn 1989). Electrophysiology recordings from acute brain slices were mostly performed on juvenile rodents. The results implied that this spontaneous firing ignited by the influx of Na^+ and K^+ ions via the HCN channels in the hyperpolarization phase, as DA neurons show a large-amplitude slow-activated current (I_h) without time-dependent inactivation in response to prolonged hyperpolarization in vitro, thus has been considered as a marker for DA neuron in SNc (Lacey, Mercuri, and North 1989), and the HCN channel is exactly the pacemaker for most other neurons with rhythmic activity. This autonomous activity was later discovered to be more robust than previously anticipated; even when the Na^+ current was completely blocked by tetrodotoxin (TTX), the subthreshold oscillations (STO) running slightly slower than the firing rate could still occur, suggesting that the Na^+ current was merely a participant instead of the activator (Ping and Shepard 1996). Later recordings from adult mouse brain slices revealed that the subthreshold oscillations were abolished in a Ca^{2+}-free medium or with cadmium (Cd^{2+}) or cobalt (Co^{2+}) treatment, implying that Ca^{2+} currents are required for pacemaking. At the same time, the subthreshold oscillation is always accompanied by a synchronized oscillation in intracellular Ca^{2+} concentration triggered by the opening of plasma membrane L-type calcium channels (Cav1.2 versus Cav1.3) and endoplasmic reticulum (ER) intracellular calcium channels. The release of Ca^{2+} out of the reservoir can be inhibited by the high-dose application of a L-type calcium channel blocker, dihydropyridines. Moreover, a prototypical potent and highly selective inhibitor of the small-conductance Ca^{2+}-activated potassium channel (SK channel), apamin, is able to block the oscillation in the hyperpolarization phase (Puopolo, Raviola, and Bean 2007). These results established a consensus about the mechanisms of spontaneous impulses in the DA neurons: the L-type calcium channel and the SK channel. Ca^{2+}

influx through the L-type forms the ascending part of the oscillation, while the subsequent opening of the activated SK channel leads to the efflux of K^+ to form the descending part. Multiple calcium channels were then found to be involved in the pacemaking process (Dragicevic, Schiemann, and Liss 2015). This notion, however, has been challenged by the discovery that the specific L-type calcium channel blocker isradipine can block all the L-type channels in a moderate concentration while maintaining the firing rate and that intracellular application of calcium buffers not only fail to slow the firing rate but surprisingly increases it (Guzman *et al.* 2009); these findings call into question that L-type calcium channel is the primary regulators of rhythm. Subsequent studies revealed that one of the main functions of L-type calcium channels is to maintain the robustness of spontaneous firing and that Ca^{2+} influx triggered by L-type channels, especially Cav1.3, together with Neuronal Calcium Sensor 1 (NSC-1), can inhibit the phosphorylation level of G Protein-Coupled Receptor Kinase 2 (GIRK2) thereby reducing arrestin-mediated dopamine receptor 2 (DR2) internalization, decreasing the desensitization of DR2, and maintaining the adaptive regulation of DR2 to the firing rate of DA neurons (Dragicevic *et al.* 2014). Thus, the drivers of spontaneous DA neuron discharges may originate from other sources, such as persistent sodium current ($I_{Na}P$) (Puopolo, Raviola, and Bean 2007; Yang *et al.* 2019).

Along with enhancing robustness in the interspike interval, L-type calcium channels provide an intracellular Ca^{2+} signal linked to the spike, which is required for homeostatic plasticity and regulation of activity-induced gene expression (Frank 2014); additionally, this Ca^{2+} signal ensures an adequate energy supply for DA neurons achieved via mitochondrial oxidative phosphorylation (OXPHOS). Due to the low intrinsic Ca^{2+} buffering capacity of SNc DA neurons, intracytoplasmic Ca^{2+} concentration $[Ca^{2+}]i$ is elevated to high nanomolar or further to micromolar levels thereafter functions throughout the cytosol and dendritic area (Guzman *et al.* 2018), promoting Ca^{2+} entry into the mitochondrial matrix and activating the tricarboxylic acid (TCA) cycle dehydrogenases to produce the reducing equivalents required for adenosine triphosphate (ATP) generation (Csordas, Weaver, and Hajnoczky 2018; Diaz-Garcia *et al.* 2021). Raised $[Ca^{2+}]i$

also enhances the transportation of the mitochondrial substrate required for OXPHOS (e.g., malate-aspartate shuttle). Axonal metabolic demands are often immense; in light of that, a large number of axonal branches of SNc DA neurons thus imposes a huge bioenergetic burden (Chamberlain and Sheng 2019; Giguere *et al.* 2019). Consequently, $[Ca^{2+}]i$ of SNc DA neurons entered through L-type channels serves as a bioenergetic feedforward signal controller to obtain the energy gain effect. However, as there is "no such thing as a free lunch", this massive energy supply inevitably aggravates the oxidative stress, and the production of large amounts of reactive oxygen species (ROS) in mitochondria contributes undermining tolerance against hypoxia, which is also thought to be the consequence of selective vulnerability, referred to as the stress pacemaker theory (Dragicevic, Schiemann, and Liss 2015; Guzman *et al.* 2018). Large amounts of Ca^{2+}-dependent mitochondrial oxidative stress are later reported in the locus coeruleus (LC) and the dorsal motor nucleus of the vagus (DMV) neurons, both of which are self-activated neurons like DA neurons (Goldberg *et al.* 2012; Sanchez-Padilla *et al.* 2014). Guzman *et al.* achieved significant therapeutic effects in animal PD models by alleviating mitochondrial oxidative stress and minimizing the loss of mitochondrial proteins by delivering L-type channel blockers (Guzman *et al.* 2018). A phase III clinical study of the L-type calcium channel blocker isradipine in PD was unfortunately declared a failure in 2020 because the drug failed to impede progression in the early stages (Maiti and Perlmutter 2020). Even so, the high-energy metabolic state induced by $[Ca^{2+}]i$ stayed in the spotlight in numerous studies. For example, an R-type calcium channel, Cav2.3, was discovered to be the most prevalent voltage-gated calcium channel subtype in the cell body of adult SN DA neurons and is considered as a negative factor for viability, but its role in pathology warrants further investigation (Benkert *et al.* 2019).

Aside from that, nigrostriatal DA neurons express a variety of potassium channels, among which changes in the A-type voltage-dependent potassium channel (Kv4.3) have been shown to raise the vulnerability to toxicity. The role of Kv4.3 is primarily to maintain the background dopamine release, and suppression of Kv4.3 activity may cause a phase-excitation pattern; as a result, dramatically boosting the

dopamine delivery (Benkert *et al.* 2019; Haghdoost-Yazdi *et al.* 2011; Liss *et al.* 2001). Overexpression of the α-Syn mutant A53T dramatically increased the burst rate of DA neurons in vivo. This higher rate is due primarily to glutathione-sensitive malfunctioning of the Kv4.3 channel, which is accompanied by elevated Kv4.3 expression, and the increased firing rate may raise the stress level of DA neurons, contributing to disease development (Subramaniam *et al.* 2014). RT-qPCR targeting nigrostriatal DA neurons in the brain of PD patients showed elevated mRNA for Kv4.3 (Dragicevic, Schiemann, and Liss 2015). Inhibition of Kv4.3 helps maintain the survival of SNc DA neurons to some degree (Yang *et al.* 2001); nevertheless, the mechanism by which aberrant Kv4.3 activity affects durability remains unknown. Another well-studied potassium channel is the inwardly rectifying potassium channel (GIRK2), which, as previously described, couples with DR2 and maintain the robustness of rhythm. The G protein-coupled inwardly-rectifying potassium channels (GIRKs), known as Kir and encoded by *KCNJ*, belong to a class of lipid-gated potassium channels that are switched on by the signaling lipid PIP2 upon activation of G-protein-coupled receptors (GPCRs). After activation, the G-protein α-subunit (Gα) is released from inactive heterotrimeric G-protein complexes (Gαβγ). The interaction between activated G-dimer (Gβγ) and GIRK channels opens the channels and allows potassium ions to efflux, resulting in membrane hyperpolarization. The affinity of GIRKs for PIP2 may be increased after activation. A high level of PIP2 could activate channels independent of G protein, whereas G protein cannot activate channels alone without PIP2. The weaver genotype mice identified A missense mutation (G953A) in the GIRK2 gene could constitutively active GIRK2wv channels which produce chronic depolarization with non-ion-selective permeability and leads to progressive degeneration of SNc DA neurons, and at one point were considered as a very popular mouse model for PD (Luscher and Slesinger 2010; Liss, Neu, and Roeper 1999). Elevated mRNA levels of GIRK2 were found in DA neurons of PD patients (Dragicevic *et al.* 2014). The deficiency of DA neurons in the striatum can also be caused by hypercholesterolemia, which affects GIRK2 activity (Dragicevic *et al.* 2014; Mathiharan *et al.* 2021; Paul *et al.* 2018). The K-ATP channel is another potassium channel of interest because its opening probability correlates with the

metabolic demands of DA neurons, and its higher activity protects neurons from hyperexcitability and excitotoxicity. The K-ATP channels are primarily expressed in medial SNc DA neurons adjacent to the VTA region, and the projection area is located in the dorsomedial striatum (DMS). The activity of K-ATP channel is to induce neuronal burst when pharmacological coactivation with NMDA receptor then triggers novelty-induced exploration.

The death of this fraction of neurons is followed by reduced novelty-induced behavior and selective persistence of interest in early PD patients (Schiemann *et al.* 2012). Last but not least, SK channels, as pacemaker participants of DA neurons, have also been reported to be involved in the pathophysiological processes of PD (Dolga *et al.* 2014; Wolfart *et al.* 2001).
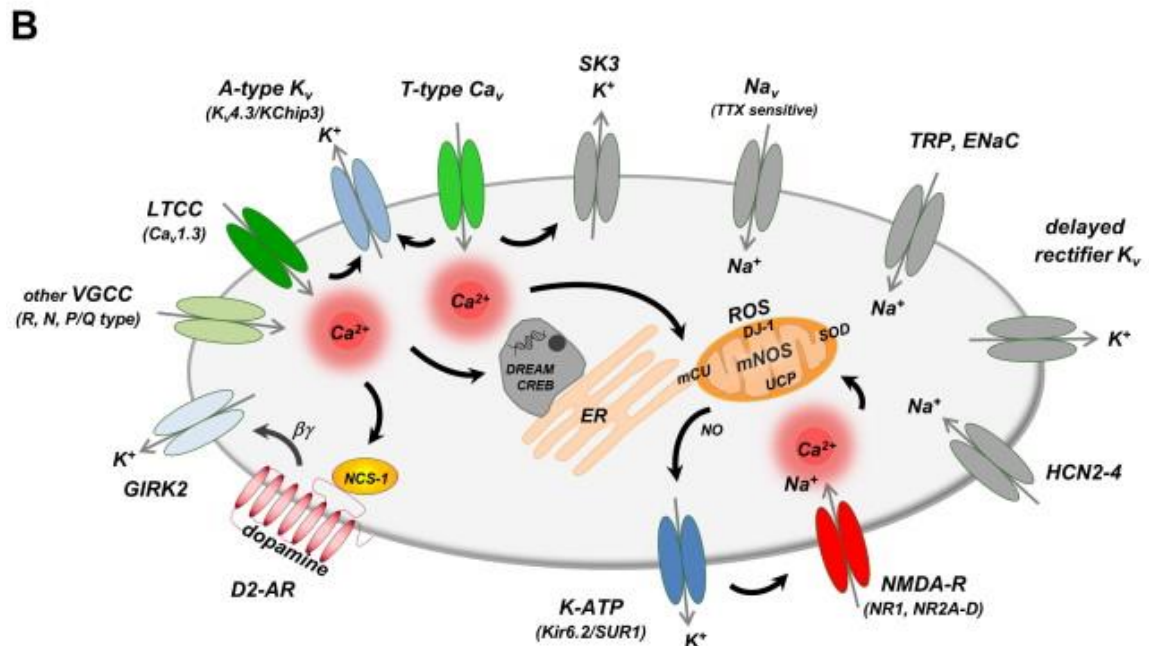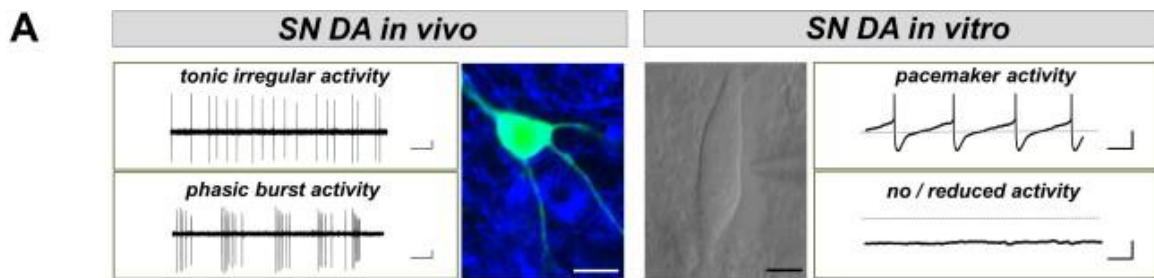
Figure 03. Distinct activity patterns and underlying ion channel expression in substantia nigra dopamine (SN DA) neurons (Dragicevic, Schiemann, and Liss 2015).

The e-phys properties of midbrain DA neurons vary by area, and this variation is intimately tied to the regions to which they project and the roles they serve. In general, midbrain DA neurons projecting to the lateral shell of the nucleus accumbens and the dorsal striatum fire at a slower rate than those projecting to the prefrontal cortex and the medial shell of the nucleus accumbens (Lammel *et al.* 2008). At least two e-phys phenotypes were also reported by several studies in the SNc area that corresponded to previously described neuron subpopulations and project regions (Lammel *et al.* 2008; Krashia *et al.* 2017; Lerner *et al.* 2015). Alterations in the excitability of associated neurons are reported in numerous neurodegeneration disorders, not just in PD. Enhanced neuronal excitability may be an adaptive response to the neuroprotection of affected neurons though alternative models emphasize hyperexcitability as a major factor in neurodegeneration (Mattson 2003). Integrating alterations in e-phys phenotypes with neuronal degeneration vulnerability requires detailed studies on the metabolic function of specific ion channels besides their impact on excitability (Roselli and Caroni 2015).

1.1.5 Nigrostriatal system in PD

It is possible to distinguish between several distinct subtypes of DA neurons that originate in the SNc, and diffusely project to various parts of the striatum to carry out specialized functions. Due to the fact that these pathological changes are closely related to the clinical manifestations in PD patients, it is critical to understand the precise path taken by different neuronal projections in the nigrostriatal system and the relationship between their excitability and PD pathology. The nigrostriatal pathway, which accounts for 75% of brain dopamine pathways, is the most significant route engaged in SNc DA neurons. Over 90% of the striatal dopamine is released for the caudate and putamen in the dorsal striatum, where it is used to modulate the initiation and termination of voluntary movements, maintain posture, motor program acquisition and habit formation (German and Manaye 1993). Because early studies on PD symptoms concentrated chiefly on the motor level,

this route is rather well understood. The nigrostriatal pathway is composed of two components: the direct pathway and the indirect pathway. Both are mutually constrained and act in concert to fine-tune the initiation and termination of locomotion, with the primary distinction being the subtype of medium spiny neurons (MSN) in the striatum: the direct pathway controls the initiation and timing of voluntary movements. The MSN, synaptically connected to SNc DA neurons contain substance P and G protein-coupled dopamine receptors 1 (DR1). These induce the synthesis of cAMP via activated adenylyl cyclase upon dopamine binding. They release the neurotransmitter GABA to activate the motor cortex by suppressing the inhibitory effect of GPi and SNr on cortical motor neurons. The indirect pathway, on the other hand, is used to antagonize the activity of the direct pathway, where DR2 and enkephalin-expressing MSN, whose excitability is inhibited by activating inhibitory G proteins, lead to an activation of GPi/SNr (Lang and Lozano 1998). This situation suggests that dopamine either increases excitability through DR1 on MSN or attenuates it via DR2. This balance favors the direct pathway somewhat more than the indirect pathway, which in turn activates the thalamus and motor cortex (Lanciego, Luquin, and Obeso 2012). In PD, a shortage of dopamine inhibits the direct route and excites the indirect pathway, resulting in thalamic inhibition and signs of diminished movements, such as hypokinesia and tonicity (***Figure 04.***).
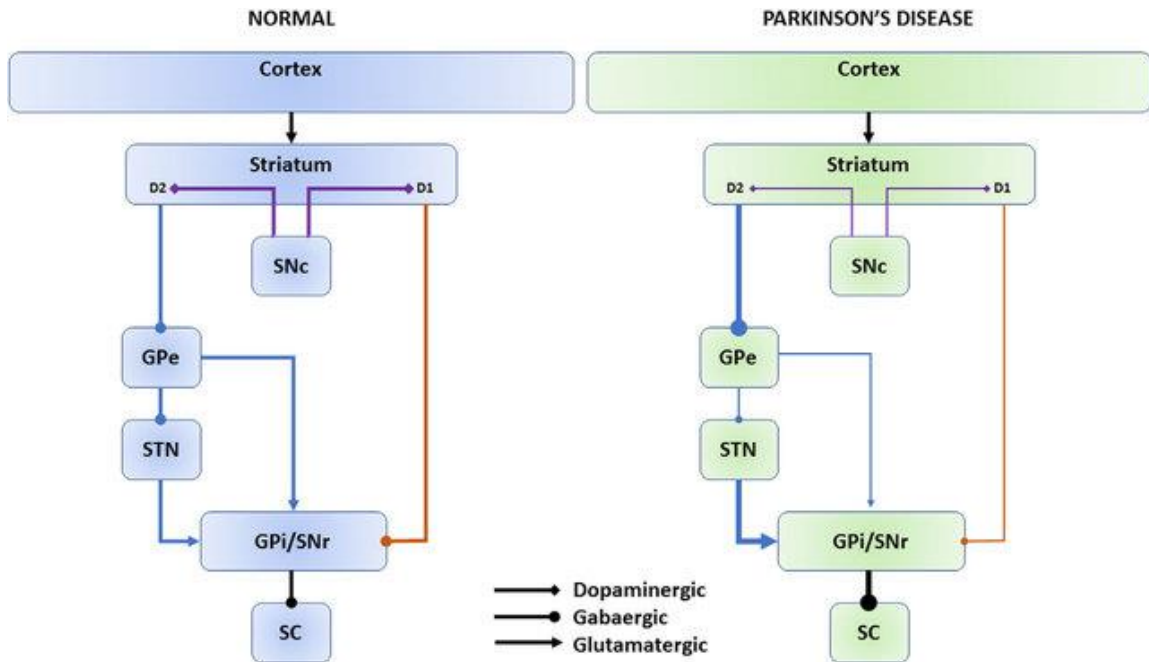
Figure 04. Direct and indirect basal ganglia pathways (Pretegiani and Optican 2017).

The nigrostriatal pathway has been gradually elucidated in recent years using cross-genetic marker strategies for combinatorial gene expression and neuronal tracing techniques, and additional branches have been unveiled based on the diversity of nigrostriatal DA neurons. Three distinct routes were identified from the SNc to the striatum, the first two of which were consistent in several studies. The first projection comes from the ventral Aldh1a1+ neurons in the SNc, casting fibers to the whole caudoputamen (CP), including rostral CP (CPR), intermediate CP (CPI) and caudal CP (CPC), which are particularly gathered in the dorsolateral and part of the medial region of striatum, showing a correspondence in the spatial relationship, that means the lateral (medial) striatum receive fibers derived from the lateral (medial) SN. They are exactly the direct and indirect pathways described above, exhibiting vulnerability in a PD mouse model. The second projection comes from Calb1+ neurons of the dorsal SNc, which intensively project medially to the CPR and partially contain the axons of Aldh1a1+ neurons to innervate the ventral medial region of the CPI and CPC, whose primary role is related to reward motivation and may be involved in voluntary exploratory movements (Lerner *et al.* 2015; Poulin *et al.* 2018). Another key finding is that the VgluR2+ DA neurons, located mainly in the lateral SNc, send axons to the CPT, which can be almost

identified as a separate route that can be strongly activated by novel environmental cues (Poulin *et al.* 2018).

Following SNc DA neuron ablation, pathway-specific abnormalities in the striatum produce many cellular and synaptic changes in the basal ganglia, resulting in hazardous neural activity across the cortex-basal ganglia-thalamic network in PD (Chen *et al.* 2021; McGregor and Nelson 2019; Parker *et al.* 2018; Parker, Lalive, and Kreitzer 2016; Sharott *et al.* 2017). These changes exacerbate the severity of motor symptoms and make the PD manifestations more nonspecific, which results in diagnostic difficulties.

1.2 Fragile X syndrome and FMRP

Fragile X syndrome (FXS) is a severe X chromosome dominant disorder that is part of the autism spectrum disorder. The cause is the transcriptional silencing of the *FMR1* gene due to an expanded trinucleotide (CGG) region of more than 200 repeats. As a consequence, the gene product, the Fragile X mental retardation protein (FMRP), is then completely lost. FMRP has an enormous impact on neurons as a shuttle protein that can bind to RNA.

1.2.1 Clinical characterization and pathogenesis

FXS is primarily caused by the silencing of *FMR1*, an X chromosome gene that encodes FMRP. Therefore, females have milder symptoms than males. Although the precise number of individuals diagnosed with FXS is unclear, one research suggested that roughly 1 in 7,000 males and 1 in 11,000 women are affected.

The number of CGG repeats in a person can be determined by a blood test performed by a health care provider or genetic counselor. Patients can be divided into four groups based on the number of CGG repeats in each copy of the *FMR1* gene, and the females are grouped according to the principle of the most repeated copies.

Normal individuals usually hold 5 to 44 repeats. Individuals with moderate repeat counts (45-54 repeats) will not have FXS and are not in danger of obtaining FXS; nonetheless, they may have a greater probability of developing symptoms of other Fragile X-related illnesses and pass these increased odds on to their offspring. Cases with so-called premutations (55-200 repeats) who do not have FXS may develop Fragile X tremor/ataxia syndrome (FXTAS). Individuals with complete mutations (>200 repeats) are FXS patients, and women with the disease have a 50% chance of passing to their children.

Symptoms at an early age with FXS include dysplasia (poor initial latch or suck with breastfeeding, recurrent emesis due to reflux, recurrent otitis media), malformations (strabismus), learning disabilities, varying degrees of psychiatric symptoms (tactile defensiveness, poor eye contact, anxiety, autism), and persistent behaviors (excited hand-flap, hand biting or chewing on clothing). In addition, seizures (partial complex seizures, generalized tonic-clonic, and disoriented seizures) are common and the most serious medical problem in children with FXS. Males with FXS usually carry some degree of intellectual disability ranging from mild to severe. Autism spectrum disorders (ASD) can also develop in early childhood. Individuals with FXS also exhibit morphological abnormalities after puberty, including long faces and arched palates, large ears, soft skin, abnormally hyperextended fingers, flat feet, and macroorchidism. However, patients with FXTAS have a more specific, predominantly motor presentation like motor tremors, rigidity, ataxia, slow movement, and hyperalgesia; therefore, they are often misdiagnosed with PD at the outset (Hagerman *et al.* 2017).

There is no cure for FXS, although some treatments can help minimize the symptoms. FXS patients who get an adequate education, therapy services, and medicine have the greatest chance of maximizing their specific strengths and capabilities. In addition, early intervention is important because the brain is still under development in children, and it provides a child with the greatest chance to develop a full range of skills.

1.2.2 FMRP and basic function in neurons

FMRP is a 632 amino acid-residue RNA-binding protein. Its structure includes three RNA-binding regions, an arginine-glycine-rich (RGG) box, two heterogeneous nuclear ribonucleoprotein K homology domains (KH1 and KH2) containing nuclear export sequences (NES) in between, and nuclear localization sequences (NLS) that contribute to nucleus anchor. Two Agn regions in the N-

terminal have the ability to bind with other proteins, thus facilitating protein-protein interactions (Richter and Zhao 2021).

It can be inferred from the structure of FMRP that it has a deep and potent influence on the proteins it targets. While FMRP is mostly found in the cytoplasm in a steady-state, it may shuttle between the nucleus and cytoplasm and alter the function of targets at multiple levels. In the nucleus, FMRP regulates DNA damage response, transcription and splicing, controls RNA synthesis by regulating the key transcription factors, and is additionally involved in RNA modification. In the cytoplasm, FMRP slows or blocks ribosome translocation and impairs the expression of its targets in translation initiation. Notably, FMRP binds directly to certain proteins, affecting their functional activity.

The breadth and scope of the FMRP effects on its' targets are also impressive. FMRP is expressed in all cell types in the central nervous system. More than 4000 RNAs in neurons of the mouse hippocampus, cortex and cerebellum were found to be potential targets of FMRP by HITS-CLIP or CLIP-seq and modified techniques, and 1/4 of them are long-range transport mRNAs, which are associated with synaptic activity, and similar results were also obtained in postmortal human prefrontal cortex tissue (Darnell *et al.* 2011; Tran *et al.* 2019; Li *et al.* 2020). FMRP-bound RNAs often exhibit the following characteristics: FMRP preferentially binds to the coding sequence of RNAs rather than non-coding sections; FMRP preferentially attaches to long-stranded RNAs; FMRP preferentially binds to autism-associated mRNAs (Richter and Zhao 2021). The roles of FMRP-binding RNAs span electrophysiology, cell signaling, synaptic formation, axonal and dendritic development, cytoskeleton and microtubule structure, RNA translocation and transcription, and epigenetic modification. It is hypothesized that this dysregulated protein translation in FXS impairs neuronal growth and function by impairing synapse maturation and plasticity, hence changing network activity throughout the brain.

1.2.3 FMRP and neuronal excitability

There is growing evidence that elevated neuronal and circuit excitability is prevalent in several brain regions of *Fmr1* KO mice, resulting in sensory and motor deficits that explain many abnormalities, including seizures, reduced thresholds for auditory epilepsy, disruption of circadian rhythms, and hypersensitivity of eye contact.

The alterations in neuronal excitability by FMRP loss involve either change in intrinsic membrane properties of the cell body or abnormalities in the processing of input (dendritic) and output (axonal) signals in the synapse. By virtue of its structure, FMRP can regulate the expression and functional activity of various ion channels and receptors from different angles, including transcription, translation, trafficking and opening. The N-terminal Agn regions can directly regulate the properties of ion channel proteins, such as Slack and BK channels, while the C-terminus can directly interact with calcium channels. The specific consequences of FMRP loss include changes in action potential initiation and firing patterns (involving various potassium and sodium channels), neurotransmitter release (involving calcium and potassium channels), and dendritic function (involving potassium, calcium, and HCN channels, as well as AMPA receptors, NMDA receptors and GABA receptors). In turn, these functional effects may be part of the underlying mechanisms that characterize FXS cognition and behavior manifestations (*Figure 05*.).

The regulation of ion channels by FMRP possesses some very important features that need to be taken into account in in-depth studies. First, FMRP may regulate the same channel in neurons in multiple ways simultaneously; for example, for BK channels, FMRP can either affect their expression level or bind directly to channel proteins to alter their opening probability (Deng *et al.* 2013). The manners of binding to BK channels can also vary, either by binding to the β4 regulatory subunit or directly to the main pore-forming α-subunit (Kshatri *et al.* 2020). As a comparison, the binding of FMRP with specific ion channels (e.g., Cav2.2) or

receptors (e.g., GluRA) can affect their trafficking to the cytosolic membrane, profoundly altering their activity without influencing their expression (Ferron *et al.* 2014; Guo *et al.* 2015).
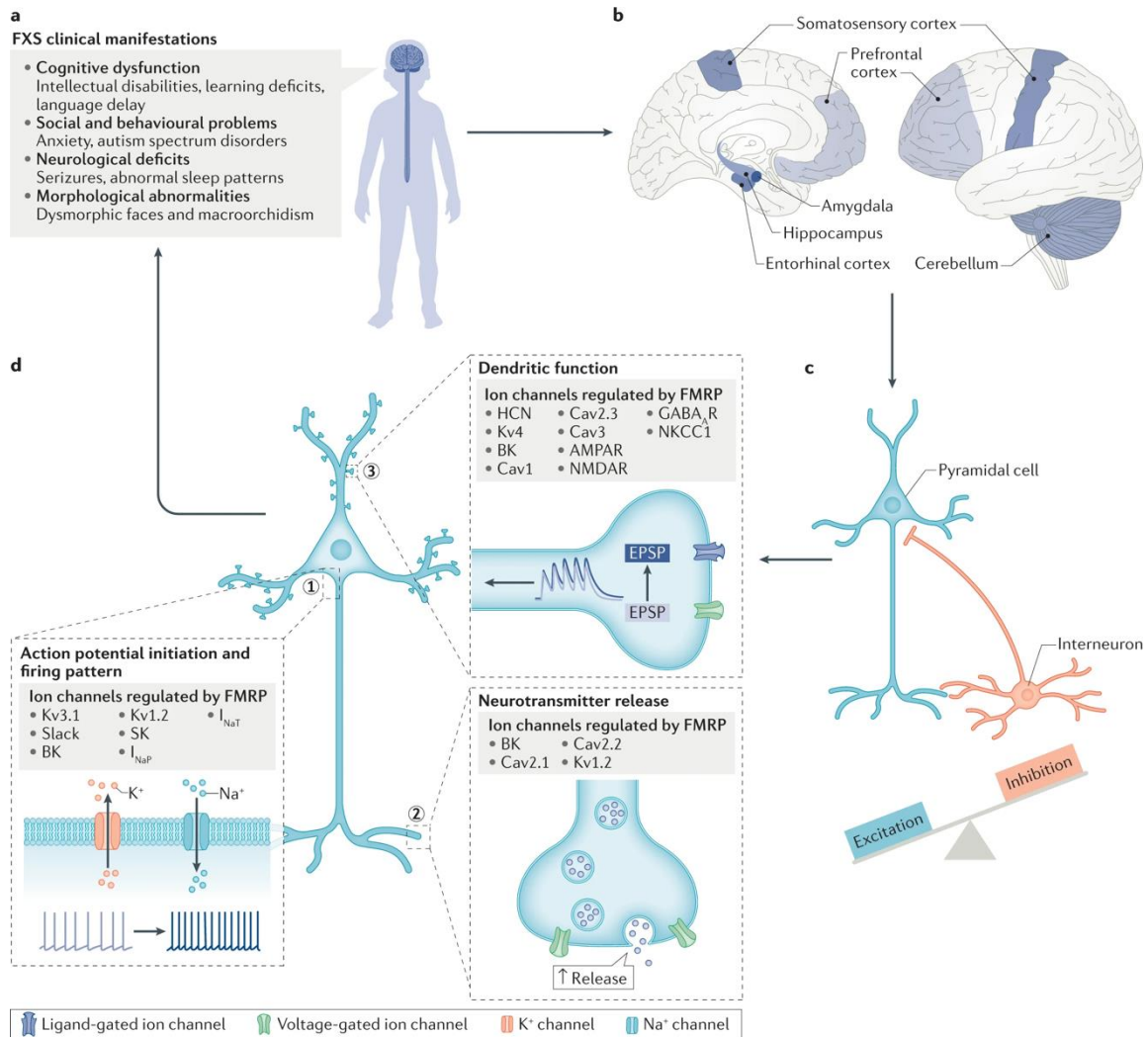
Figure 05. Overview of channelopathies in FXS (Deng and Klyachko 2021).

While FMRP deficits lead to overall neuronal and circuit hyperexcitability in almost all cases, the control of individual ion channels by FMRP can be bidirectional, depending on the types of neurons and the areas in which they are located. For example, the regulation targeting HCN channels, whose function is elevated in CA1 dendrites in the *Fmr1* KO mouse model, is reduced in L5 PFC dendrites (Brandalise *et al.* 2020). It is now thought that this bidirectionality stems from the background differences in the expression of various molecules. The

diversity in the way FMRP regulates ion channels makes the multiple directions have completely different sensitivities for a certain type of neuron (***Figure 06.***).
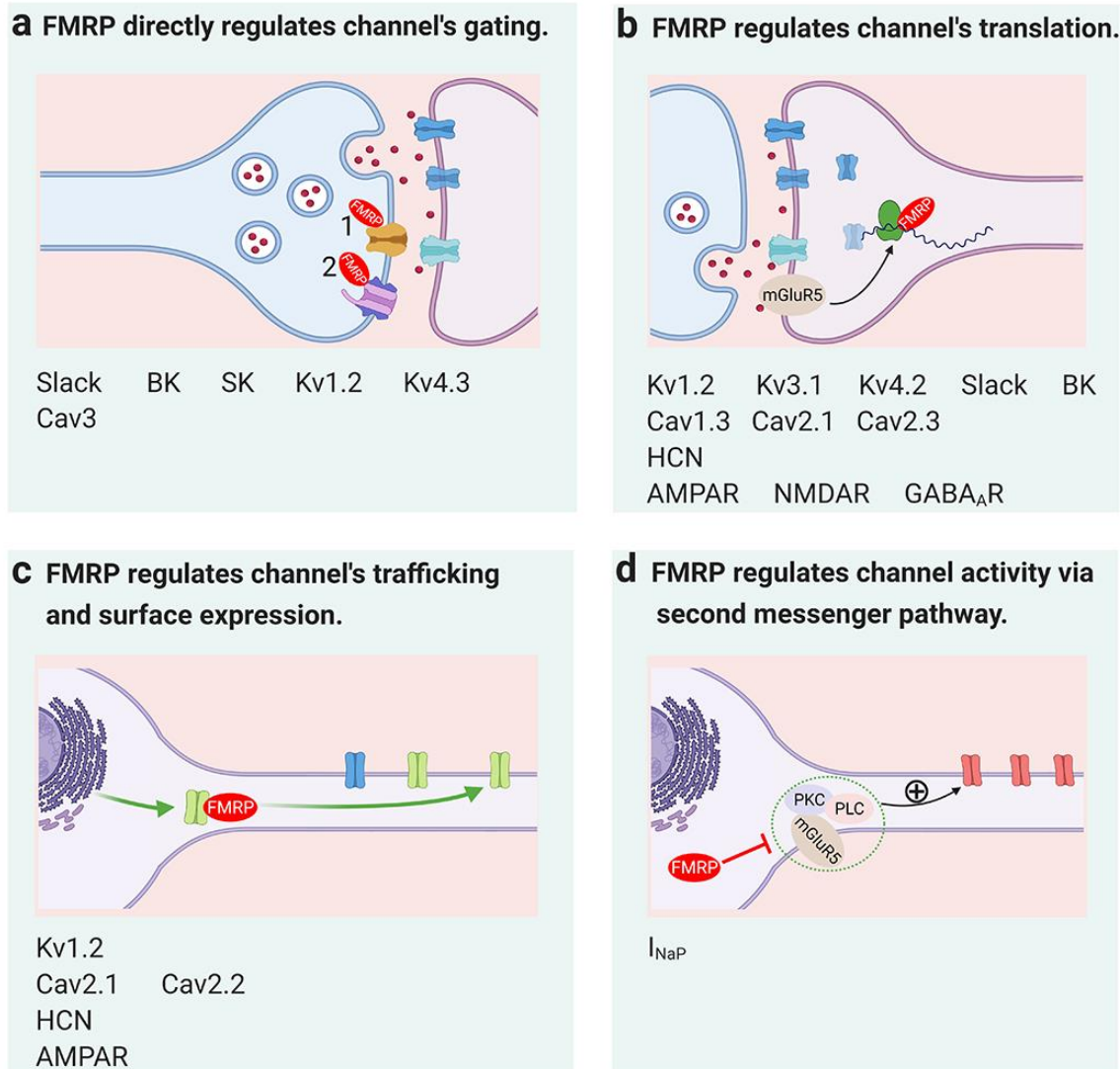
Figure 06. FMRP controls ion channel functions through multiple mechanisms.

1.2.4 FMRP and Parkinson's Disease

Patients with FXS do not show any sign of the typical PD, but symptoms of PD in FXTAS have been commonly reported, with almost all non-motor and motor symptoms, in patients with FXTAS by mid to late stage (Fay-Karmon and Hassin-Baer 2019; Salcedo-Arellano *et al.* 2020). The LB pathology was also found to be present in some FXTAS cases (Sacino *et al.* 2019). Moreover, impaired nigrostriatal pathways and associated DA deficits are common in FXTAS patients, and DatScan can detect this abnormality (Hall *et al.* 2010; Madeo *et al.* 2013). Notably, unlike FXS, the immediate result of the premutation is that the transcription of the *FMR1* gene is not silenced but heavily enhanced, resulting in up to nearly 8-fold more FMRP mRNA than the normal (Tassone *et al.* 2000), with slightly reduced FMRP expression in neurons and glia (Greco *et al.* 2006), considering the pathogenesis may be closely related to the toxicity of rampant FMRP mRNA by protein sequestration. Counterintuitively, the number of CGG repeats in premutation shows somewhat negatively correlated with the probability of a PD phenotype. Seven out of eight FXTAS cases were diagnosed with PD having CGG repeats between 57 and 79, and the closer association between moderate CGG repeats number (40-54) instead of premutation and clinical PD was found recently (Loesch *et al.* 2018; Salcedo-Arellano *et al.* 2020).

The previous work from our group further identified a link between FMRP and PD. FMRP was discovered to be reduced in cultured DA neurons as well as the SNc region in the mouse brain in response to α-Syn overexpression. FMRP was also absent in the SNc of PD patients and the individuals with early stages of incidental Lewy body degeneration (iLBD). *FMR1* expression in response to α-Syn was controlled via Protein Kinase C (PKC) and cAMP response element-binding protein (CREB). α-Syn overexpressing neurons demonstrated an increase in N-type calcium channels, increased phosphorylation of ERK1/2, eIF4E, S6, and increased expression of Matrix Metalloproteinase 9 (MMP9). FMRP influenced neuronal function in a PD animal model because Fmr1 knock-out mice were resistant to the impact of α-Syn on electrically evoked striatal dopamine release. In summary, the

findings encourage the investigation of what FMRP plays in the course of PD (Tan *et al.* 2020).

2. Aim of the study

Before the emergence of Lewy bodies in PD, structural and functional changes are likely to occur. A better knowledge of the early pathogenic alterations in SNc DA neurons, as well as the molecular and cellular processes that contribute to them, would likely aid in the development of new therapeutics to slow the progress of PD. The loss of FMRP is a unique molecular event that happens prior to the appearance of Lewy bodies, and FMRP regulates neuronal excitability by modulating numerous neuronal genes, making the FMRP loss possibly have a far-reaching impact on the progress of PD. By identifying all of the functional repercussions of FMRP loss in SNc DA neurons under physiological circumstances, we may be able to comprehend the PD pathophysiology better. Our specific aims therefore were:

1. Investigating the effect of FMRP on neuronal excitability in SNc DA neurons.
   We investigated the normal action potential and firing rate of SNc DA neurons in *Fmr1* knock-out mice using patch clamp recordings to test if there is any change in the excitability phenotype caused by the FMRP loss. In addition, we performed treatment with specific antagonists/agonists on different ion channels to examine the molecular mechanism of altered neuronal excitability.

2. Delineating the role of FMRP on the nigrostriatal pathway.
   We determined whether the expression of certain nigrostriatal pathway-related molecules is altered in Fmr1 knock-out mice by immunofluorescent staining on the brain slices containing the dorsal striatal region to explore the alteration of nigrostriatal pathway excitability by FMRP and the possible mechanisms. Mass spectrometry proteomics profiling of mouse dorsal striatum tissue was used to identify possible targets related to PD that may be altered by FMRP.

3. Materials and methods

3.1 Materials

3.1.1 Antibodies

Antibody	Cat. No.	Dilution (WB)	Dilution (ICC/IHC)	Supplier
FMRP	4317S	1:1000		Cell Signaling
FMRP 5C2	834701		1:200	Biolegend
Phospho-S6 (Ser244/247)	44-923G		1:250	Thermo Fisher
Tyrosine Hydroxylase	PA1-4679	1:1500		Thermo Fisher
Alpha-synuclein (14H2L1)	701085		1:500	Thermo Fisher
clone DaT-Nt	MAB369	1:1000	1:100	Millipore
GFP antibody	GTX113617		1:500	GeneTex
Anti-D1 Dopamine Receptor antibody	D2944		1:100	Millipore
Anti-Dopamine D2 Receptor Antibody	AB5084P	1:1000	1:100	Millipore
Anti-α-Tubulin antibody	T6074	1:10000		Sigma
Na,K-ATPase Antibody	3010S	1:1000		Cell Signaling
Donkey anti-Rabit IgG H&L Alexa Fluor® 488	A32790		1:500	Invitrogen
Donkey anti-Sheep IgG H&L Alexa Fluor® 488	A11015		1:500	Invitrogen
Donkey anti-Sheep IgG H&L Alexa Fluor® 555	A21436		1:500	Invitrogen
Donkey anti-Mouse IgG H&L Alexa Fluor® 555	A32773		1:500	Invitrogen
Donkey anti-Sheep IgG H&L Alexa Fluor® 568	A21099		1:500	Invitrogen
Donkey anti-Rabbit IgG H+L Alexa Fluor® 594	A21207		1:500	Invitrogen
Donkey anti-Mouse IgG H&L Alexa Fluor® 647	A32787		1:500	Invitrogen
Alexa Fluor™ 647 Streptavidin	E35351		1:500	Invitrogen

Table 01. Antibodies used for WB and immunofluorescent staining.

3.1.2 Compounds & Chemicals for electrophysiology

Compounds	Cat. No.	Working Concentration	Supplier
Kynurenic acid	K3375-5G	1.25mM	Sigma-Aldrich
(+)-MK 801 maleate	0924	10 µM	Tocris
Picrotoxin	1128	100 µM	Tocris
Amphotericin B	A4888	10-40µg/µl	Sigma-Aldrich
Rhodamine-Dextrane 3000MW	D3308	0,02%	Invitrogen
TTX	1069	1 µM	Tocris
Riluzole hydrochloride	0768	10 µM	Tocris

Table 02. Compounds & Chemicals used for the patch clamp experiment

3.1.3 Buffers and reagents for Mass Spect proteinomics

Buffers and reagents	
STET Lysis buffer	50 mM Tris, pH 7, 150 mM NaCl, 2 mM EDTA, 1%(v/v) Triton X-100 + 1:500 Protease Inhibitor (Roche)
ABC 50mM	3.95 mg/mL in LC-MS grade water
DTT 200mM (-20°C)	Dilute frozen 1M DTT stock with 50mM ABC (1:5 dilution)
IAA (iodoacetamide)	73.98 mg/mL in 50mM ABC (final conc.400mM)
Acetonitrile (ACN)	100%
Ethanol 80%	Mix with LC-MS grade Ethanol with LC-MS grade water
LysC 0.03 µg/µl	Dilute frozen 0.5 µg/µl aliquots with 50 mM ABC (For 100 µl: 6 µl in 94 µl ABC)
Trypsin 0.03 µg/µl	Dilute frozen 0.5 µg/µl aliquots with 50 mM ABC
formic acid (FA)	Use 0.1% FA for wash and beads elution
SeraMag Beads A und B	Sera-Mag SpeedBeads A: (Fisher Scientific; CAT No. 09-981-121, Magnetic Carboxylate Modified)
	Sera-Mag SpeedBeads B: (Fisher Scientific; CAT No. 09-981-123, Magnetic Carboxylate Modified)
	Capacity ~100 µg of protein per µg of beads
	Best use > 0.1 µg/µL in the protocol as it is beneficial

Table 03. Buffers and reagents for Mass Spect proteinomics.

3.1.4 Primers for genotype

Gene	Primer Name	Sequence 5' to 3'
Fmr1	Forward Primer	CCAACAAACCTGCCACAAAAG
	Reverse Primer	GCACACATTTGCCGTAAGTCTT

Table 04. Primers for genotype

3.2 Animal-related methods

EU Council Directive 2010/63/EU, National Research Council's Guide for the Care and Use of Laboratory Animals, and the local institutional committee's requirements were followed for all animal operations. All the experiments were conducted in accordance with local regulations.

3.2.1 Animal breeding and genotyping

For this study, we utilized C57BL/6J or *Fmr1* knock-out mice (B6.129P2-*Fmr1*tm1Cgr/J, Stock No.: 003025) bought from the Jackson Laboratory are housed in ordinary circumstances and have access to food and drink at all times. Adult (~PN100) C57BL/6J, and *Fmr1* knock-out female mice are bred at DZNE Standort München. The *Fmr1* knock-out female is back-crossed with C57BL/6J males, leading to 50% *Fmr1* heterozygous females and 50% knock-out males. In order to get rid of the gender-based bias, only female mice are used for the whole project.

For the genotyping, the mouse-ear sample was alkalized into lysis in 50 µl 50 mM NaOH, boiled at 95°C for 30 minutes, then neutralized with 50 µl 1.5 M Tris pH 8.8 and vortex until the tissue was dissolved. Primers used for genotype are listed in above. The sample can go through the PCR then: initial incubation at 5 min at 94 °C was followed by a touchdown 10 cycles of 30 sec from 65 °C to 60 °C at -

0.5°C steps and continued by normal 28 cycles of 30 sec at 60 °C with elongation at 72°C for 7 minutes. Gel running was performed on a 2% agarose gel at 130 V for 30 minutes, and images were captured in the gel imager (BIO-RAD, Gel Doc XR+ System, Germany).

3.2.2 Animal surgery

Adenoassociated virus (AAVs) that expresses α-Syn or GFP was stereotaxically injected into the specific brain region to mimic their overexpression. Premade AAV5-α-Syn and AAV5-GFP viruses used for this project are described in our previous publication(Tan *et al.* 2020). Young mice (~PN21) were anesthetized with 1.4% Ketamine and 0.12% Xylazine intraperitoneally. The mouse head clamped by two ear bars in between was fixed firmly on a stereotaxic plate (Stoelting), then gave eye ointment and disinfected the surgical areas with a 75% alcohol-dipped swab. Make a skull-midline incision by scalpel in front of the ear about 1 cm in length. After the retractor has exposed the field of view, use a coordinate ruler to measure the bregma and lambda to confirm that the head is horizontal. Simultaneously pinpointed the SNc region on both sides of the mouse, the coordinates of which relative to the bregma are: anterior -3.16 mm, lateral ±1.50 mm, ventral -4.50 mm. 2-mm wide burr hole was drilled by a cranial driller on either side to make an approach for a 33-gauge needle on a Hamilton syringe containing 2 x 10^{12} viral particles of AAV5-α-Syn, AAV5-GFP in 2 μl PBS. The virus injection was done at a rate of 0.2 μl/min to the SNc region, and an additional 5 min for the needle to stay to get rid of the hemorrhage until retracting. Subsequent to the surgery, the mouse was kept at 35°C in the incubator to restore normal body temperature. Once it had been awakened from anesthesia, the mouse was returned to the cage, where it would be kept along and given ad libitum access to food and water until being sacrificed for e-phys recordings.

3.3 Electrophysiology

3.3.1 Perforated patch clamp

SN DA neurons were identified according to their e-phys fingerprints, such as regular slow-firing (0.5-3Hz), broad action potential (AP) duration (>2ms), dominant sag component represented as the slow Ih-current, and further confirmed by TH-immunostaining in retrospect. Neurobiotin-streptavidin tracing was combined with TH-immunohistochemistry to label every neuron that had been recorded. Only TH-positive and neurobiotin-marked DA neurons in the SNc region were analyzed in this study.

Normal artificial cerebrospinal fluid (aCSF) is used for brain slice recovery, incubation and recording. The recipe (in mM) is 125 NaCl, 2.5 KCl, 2 MgCl2, 2 CaCl2, 1.2 NaH2PO4, 10 HEPES, 21 NaHCO3, 5 glucose adjusted to pH 7.2 with 2.5M NaOH, resulting in an osmolarity of ~310 mOsm. Glycerol-based artificial cerebrospinal fluid (GACSF) prepared by replacing the 125mM NaCl with 250mM Glycerol is used for brain dissection and slicing. Mouse (~PN100) was anesthetized with isoflurane and subsequently decapitated. Quickly took out the brain and trimmed the frontal lobe and cerebellum within one minute to achieve a block of tissue containing the mesencephalon. SNc-containing coronal sections (270 μm) were obtained under ice-cold (0-4°C), carbonized (95% O2 and 5% CO2) GACSF using a vibratome (VT 1200S, Leica). The slices were then transposed into the normal aCSF and kept for 30 min at 35°C in a water bath for initial recovery. The slices were stored at room temperature (24°C) for at least 45 min before recording and only be used later for up to 8 hours. The slice was transferred to a recording chamber (~2 ml volume), fastened by a net anchor and continuously superfused with carbogenated aCSF at a flow rate of ~4 ml/min. The whole recording was carried out at 30~31°C. Recordings and electroporation were performed with an EPC10 amplifier (HEKA) controlled by the software PatchMaster (version 2.32; HEKA). In parallel, the data were sampled at 40 kHz with a four-pole Bessel filter

at 2 kHz. The liquid junction potential (LJP) of 14.8mV was calculated with a Patcher's Power Tools plug-in for Igor Pro 6 (version 6.37, Wavemetrics) and compensated in PatchMaster.

For perforated patch clamp, intracellular solution devoid of ATP and GTP containing (in mM): 128 Kgluconate, 10 KCl, 10 HEPES, 0.1 EGTA, 2 MgCl2 and adjusted to pH 7.3 with KOH resulting in osmolarity of ~300 mOsm was prepared. Fire polished borosilicate capillaries (GB150-8P, Science Products) were used to make recording electrodes with tip resistances ranging from 3 to 6 MΩ, pulled by a vertical pipette puller (PC-10, Narishige). Amphotericin B powder (A4888, Sigma-Aldrich) was aliquoted into 1-2mg. On the day of the experiment, one aliquot was dissolved into 25µl dimethyl sulfoxide (DMSO) per milligram with sonication; then, 5 µl was added to the 1ml intracellular solution to make a final concentration at around 0.2µg/µl. Tetramethylrhodamine-Dextrane 3000MW (D3308, Invitrogen) or Neurobiotin Tracer (SP-1120, VECTOR) were added into 1ml intra-solution as well to fulfill 0.02% and 0.2%, respectively. The patch pipette was tip-filled with the pure intern solution and back-filled with amphotericin B, Rhodamine-Dextrane or neurobiotin-containing intracellular solution. Once obtain a Giga-seal (>1.5GΩ) configuration when approaches the neuron, quickly compensate electrode capacitance through the "C-Fast" function in PatchMaster and wait around 10-20 minutes until it forms a "stable perforated condition" for recording. The stable perforated condition is defined by a lower access resistance (Ra) around 30-45 MΩ, stable AP amplitude above 20mV without significant change, and a regular firing rate (0.5-3Hz). The experiments will be discarded if the whole-cell configuration is formed by several signs: A abrupt drop of Ra instead of a mild descending, Ra less than 30MΩ, and a diffusion of Rhodamine-Dextrane into the neuron monitored by a fluorescent microscope. To block glutamatergic and GABAergic synaptic input, the aCSF for recording in the bath contained 1.25mM Kynurenic Acid (K3375, Sigma-Aldrich), 10µM (+)-MK801 (0924, Tocris), and 100µM Picrotoxin (P1675, Sigma-Aldrich). All the other protocols are running in the current clamp except for the firing recordings. The amplifier bridge circuit,

thereafter, was adjusted to compensate for electrode resistance and monitored continuously throughout the experiment.

The following compounds were used to modulate the spontaneous firing: TTX, Dopamine, Quinpirole and Riluzole were all diluted in aCSF. Sulpiride was diluted in DMSO. 1μM TTX in aCSF was perfused for the 30s during the recording to induce subthreshold oscillation, followed by a 5min washout with normal aCSF. Riluzole (10μM) was applied directly in aCSF during the whole incubation.

After recordings, the electroporation protocol (100mV step square wave at 2Hz) was run for 10 min to inject the Neurobiotin. The slices post-record was fixed in 4% paraformaldehyde (PFA) for a short time (20 minutes) and stored in PBS at 4°C until further immunofluorescence workflow.

3.3.2 Whole-cell voltage-clamp recordings

The procedures of whole-cell voltage-clamp recordings are almost the same as the perforated current clamp. The experiment was mainly performed in younger mice (~PN30) with viruses injected. aCSF contained (in mM): 125 NaCl, 25 NaHCO3, 2.5 KCl, 1.25 NaH2PO4, 2 CaCl2, 1 MgCl2 and 25 glucose and was gassed with carbogen to keep the pH at 7.4 and osmolarity at 300-310 mOsm/Kg. Half of the NaCl was replaced with 75mM sucrose to prepare sucrose-base aCSF for slice preparation. The internal solution contains in mM: 125 K-methylsulfate, 10 KCl, 10 Phosphocreatine-Na2, 10 HEPES, 2 MgCl2, 0.025 EGTA, 4 ATP-Mg2, 0.3 GTP-Na3, 0.2% neurobiotin tracer; pH was adjusted to 7.2 with KOH, osmolarity was 280-290 mOsm/Kg. The recording was performed without cell capacitance and serial resistance neutralization at room temperature. Neurons were passively filled with neurobiotin during the recording, so the electroporation procedure was omitted.

In order to isolate the A-type potassium current, two steps of voltage depolarization were applied (Routh, Johnston, and Brager 2013). In the first step, the neuron was

depolarized from -100mV to 50mV for 2 seconds, and the current response was recorded. For the second step, the same neuron was clamped at -30mV for at least 30s to completely inactivate the transient voltage-dependent potassium channels and depolarized to the 50mV for 2 seconds again to acquire the current trace without a fast A-type component. Finally, subtracting the trace from the second step with the first one, the fast A-type K outward current is then isolated. 500nM TTX was always applied in the bath during the recording to make the outward current more evident.

3.4   Protein biochemistry

3.4.1 Immunostaining and histological analysis

Immunostaining is a prerequisite for the 270μm thick slices after patch clamp to retrospect the recorded neurons. The main workflow follows a published protocol (Karadottir and Attwell 2006). Briefly, the post-fixation slices were washed in PBS for 15 min with shaking (300 rpm, microplate shaker, VWR) 3 times, then incubated in the blocking solution (5% normal donkey serum, 2% BSA and 0.5% Triton X-100) for 6-8 hours at room temperature (RT). The primary antibodies were present in the same blocking solution and applied overnight at RT. Thereafter, washed the slices with PBS for 15 min 3 times and incubated with secondary antibodies for 6 hours. Afterward, washed the slices another 3 times in PBS and treated with DAPI in the last wash. Finally, sections were mounted on glass slides, and the coverslip was fixed with a fluorescence mounting medium (ROTI®Mount FluorCare) for confocal imaging.

Primary antibodies for the thick slices include Rabbit anti-pS6 (Ser244/247) 1:250, Sheep anti-TH 1:1500, Mouse anti-FMRP 5C2 1:200. Secondary antibodies include Donkey anti-rabbit 488 1:500, Donkey anti-sheep 555 1:500, Donkey anti-mouse 594 1:500, and Streptavidin 647 1:500.

For immunofluorescence (IF) of mouse brain tissue, the animals were anaesthetized with isoflurane inhalation, then sedated with a mixture of Ketamine and Xylazine, and transcardially perfused with 50ml PBS and 50ml 4% PFA. The brains were promptly removed and submerged in 4% PFA for 24 hours at 4°C, followed by another 72 hours in 30% sucrose at 4°C until it sank to the bottom. The postfixed brains were directly frozen at -80°C, coronal slices containing SNc and striatum regions were cut at a thickness of 25μm using a cryotome (Thermo Fisher CryoStar NX70), and the free-floating sections were transferred to cryoprotectant containing: 30% Ethylene glycol, 30% Glycerol, 0.002% sodium azide, in 0.1 M PB (pH 7.35) for future applications. Before staining, slices were washed three times in PBS, followed by an antigen retrieval procedure, which was performed by boiling the slides attached with sections in sodium citrate buffer (10 mM Sodium citrate, 0.05% Tween 20, pH 6.0) for 20 min at 98°C. The staining steps are mostly the same as the thick slices with some minor differences: 1. Thin slices staining was performed on a glass slide instead of free-float; 2. The slices were incubated in the primary antibody at 4°C; 3. the blocking and secondary antibody incubation time was shortened to 1 hour; The slices were finally mounted in the medium with DAPI for subsequent scanning.

Primary antibodies used for the thin slices include all the mentioned primary antibodies plus Rat anti-DaT 1:200, Rat anti-DR1 1:250, and Rabbit anti-DR2 1:100. All mentioned secondary antibodies plus Donkey anti-sheep 568 1:500, and Donkey anti-rat 647 1:500 were included.

All images were captured using a Leica SP5 confocal microscope. For thick slices, fluorochromes were excited at 405nm, 488nm, 555nm, 594nm, and 647nm for DAPI, pS-6, TH, FMRP and neurobiotin, respectively. For thin SNc slices, there is no neurobiotin channel that can make the TH channel move to 568nm and FMRP to 647nm to decrease signal crossing. DaT or DR1 occupy 488nm, and TH and DR2 take 568nm and 647, respectively, in striatum slices. Parameters are set to avoid signal saturation and keep confocal settings identical for all analyzed

neurons/animals. Analysis always uses the open-source image analysis platform FIJI (http://fiji.sc/Fiji). Regions of interest (ROI) of TH-positive neurons in SNc were selected manually according to the TH channel. Neurons are grouped into FMRP positive or negative based on the FMRP channel. Only neurobiotin-positive neurons will pick up for the e-phys analysis in thick slices.

3.4.2 Western blot

Striatum tissue was collected from 2 mm thick fresh brain slices. After anesthesia, the brain was quickly taken out and held in stainless steel brain matrices (RBMS-200C, Kent Scientific corporation) in ice-cold PBS; 2 mm fresh brain slice were cut, and the dorsal striatum tissue was punctured out from the slices. All operations were carried out on ice or in ice-cold PBS in case of protein degradation.

300ul of STET Lysis buffer (50 mM Tris, pH 7, 150 mM NaCl, 2 mM EDTA, 1% Triton X-100, 1:500 Protease Inhibitor) was added per 10mg of dorsal striatum tissue in Precellys Tubes with Glasbeads, then homogenized using precellys evolution homogenizer (P000671-CLYS2-A.0, Bertin instrument) with 6500 rpm in 2*30s cycles. After homogenizing, the cell lysates were aggitated for 30 minutes on the ice and centrifuge at a speed of 16,000 rcf for 15 minutes. The supernatants were obtained for the following experiments.

Protein concentration was determined by Pierce™ BCA Protein Assay Kit (Thermo Fisher Scientific) according to the manufacturer's instructions.

Laemmli buffer was added to the samples according to the calculated concentration. After that, samples were denatured by heating at 95℃ for 5 minutes, and 15µl samples were loaded into AnykD™ Criterion™ TGX™ precast gels (Bio-Rad Laboratories). Gels were ran at constant voltage with Tris-glycine running buffer and transferred onto polyvinylidene difluoride (PVDF) membranes which have been activated with methanol. Membranes were blocked in 5 % skimmed milk in

Tris-buffered saline with 0.1% Tween20 for 30 minutes at room temperature and incubated at 4°C overnight under gentle shaking with primary antibody (diluted in 5% skimmed milk or 5% BSA, according to each antibody datasheet recommendations). The membranes were washed and incubated with respective secondary antibodies in 5% milk for 1 hour at room temperature. Clarity™ Western ECL Substrate Kit or SuperSignal ™ West Femto Maximum Sensitivity Substrate were used to detect signals. Band intensities were quantified by Image Studio™ software (LI-COR Biosciences) and were normalized to the housekeeping protein Tubulin.

3.4.3 Mass Spectrometry

We combined 20µl of SeraMag A and 20µl of SeraMag B beads and washed them three times with 200µl of LC-MS grade water; we stored the beads in 100µl of water in the fridge (4 µg/µL beads) for subsequent procedures.

We added 2.5µl DTT (200mM) to the 30µl protein sample followed by the protein preparation procedures mentioned above, vortexed and centrifugate the samples shortly, and incubated them for 30 min at 45°C (Thermomixer 1200rpm) during the reduction. Then, 5µl IAA (400mM) were added and the samples incubated for another 30 min at 24°C in the dark for alkylation. After that, 2.5 µl DTT (200 mM) was added to quench the reaction and form a total 40 µl volume of sample. 10µl clean beads were added (~40 µg) to 50 µL, vortexed vigorously and ACN 100% added to a final concentration of 70% (v/v) ACN and mixed immediately; thereafter, the samples were incubated for 30min at RT, spun down and placed in the magnetic rack for 2 min. The supernatant was discarded. The beads were washed with 200µl ethanol 80% followed by vortexing them for 30s four times. After the wash, the protein were removed from the beads by adding 10 µl of Trypsin (0.03 µg/µl) after treating the beads with 10µl of LysC (0.03 µg/µl) , then spun down and incubated overnight (16h) at room temperature.

On the second day, the beads were centrifuged for 1 min at 16,000g, the tubes placed on a magnetic rack to attache them to the wall for 2 minutes to thoroughly remove the beads, transfered the remains to Costar Spin-X 0.22µm filter, which is washed with 200 µL of 0.1% FA before ahead. At the same time, we performed elution on the beads with 20µl of 0.1% FA, sonicated the beads for 2 x 30 s in the water bath, and put the beads tube in a magnetic rack for 2 min and transfer the supernatant to the same sample collection tube. Add 2 µL of 8% FA to the Costar Spin-X 0.22 µm filters to acidify the sample, then spin 2 min at 2,000 g. The flow then goes through SpeedVac Vacuum Concentrators (SPD120, Thermofisher) to condense the dry peptides, finally resuspending the pellet in 18 µl 0.1% FA for further overall peptides concentration measurement by Qubit analysis (Qubit 4 Fluorometer, ThermoFisher).

The LC-MS/MS workflows are deployed by timsTOF Pro (Bruker), and samples are loaded on the machine. After two days of running, raw timsTOF data is transformed to mzBIN format and analyzed with MSFragger to identify peptides. FDR-filtered reports are generated at the PSM, peptide ion, peptide, and protein levels, using Philosopher (PeptideProphet, ProteinProphet, FDR estimate). MaxQuant software is used for inspection of raw data and identification and quantification results. Perseus framework is used for results visualization and export.

3.5 Statistical analysis

Data analysis and graphical illustrations were performed using PatchMaster software (v2x90.2, HEKA Electronics), AxoGraph X Office (versio1.7.6, @John Clements), MATLAB R2020a (MathWorks), Anaconda 3 (Anaconda Inc.), GraphPad Prism 9 (GraphPad Software, Inc.), Adobe Illustrator CC2021 (Adobe Systems Software), and Fiji (https://imagej.net/Fiji) software.

Perforated patch clamp data were mainly analyzed by MATLAB and python scripts. https://github.com/gaopan64/HEKA_PatchMaster_DataAnalysis is the open-source repository where the scripts are stored.

GraphPad Prism 9 was used to run statistical tests for statistically significant differences, as stated in the text. If the data were regularly distributed, parametric statistical tests were used. The D'Agostino-Pearson omnibus normality test was used to verify the normal distribution. There were no paired tests utilized unless otherwise noted. There are four levels of statistical significance: *, **, ***, and ****. In graphs, data are presented as mean, standard deviation (SD) or standard error of measurement (SEEM). Even if the data were regularly distributed, more cautious non-parametric tests were used in studies with low sample numbers.

4. Results

4.1 α-Synuclein overexpression in SNc DA neurons

Our previous work has demonstrated that α-Syn overexpression decreases the FMRP abundance in SNc DA neurons. By using LUHMES cells, we found many electrophysiological changes like the AP duration and N-type calcium currents that may be modulated by FMRP (Tan *et al.* 2020). However, data from mouse brain slices ex vivo were missing. Therefore, we established an α-Syn overexpression model in acute brain slices for electrophysiology recordings. Within the scope of additional unpublished experiments, we first established patch clamp electrophysiological recordings from SNc DA neurons in acute mouse brain slices. We injected the mice (~PN21) with an adenovirus into the SNc to overexpress human α-Syn or GFP in these neurons as decribed previously (Tan *et al.* 2020). After one week, the animals were sacrificed, their brains were removed, and acute brain slices were prepared for patch clamp recording (***Figure 07.***).
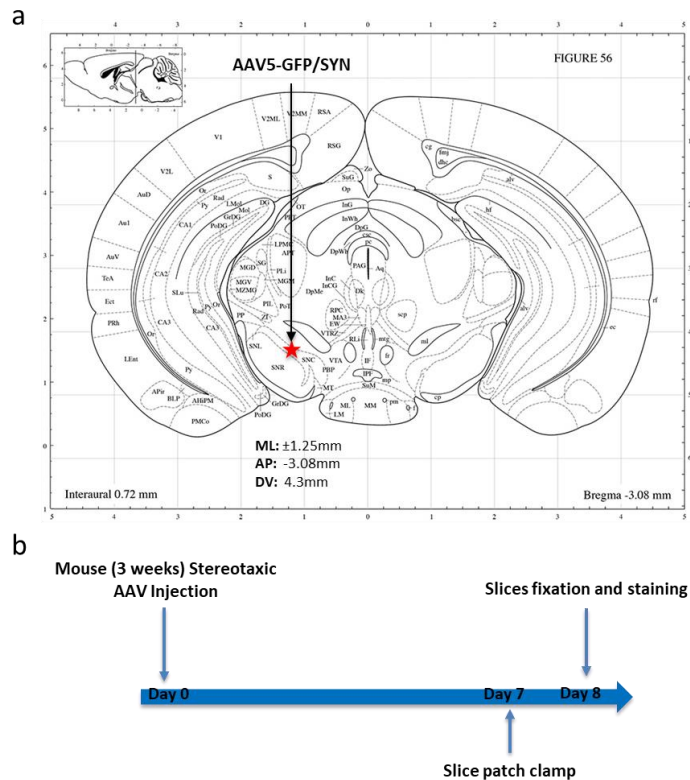
Figure 07. Schematic diagram for the experiment. *a) The coordinate of mouse brain and the precise position of the substantia nigra pars compacta into where is AAV injected. b) The workflow of the experiment.*

4.1.1 Electrophysiological Characteristics of SNc DA Neuron

The first step in this section was to measure the e-phys characteristics of SNc DA neurons from wildtype mice. Two distinct phenotypes of neurons could be found in the SNc area (***Figure 08.***). We found the spontaneous firing of TH-positive neurons not to be stable during the recording, possibly due to a 'run-down effect' (Belles *et al.* 1988); the firing slowed down and was finally dimishied in a very short time, even in the presence of the intracellular solution (ICS) containing Phosphocreatine-Na2 (Graziane and Dong 2016). In such a scenario, the firing spike analysis is almost impossible with the whole-cell mode in DA neurons.

The experiment also identified GABAergic neurons in substantia nigra by their electrophysiology features. Dopamine neurons in the SNc remain susceptible to GABA inputs in coronal brain sections, especially those dominated by GABAergic neurons in the SNr. GABA receptor blockers were added during the whole experiment to eliminate their effect on SNc DA neuron excitability.
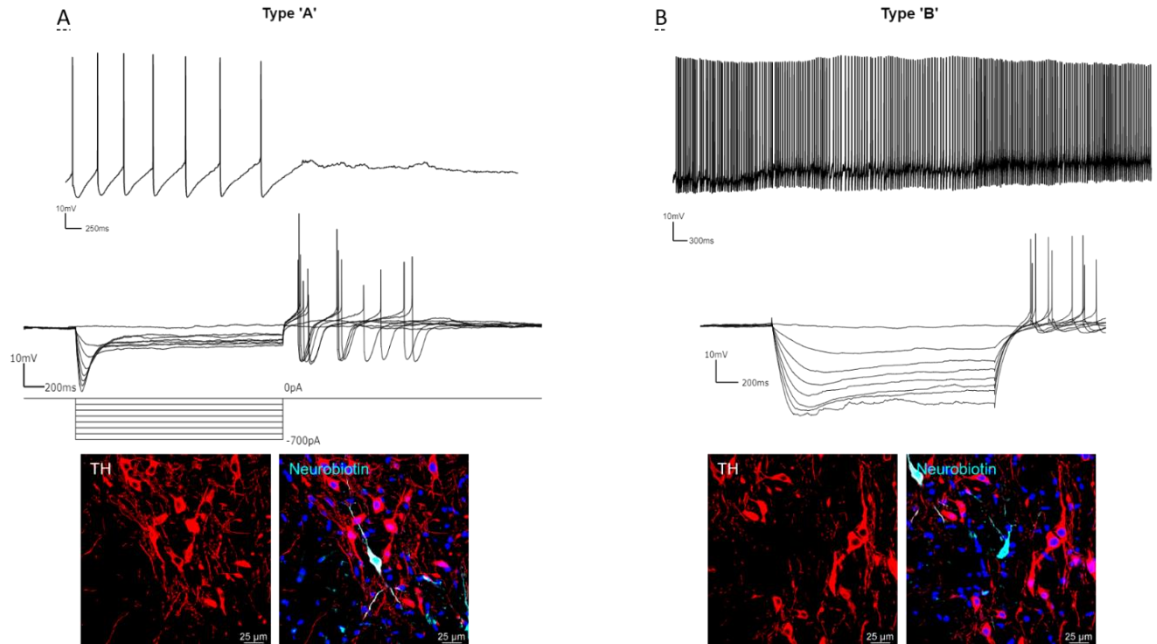
Figure 08. Two distinct phenotypes of neurons could be found in the SNc area. *A). Shows a kind of neuron exhibiting slow-firing (upper panel), and predominant hyperpolarization current (middle). Immunofluorescent staining identified it as TH-positive neurons (bottom). B). Shows another kind of neuron exhibiting a much higher firing rate (upper panel), and no hyperpolarization current (middle panel). Immunofluorescent staining identified it as TH-negative neurons, presumably GABAergic neurons (bottom, Scale Bar = 25µm).*

4.1.2 Unchanged Electrophysiological Properties of the Cell Membrane and HCN Current

We then examined if α-Syn could impose any change on passive membrane properties including membrane resistance and capacitance (Eckert, Paschke, and Hülser 1991; Gentet, Stuart, and Clements 2000) and found no difference for these passive parameters between the GFP and α-Syn AVV injection groups (***Figure 09. b***). That implies α-Syn overexpression doesn't influence the total ion channels' open probability or the membrane area in our model system (Pacheco *et al.* 2015).

We proceeded to examine the HCN current in both groups. Given the challenge of measuring firing spike rate in the whole-cell mode due to the run-down effect, we concentrated on the fundamental channels that contribute to neuron excitability, including the HCN channel. Although the firing of dopamine neurons is mainly stimulated by channels other than HCN, as noted earlier, HCN remains a pacemaker in most neuron types (Herrmann, Schnorr, and Ludwig 2015). The absence of disparity between the two groups indicates that the neurons may display comparable Ih current during hyperpolarization. (***Figure 09. c***).
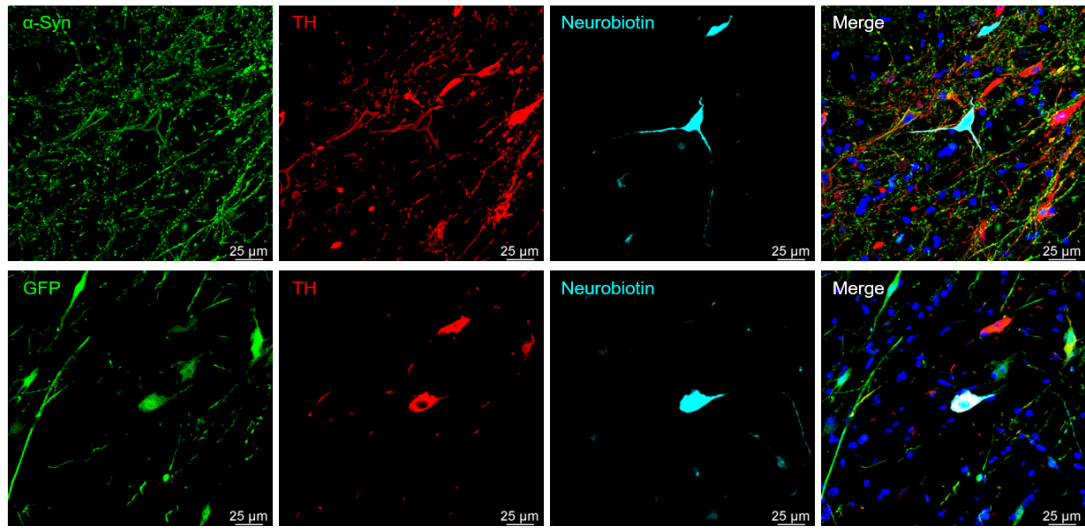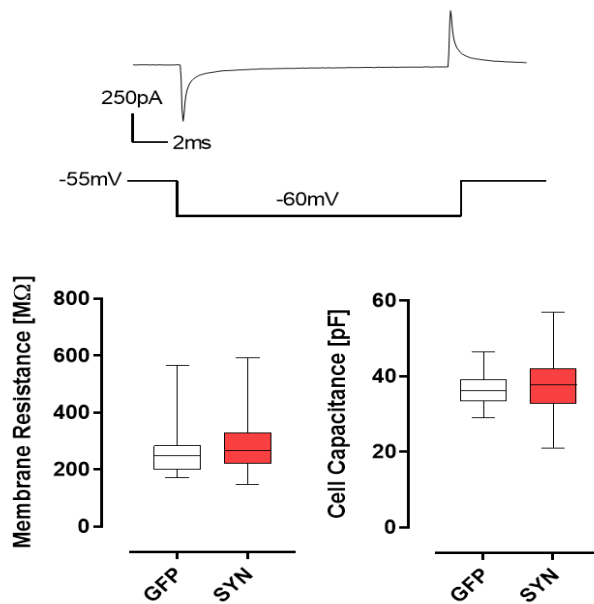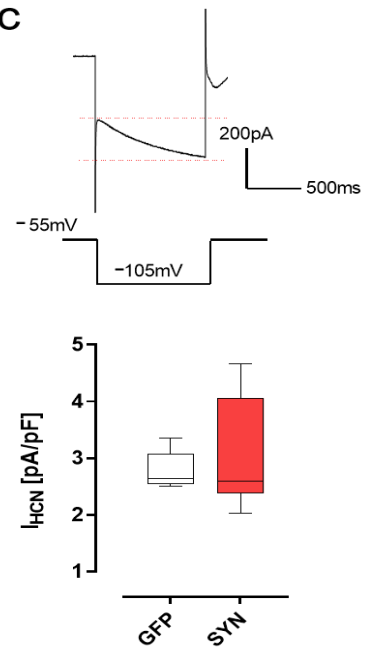
Figure 09. α-Syn overexpression in SNc DA neurons has no effect on passive membrane properties, neuron size and HCN current. *a) After the acute brain slice patch clamp, neurons are marked with neurobiotin and co-stained with GFP/α-Syn and TH antibodies to ensure their identities. Scale Bar =25μm. b) No difference is found in membrane resistance (p=0.5542), cell capacitance (p=0.3859) and , c) HCN current (p=0.6878) between GFP (n=24) and α-Syn overexpression (n=33) groups. For comparison of the means, an unpaired t-test was used; Data are shown as Min & Max with the mean value.*

4.1.3 α-Synuclein overexpression impaired outward current in SNc DA neurons

Induced action potentials (APs) were recorded from DA neurons in brain slices that had been injected with α-Syn or GFP as a control. We observed an increase in AP duration in α-Syn-infected neurons (***Figure 10. a***). Consistent with the regulation of AP shape and duration by FMRP, we identified a reduction in the current density of the A-type potassium current in α-Syn-transduced neurons (***Figure 10. b,c***). Together with our previously published data, these preliminary findings illustrate the establishment of electrophysiological techniques that are necessary to further explore FMRP-associated neuronal excitability in SNc DA neurons ex vivo. They also suggest that overexpression of α-Syn alters DA neuron APs, potentially via FMRP-modulated target genes.
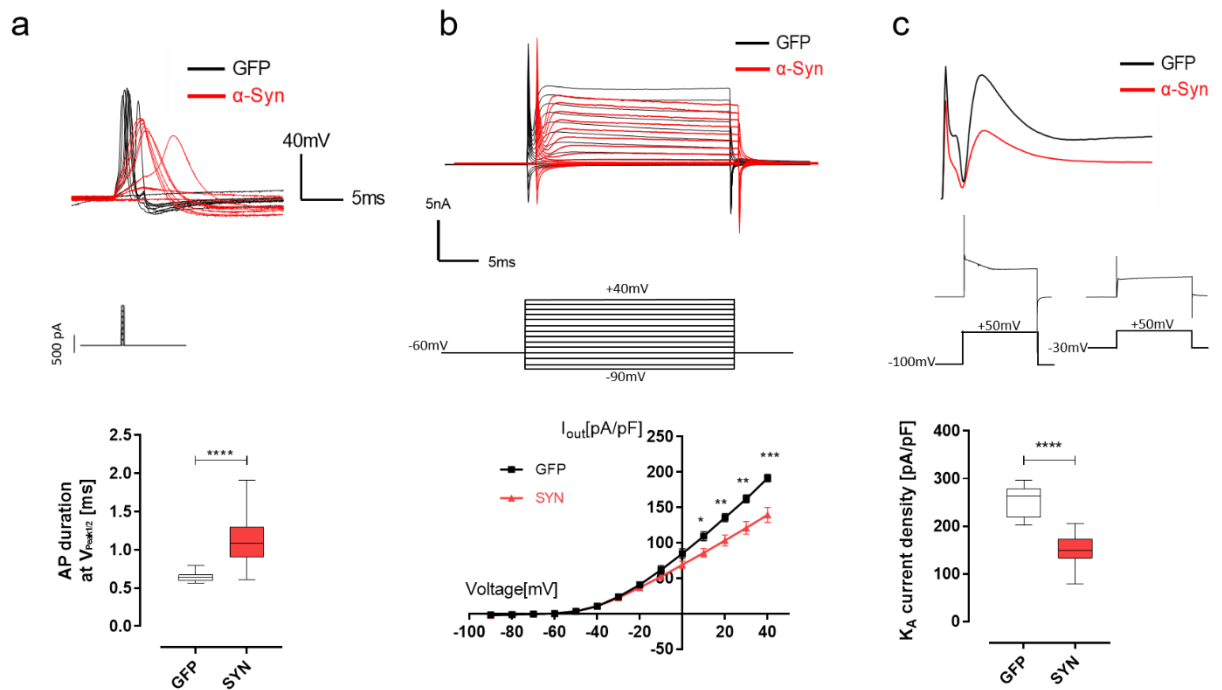
Figure 10. α-Syn overexpression impaired outward current in SNc DA neurons. *Electrophysiological examination of SNc DA neurons from GFP- and α-syn-transfected neurons. Induced action potentials (iAPs) in SNc DA neurons from mouse brain slices transduced with GFP (n=36) or α-syn (n=42) (upper) and the protocol used for induction (middle) and the analyzed results (bottom). a) The AP-duration is significantly increased in α-syn-transduced neurons. b) The overall outward current is decreased in α-syn overexpression neurons compare to the GFP overexpression group at the presence of 1μM TTX. c) Through A-type current subtraction method mention above, A-type outward current in α-syn-transduced cells is also decreased. For comparison of the means, an unpaired t-test was used; **P < 0.01, ***P < 0.001, **** P < 0.0001 . Data are shown as Min & Max with mean value.*

4.2   FMRP and SNc DA neuron excitability

We utilized an α-Syn overexpression model to investigate potential alterations in electrophysiological properties of SNc DA neurons. The observed changes are reminiscent of the modulatory role of FMRP on neuronal excitability. Given that the level of FMRP is already reduced in SNc DA neurons during the early stages of PD, and that the decline in striatal DA levels precedes the death of SNc DA neurons, the release of DA is closely linked to neuronal excitatory impulses. Thus, it is intriguing to explore whether FMRP is involved in the early pathogenesis of PD via its modulation of neuronal excitability, particularly DA release in the striatum. Therefore, we sought to investigate how FMRP influences the excitability of SNc DA neurons as the primary research question for this study, *Fmr1* heterozygous (HET) and knock-out (KO) compared to wild-type (WT) mice were bred, followed by perforated patch clamp and immunofluorescence procedures (***Figure 11.***).

Figure 11. Fmr1 heterozygous (HET) and knock-out (KO) compared to wild-type (WT) mice used for the experiment.
a) Flow chart illustrating the principal design of the experiment. b) Representative picture from a gel electrophoresis illustrating the genotyping results from Fmr1 KO, HET and WT mice. Note the WT allel at 400 bp and the WT allel at 131 bp.
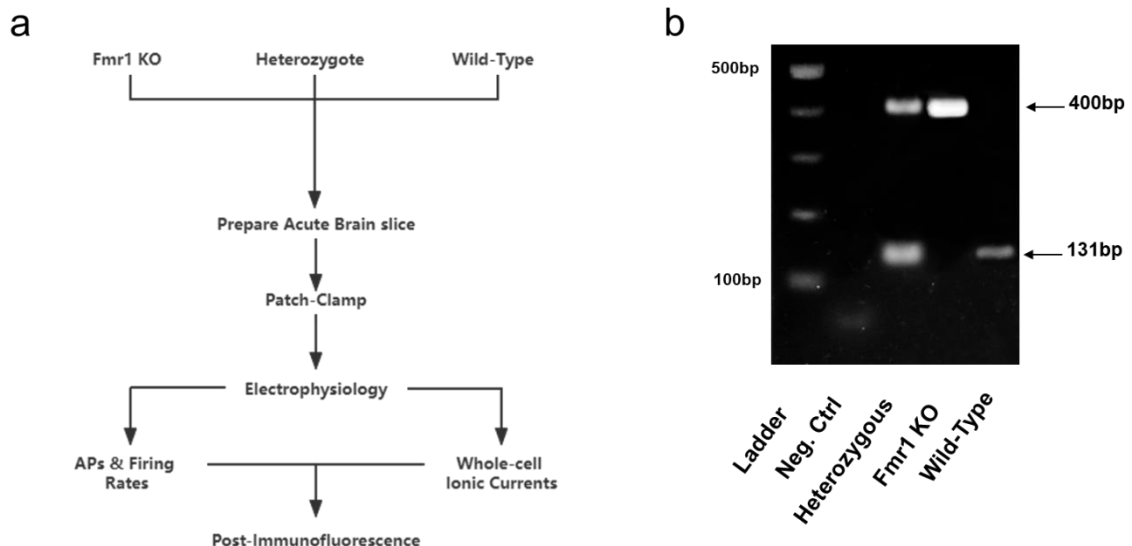
4.2.1 pS6-positive neurons account for a higher ratio in *Fmr1* HET mice

Neuronal excitability can be assessed either by functional assays, such as patch clamp electrophysiology or else, by quantifying the abundance of activity-induced molecules. Among these, phosphorylated ribosomal protein S6 (pS6) is a potent marker for activated neurons, and the phosphorylation is believed to occur sequentially on serine residues (in the order Ser 236,235,240,244, and 247). Notably, phosphorylation at the C-terminus (Ser 244 and 247) is less frequent than at the N-terminus. Therefore, C-terminal phosphorylation of pS6 is considered a reliable marker for highly active neurons with elevated excitability. (Knight *et al.* 2012). In order to investigate the phosphorylation level of pS6 in *Fmr1* mutant mice, we co-stained the pS6 (Ser 244 and 247 phosphorylated) with FMRP and TH. Although SNc DA neurons were highly positive in pS6, there was no significant difference regarding the pS6 intensity or the ratio of pS6-positive and -negative neurons in all three groups (*Figure 12.*). However, we found that the pS6-positive neurons accounted for a higher ratio in FMRP-negative neurons than in FMRP-positive counterpart in *Fmr1* HET mice, and in certain stained brain sections, a clear boundary was observed between pS6-positive cluster and FMRP-positive populations (*Figure 13.*). The *Fmr1* HET mice exhibit a mosaic of FMRP-positive and FMRP-negative phenotypes due to random X-chromosome inactivation (Bland *et al.* 2021), but all four types of neurons (FMRP+/pS6+, FMRP-/pS6+, FMRP+/pS6-, FMRP-/pS6-) are not distributed evenly in SNc region. Typically, FMRP-/pS6+ neurons are the most abundant, followed by FMRP+/pS6+ neurons, and FMRP+/pS6- neurons with double-negative neurons representing a miniscule proportion. The extensive prevalence of pS6+ neurons suggest a high load of physiological activity in SNc DA neurons (*Figure 13.b*).

Our findings indicate that in *Fmr1* HET mice, the absence of FMRP in SNc DA neurons is strongly related to an increased activity. pS6 is ordinarily related to protein translation and FMRP is believed to be a translational suppressor, so FMRP loss results in such an increase in translational activity. Nevertheless, we found no difference in pS6 between WT and *Fmr1* KO groups (*Figure 12.*).

We concluded that the *Fmr1* HET mice could be considered as a potential model to investigate the FMRP effect on SNc DA neurons as they offer an internal control due to the mosaic architechture of FMRP. *Fmr1* KO mice are global knockout, implying potentially widespread changes of the brain's network activity, thus possibly occluding the specificity of physiological phenotypes. In accord, several studies reported FMRP's non-cell-autonomous effect on the functions of neurons in different brain areas (Bland *et al.* 2021; Patel *et al.* 2014; Golovin, Vest, and Broadie 2021). Conversely, FMRP in DA neurons is randomly silenced in *Fmr1* HET mice, thus providing a suitable internal control. Besides that, as per our previous findings, FMRP expression level is decreased in response to α-Syn overexpression but not completely silenced, and heterozygous mice still maintain low-level FMRP expression, which may be theoretically more suited to mimic PD pathology.
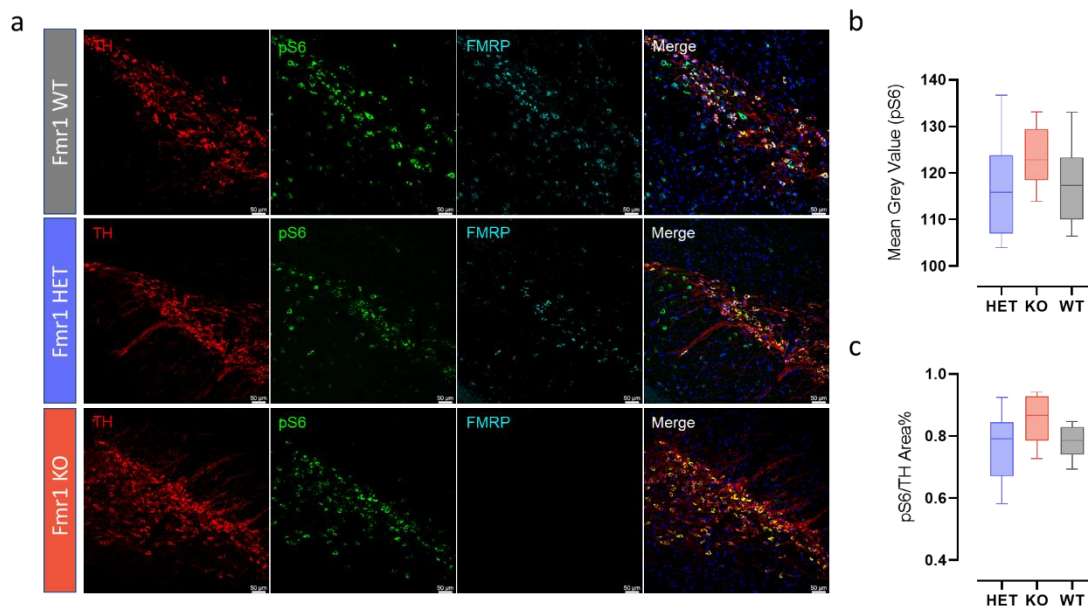
Figure 12. pS6 staining in Fmr1 WT, HET and KO mice. *a) Representative photomicrograph from immuno-fluorescence staining of DA neurons in Fmr1 WT (n=9) , HET (n=9), and KO (n=7) mice brain tissue. Tissue sections were stained with antibodies against TH (red), pS6 (green) and FMRP (cyan) revealing a higher ratio of pS6-positive neurons in SNc region. Scale Bar = 50µm. b) Bar graph illustrating the mean pS6 intensity in all three goups. No significant differences were found between all groups (HET vs. KO, p=0.3843; HET vs. WT, p=0.9908, KO vs. WT, p=0.5380). c) Bar graph illustrating the pS6-positive neurons ratio in all DA neurons marked by TH in the SNc region (HET vs. KO, p=0.1752; HET vs. WT, p=0.9396, KO vs. WT, p=0.3210). For comparison of the means, a one-way ANOVA with Tukey's post hoc test was used. Data are shown as Min & Max with mean value.*
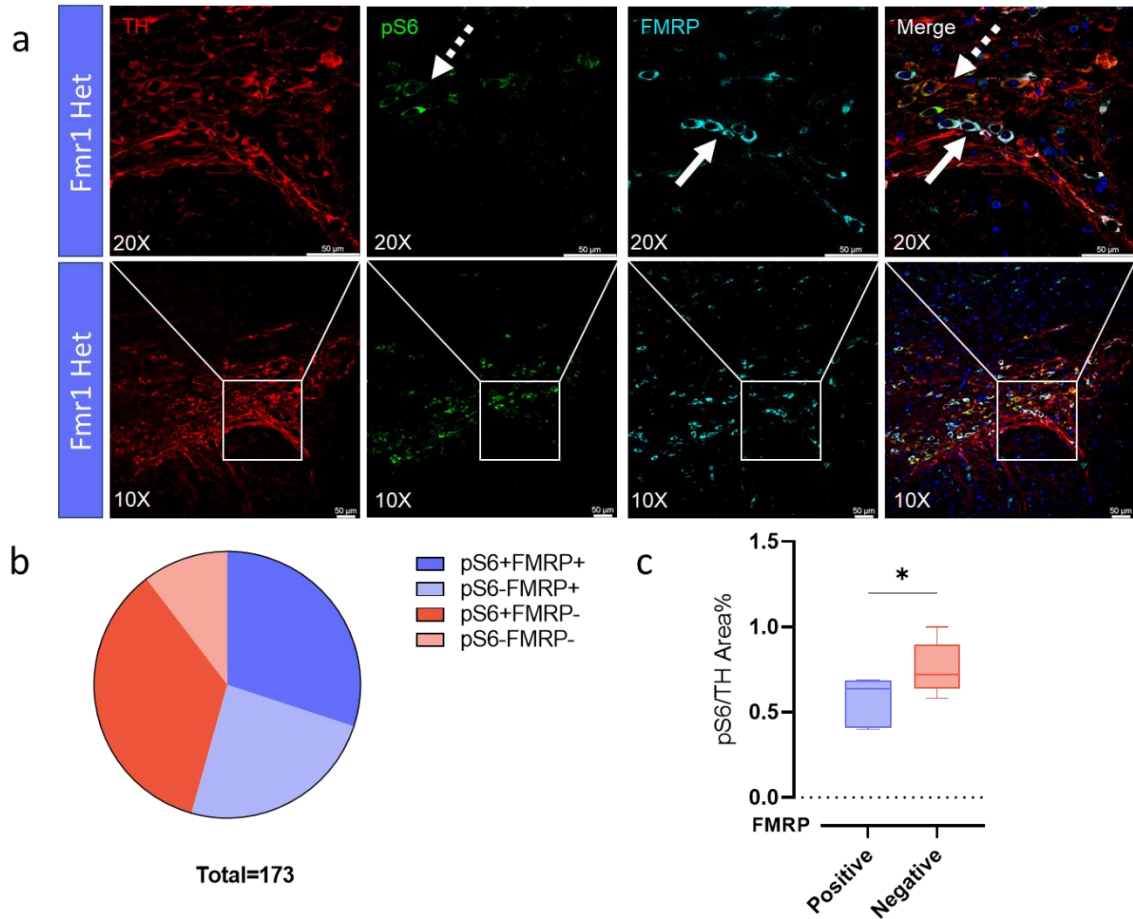
Figure 13. pS6-positive neurons accounted for a higher portion in FMRP negative neurons than in FMRP positive neurons in Fmr1 HET mice. *a) Lower row: Representative photomicrograph from immunohistochemical staining of DA neurons in Fmr1 HET mouse brain tissue, Scale Bar = 50µm. Upper row: high magnification (20X) from the lower row shows clusters of neurons, FMRP+ (Arrow with line) and pS6+ (Arrow with dash) has obvious boundary, Scale Bar = 50µm. b) Venn plot illustrating a distribution of all types of neuron based on the staining result. c) Bar graph illustrating the pS6-positive neurons ratio is higher in FMRP-negative neurons than -positive neurons in SNc slices (n=7) from three Fmr1 HET mice (p=0.02). For comparison of the means, a student t-test was adopted. *P < 0.05; Data is shown as Min & Max with mean value.*

4.2.2 Neuronal excitability is higher in FMRP-negative neurons in *Fmr1* HET mice

We then applied patch clamp recordings to clarify if neuronal excitability is indeed affected in FMRP-negative neurons. Considering that the "run-down effect" is prevalent when recording DA neurons under a whole-cell mode, we resorted to a perforated patch clamp technique to avoid such a potential run-down effect (Lippiat 2008). Of course, the whole-cell mode was still applied after recordings to mark the neurons with neurobiotin by electroporation (*Figure 14.*).

We first recorded spontaneous APs in DA neurons in acute brain slices from *Fmr1* HET mice. The result is consistent with the pS6 staining result in HET mice, since FMRP-negative neurons have a higher firing rate than FMRP-positive neurons (*Figure 15. a,c, and d*). At the same time, after clamping the rest membrane potential (RMP) at -70mV to silence the neurons, FMRP-negative neurons were reactivated with lower rheobase input current (*Figure 15. b,e*).

In order to investigate what currents may contribute to the excitability change, spike analysis was conducted in Matlab (*Figure 16. a*). Therefore, we calculated the derivative of voltage with respect to time (*Figure 16. b*). We defined the threshold as the voltage when it starts to decrease (dv/dt = 50mV/ms), the fast afterhyperpolarization (fAHP) as the voltage at 3ms after the spike peak, the half-width as the AP duration at the membrane voltage halfway between AP threshold and AP peak, and afterhyperpolarization (AHP) as the lowest voltage between spikes mainly induce by SK channel. The result showed that even though both types of neurons exhibit robust firing rate, the half-width, fAHP, and threshold are all decreased in FMRP negative neurons while the peak value, AHP and the slope of threshold has no significant change (*Figure 16. c-h*).
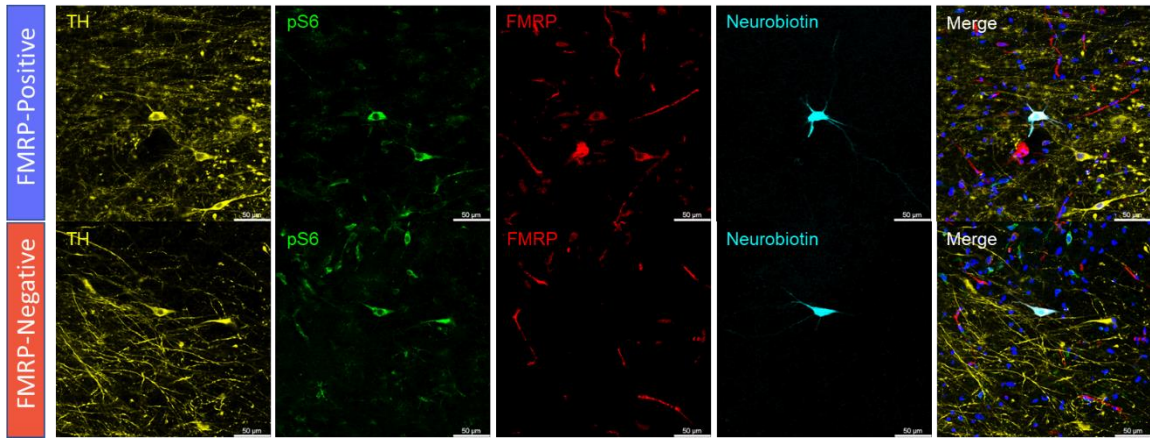
Figure 14. Thick slices of immunofluorescence staining after perforated patch clamp recordings. *Scale Bar = 50 µm*
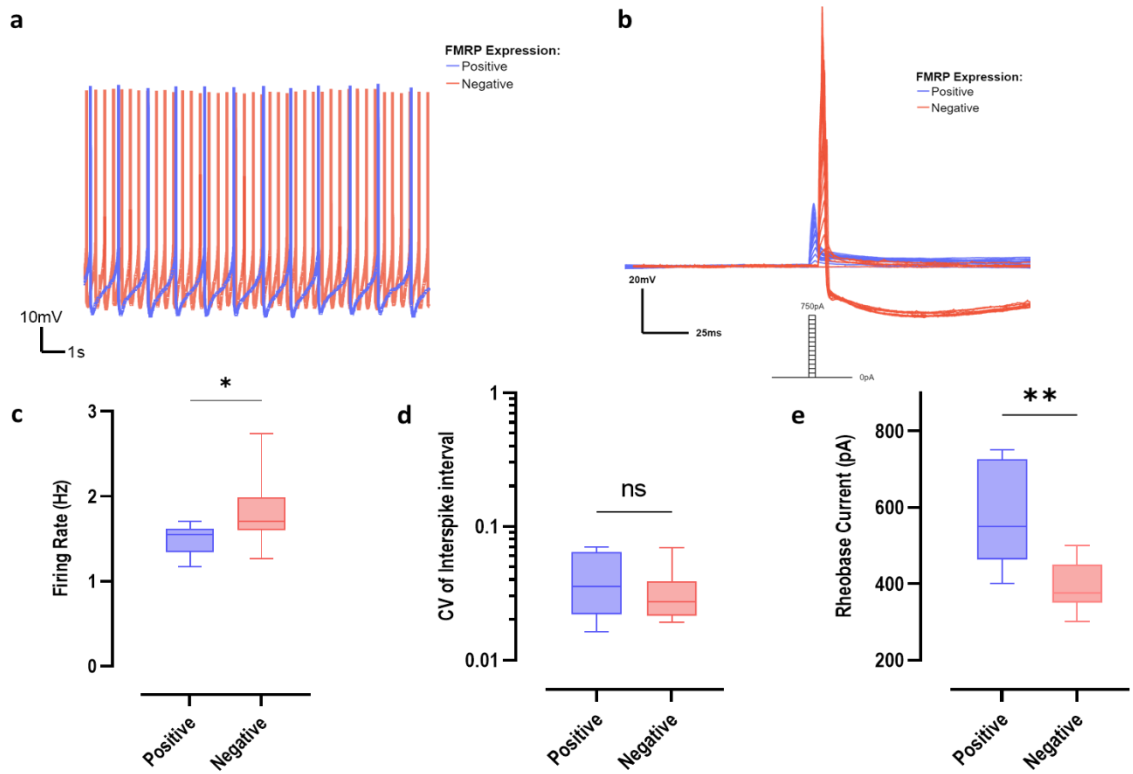
Figure 15.Neuronal excitability is higher in FMRP-negative neurons in Fmr1 HET mice. *a) Recording digraph illustrates higher spontaneous firing frequency in FMRP-negative neurons compare to the FMRP-positive counterpart. b) Recording digraph shows that FMRP-positive neurons are more resistant to the depolarized current steps of input. c) Bar graph demonstrate the significance in firing rate between FMRP-positive (n=10) and -negative (n=13) clusters (p=0.0215). d) Bar graph exhibits the coefficients of variation of interspike intervals between FMRP-positive and - negative clusters (p=0.2709). e) Bar graph shows that the rheobase current is lowered in the FMRP-negative neuron group (p=0.0041). For comparison of the means, a student t-test was adopted. *P< 0.05,**P < 0.01; Data is shown as Min & Max with mean value.*
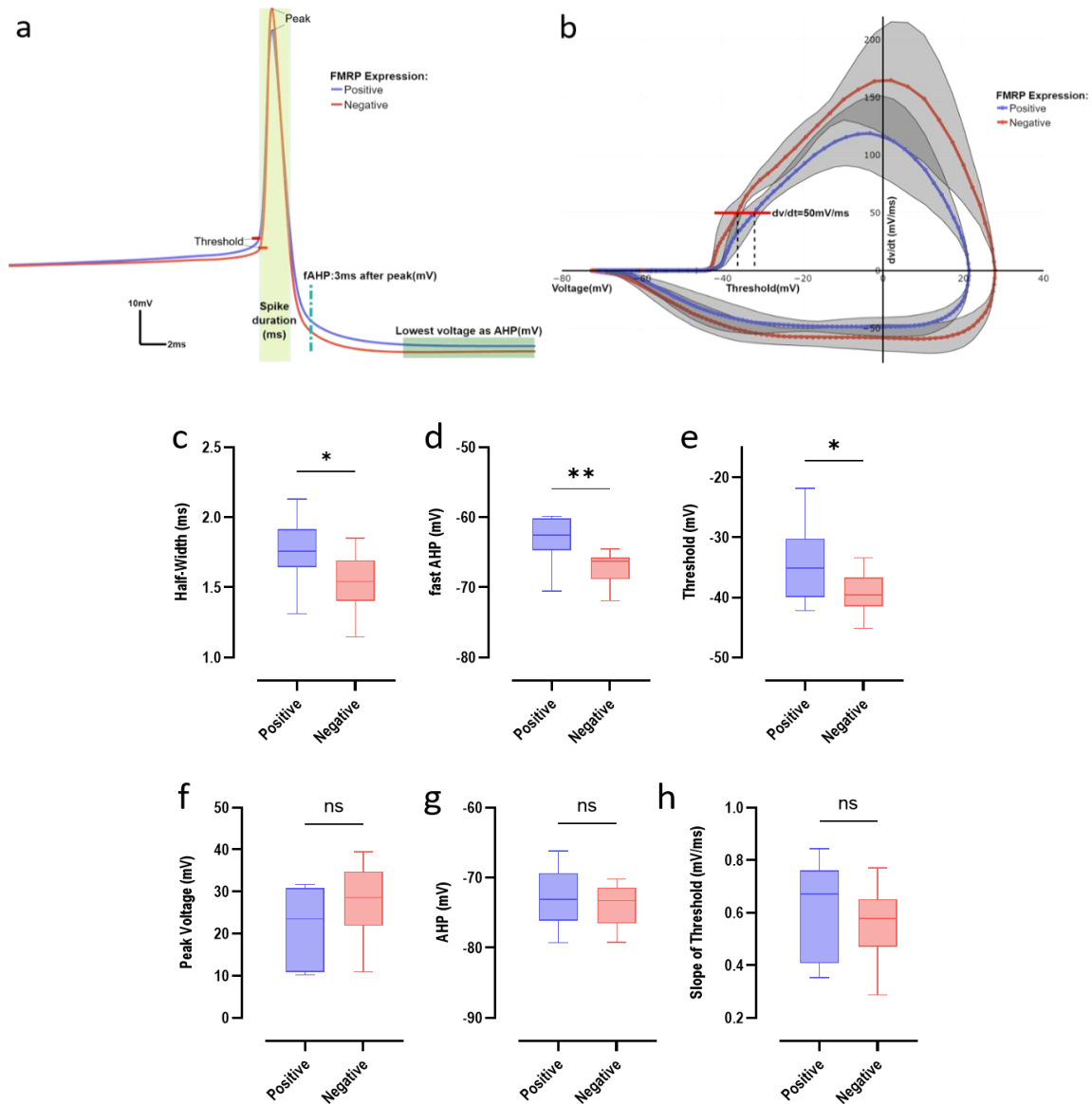
Figure 16. Firing spike analysis results between FMRP-positive and -negative neurons in Fmr1 HET mice. a) Digraph illustrates an averaged firing spike shape from the FMRP-positive and -negative neurons. b) The calculated derivative of voltage with respect to time shows that FMRP-positive and -negative neurons hold a completely distinct spike course. c-d) Bar graph demonstrate the significance in half-width (p=0.0228), fast AHP (p=0.0044), and threshold (p=0.0275) between FMRP positive (n=10) and negative (n=13) neurons. f-g) Bar graph shows no significance in peak amplitude (p=0.0884), AHP (p=0.4274) and slope of threshold (p=0.3682). For comparison of the means, a student t-test was adopted. *P< 0.05,**P < 0.01; Data is shown as Min & Max with mean value.

4.2.3 Increased excitability of FMRP-negative neurons is modulated by persistent sodium current

Next, we quantified the magnitude of distinct ion channel conductances in SNc DA neurons from *Fmr1* KO and HET mice, post-staining verified their FMRP expression level. In fact, there are numerous ion channels that are regulated by FMRP and, at the same time, are known to modulate SNc DA neuron excitability (***Figure 17.***).
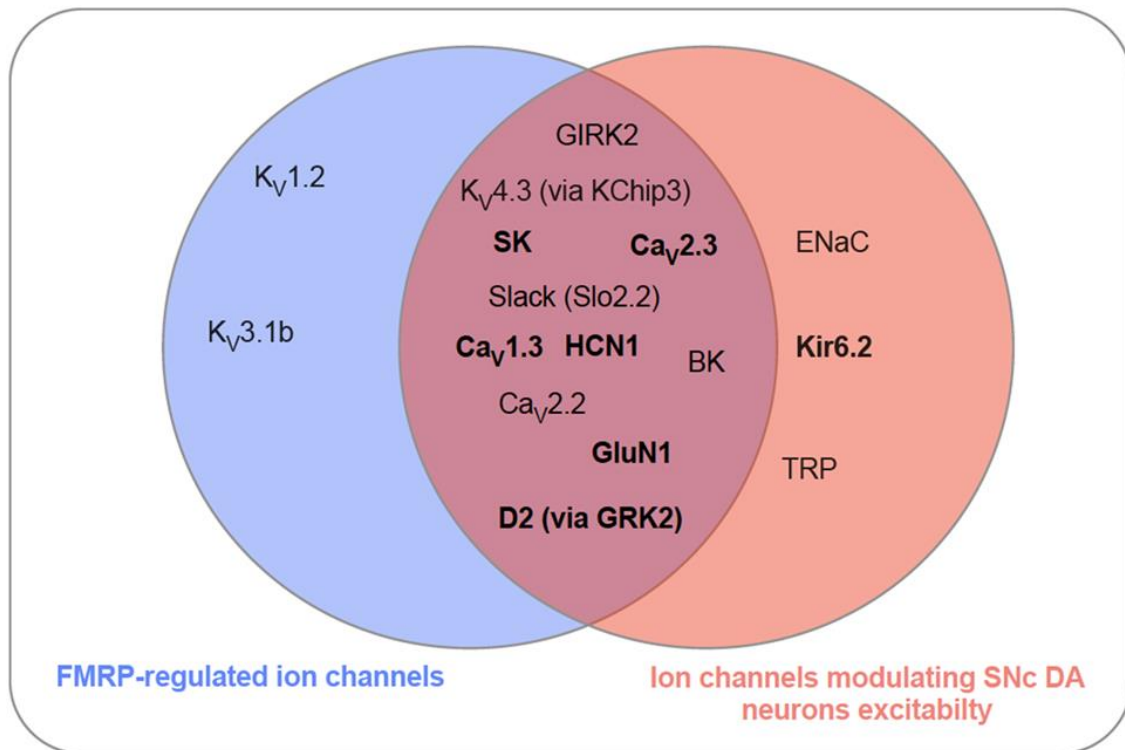
Figure 17. Venn plot illustrating the interplay between FMRP-regulated and PD-associated ion channels in SNc DA neurons.

First, we measured the current driven by the HCN channel. Therefore, neurons were silenced by clamping at -70mV, then incremental steps (-100pA) of current from 0 to -700pA were applied to depolarize the neurons. Sag ratios, the ratio between the steady-state decrease (SSD) in the voltage and the largest falling decrease (LFD) in the voltage, were measured after the hyperpolarizing current step, and rebound delay, the delayed time before the first spike after the hyperpolarizing current, was also included. No significant change was found in the HCN current (***Figure 18.***).
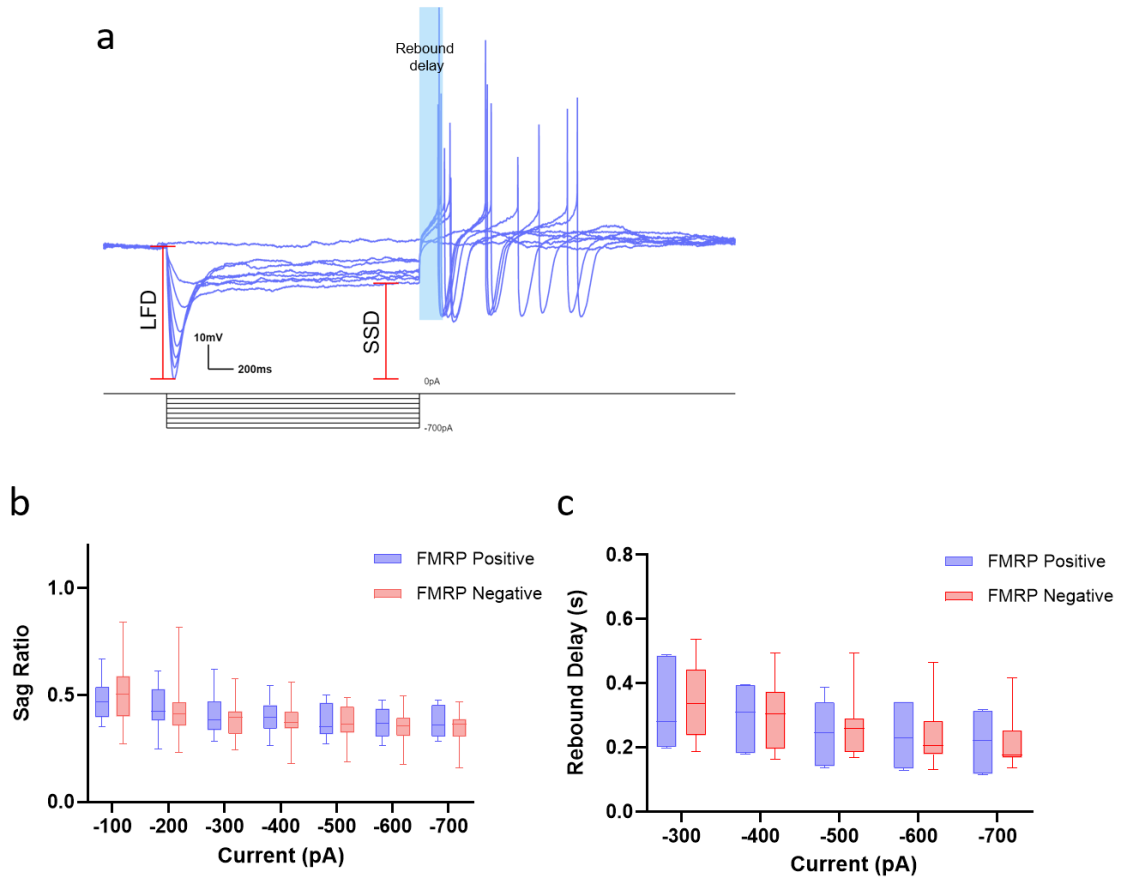
Figure 18. HCN channel condition in FMRP-positive and -negative neurons. *a) Illustration represents the sag ratio and rebound delay after the hyperpolarizing current steps stimulus. b-c) bar plot shows no significant difference was found between FMRP-negative (n=7) and -positive neurons (n=7) in sag ratio and rebound delay. For comparison of the means, ordinary two-way Anova with multiple t-test was adopted. Data are shown as Min & Max with mean value.*

Second, a number of depolarized current stimuli was applied to induce slow afterhyperpolarization (sAHP), which is modulated by the Slack channel (Wilson and Goldberg 2006; Wallen *et al.* 2007; Brown *et al.* 2010). Similar to the HCN channel, we didn't find a difference in the sAHP amplitude, although the increased excitability resulted in a higher number of spikes for FMRP negative neurons (**Figure 19.**).
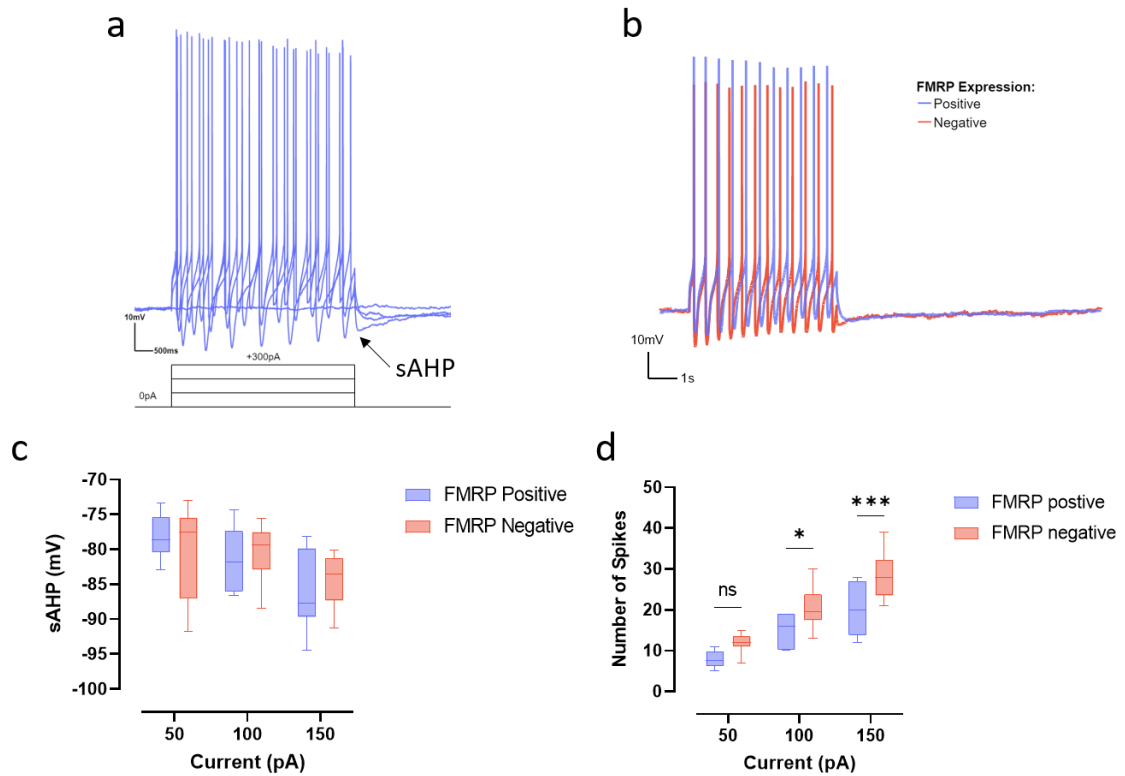
Figure 19. Steps of Depolarized stimulus exerted on DA neurons. *a-b) Representative traces of stimulated firing in response to the depolarized current injection. c) Bar plot shows no significant difference was found between FMRP-negative (n=12) and -positive neurons (n=8) in slow afterhyperpolarization (sAHP). d) Bar plot counting the firing spikes between two groups. FMRP-negative neurons have a higher number of spikes at the same level of stimulation(p=0.0216 with 100pA current, p=0.0003 with 150pA current). For comparison of the means, ordinary two-way Anova with multiple t-test was adopted. Data are shown as Min & Max with the mean value.*

Since spontaneous firing of DA neurons was driven by the basic intrinsic excitability shown as a subthreshold oscillation (STO) as mentioned above, the potent sodium channel blocker TTX (1μM) was perfused to unmask STOs and examine it in FMRP-negative and -positive neurons. To our surprise, the STO activity in both groups was similar during the perfusion, and the firing rate of each group could partially be recovered by washing out the TTX (***Figure 20.***). This result thus suggests the voltage-gated sodium channels to contribute to the higher firing rate in FMRP-negative neurons.
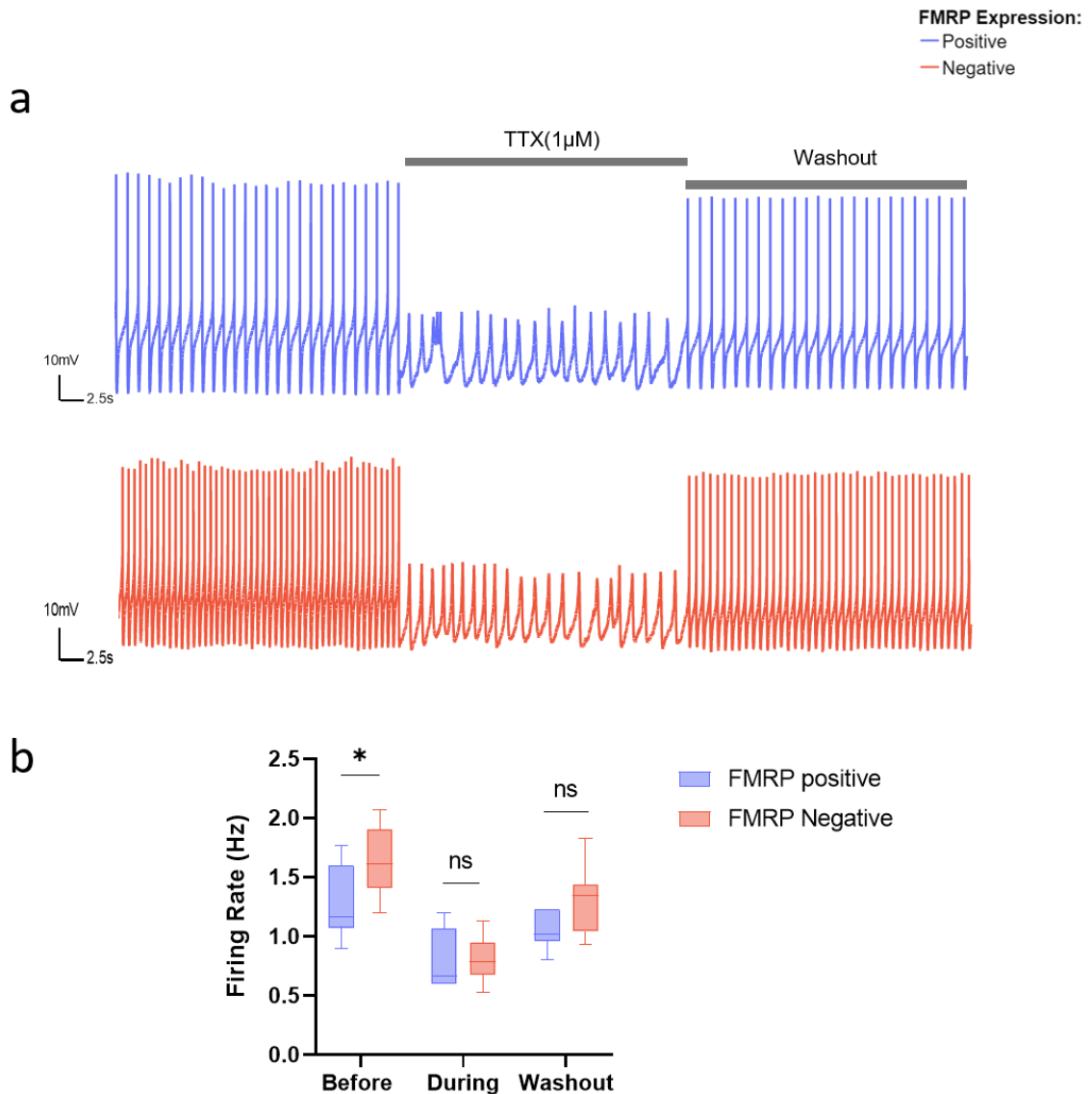
Figure 20. Subthreshold oscillation of DA neurons induced by TTX perfusion. *a) Recording traces of the spontaneous activities before, during and after TTX (1μM) perfusion. b) Bar plot shows that FMRP-negative neurons fire at a higher rate before TTX perfusion, but the TTX perfusion kills the difference between the two groups (FMRP-positive vs. -negative, n=7, 10 respectively, p=0.0272 before TTX perfusion). The TTX washout only partially recovers the firing rate. Ordinary two-way Anova with multiple t-test was adopted for the data analysis. ns = no significance , *P< 0.05.Data are shown as Min & Max with the mean value.*

Considering that the increased excitability is related to a sodium current, and that the threshold is decreased in FMRP-negative neurons, we presumed the persistent sodium current to be involved in the higher excitability of DA neurons (Deng and Klyachko 2016). In order to test this hypothesis, we applied the INaP-specific blocker riluzole (10 μM) to incubate the slices during patch clamp recordings. We found that riluzole administration indeed decreases the firing rate in both groups

and normalized the differences in AP frequency, duration, fast AHP and threshold (***Figure 21.***).
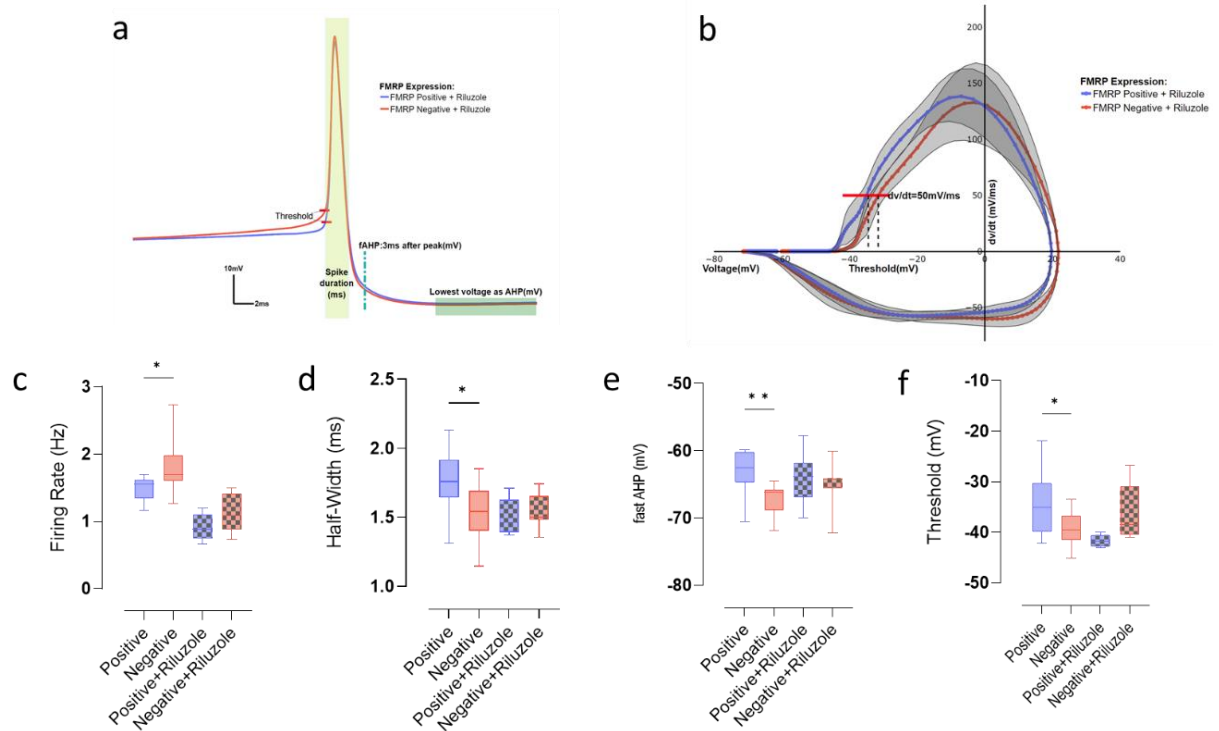
Figure 21. In riluzole-treated brain slices, FMRP-positive and -negative DA neurons exhibited similar firing properties. *a) Digraph illustrates an averaged firing spike shape from the SNc DA neurons during riluzole administration. b) Derivative of voltage with respect to time shows that riluzole-treated DA neurons have a similar spike shape between FMRP-positive and -negative phenotypes. c-f) Bar graphs demonstrate that riluzole administration rescues the difference in frequency, AP duration, as well as the fast AHP and threshold between FMRP-positive and -negative DA neurons (FMRP-positive vs. -negative, n=6, 7 respectively). For comparison of the means, one-way Anova with multiple t-test was adopted. *P< 0.05,**P < 0.01; Data is shown as Min & Max with mean value.*

4.2.4 FMRP modulation on neuronal excitability of SNc DA neurons is not cell-autonomous

In order to investigate the global effect of FMRP on neuronal excitability, we investigated basic measures of neuronal excitability of the DA neurons in WT mice. Therefore, we applied patch clamp electrophysiology recordings in acute brain slices from *Fmr1* WT and KO animals. Surprisingly, we found the firing rate, the threshold, as well as the afterhyperpolarization to exhibit no significant difference between the two groups of neurons; only the half-width in the *Fmr1* KO group has

been found to be shorter compared to WT neurons (***Figure 22. a-f***). Likewise, when we injected steps of depolarizing current (***Figure 22. g***) and recorded the resulting induced APs (iAPs), we found no difference between the *Fmr1* KO and WT mice.

Figure 22. Firing spike analysis of DA neurons in SNc DA neurons from Fmr1 KO mice and WT mice. *a) Digraph illustrating an averaged firing spike shape in DA neurons from Fmr1 KO and WT mice. b) Plot of the calculated derivative of voltage with respect to time illustrating a similar spike course between Fmr1 KO and WT. c-f) Bar graph demonstrating the an increase in half-width (p < 0.0001), but no difference in firing rate, and threshold between the neurons from Fmr1 KO (n=52) and WT mice (n=62). g) Bar graph illustrating the number of spikes in DA neurons from Fmr1 KO (n=6) and Wild-type mice (n=7) in response to a depolarizing current injection (x-axis). For comparison of the means, a student t-test was adopted. Ns = no significance, **** P < 0.0001; Data is shown as Min & Max with mean value.*

In summary, the result demonstrated DA neurons in *Fmr1* HET mice to fire at a slower rate compared to both WT and KO groups, with no discernible difference found between WT and *Fmr1* KO except for the half-width (***Figure 23. a-b***). The differences in firing rate between all the three groups might be attributed mostly to the variation in threshold and fast-afterhyperpolarization (***Figure 23. c-d***).
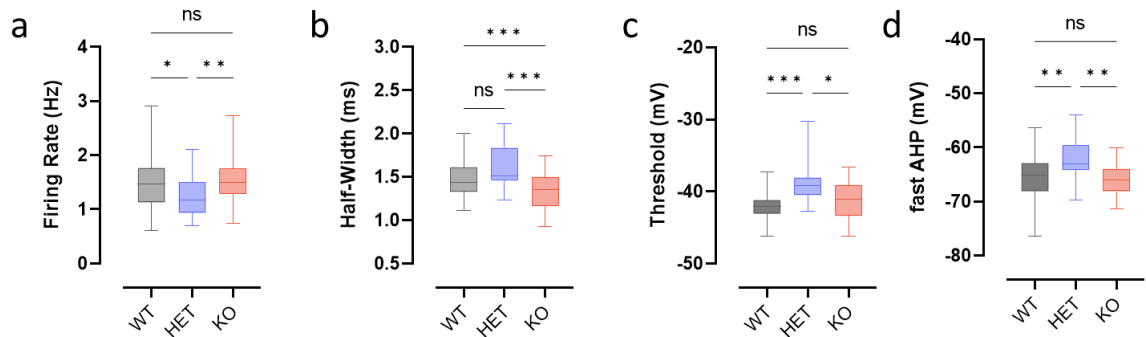
Figure 23. FMRP modulates neuronal excitability in a non-cell-autonomous manner. *a) Bar graphs illustrating that DA neurons in slices from Fmr1 HET mice (n = 31) fire at a lower rate than those in Fmr1 KO mice (n = 52, p= 0.0076) and wild-type mice (n = 62, p = 0.0318). b) Spike half-width in DA neurons in Fmr1 KO (n=60) is shorter than those in Fmr1 HET mice (n=19, p=0.0005) and wild-type mice (n=51, p=0.0005). c) Firing threshold of DA neurons in Fmr1 HET (n=17) mice is higher than in neurons from Fmr1 KO mice (n=52, p= 0.0139) and wild-type mice (n=50, p= 0.0009). g) Fast AHP of DA neurons in Fmr1 HET (n=19) mice is higher than Fmr1 KO mice (n=60, p= 0.0024) and wild-type mice (n=51, p=0.0057). For comparison of the means, one-way ANOVA with Brown-Forsythe and Welch tests for SDs correction was adopted. Ns = no significance, *** P < 0.001, **P < 0.01, *P< 0.05; Data is shown as Min & Max with mean value.*

4.2.5 G-protein-gated potassium channel may be relevant in FMRP-mediated non-cell-autonomous excitability tuning.

From the aforementioned data, we intended to explorte how FMRP affects neuronal excitability of DA neurons in a non-cell-autonomous manner. To identify multiple FMRP targets associated with DA neuron excitability, mass spectrometry was conducted on striatum samples from n = 9 mice divided into three groups (*Fmr1* KO, HET and WT, n = 3 per group). Among other targets, we found the expression of the G-protein-gated potassium channels subunit KCNJ3(GIRK1/Kir3.1) to be increased in WT as compared to KO and HET animals (***Figure 24.***).
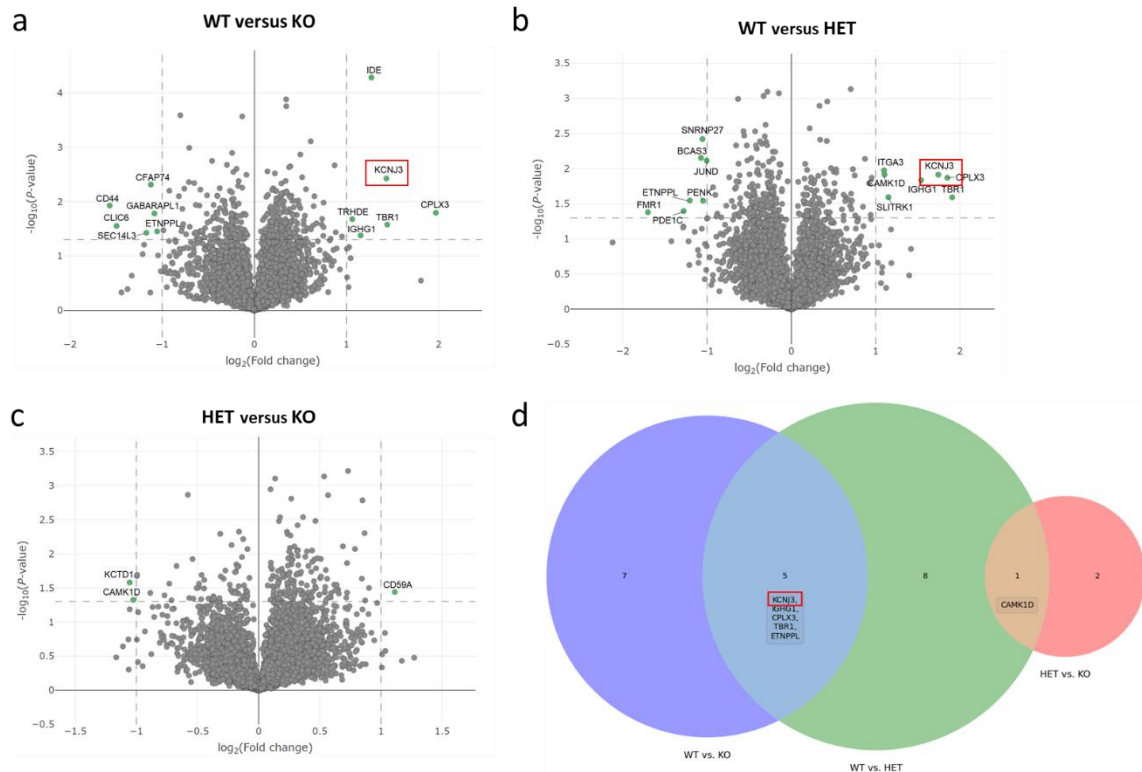
Figure 24. Volcano and Venn plots of the differently expressed proteins identified by LC-MS/MS. *The volcano plot shows the fold change (x-axis) versus the significance (y-axis) of the total proteins identified. The significance (non-adjusted p-value) and the fold-change are converted to −log10(p-value) and log2(fold-change), respectively. The vertical and horizontal dotted lines show the cut-off of fold-change = ±1 and of a p-value = 0.05, accordingly. a-c) 12 out of 7601, 14 out of 7452, and 3 out of 7437 proteins were expressed substantially different in WT vs. KO, WT vs. HET, and HET vs. KO animals, respectively, as shown by the volcano digraphs. d) The expression of KCNJ3 (kir3.1) was determined to be higher in the HET and KO groups compared to the WT group, but no significant difference was found between the HET and KO groups.*

We also analyzed the abundance of the KCNJ6 (GIRK2/Kir3.2) via Western blot because KCNJ6 values were missing from our Mass Spectrometry data. Many studies reported that the KCNJ6 is affected in a similar direction like KCNJ3 (Signorini *et al.* 1997; Torrecilla *et al.* 2002; Marker, Stoffel, and Wickman 2004; Harashima *et al.* 2006), and KCNJ6 is an important participant in PD pathology as mentioned above. In accord with our MS data, a greater KCNJ6 abundance in striatum tissue was found in *Fmr1* KO and HET mice as compared to WT animals (***Figure 25. a-b***). This result has been verified further by additional immuno-fluorescence labeling on DA neurons in brain slices from the SNc area (***Figure 25. c-d***). Conversely, we found no difference between the *Fmr1* KO and HET groups in terms of the KCNJ6 signal, and this was true for both FMRP-positive and -negative neurons in *Fmr1* HET mice (***Figure 25. e***).

In line with earlier findings demonstrating that DA neurons in the medial SNc have more KCNJ6 than those in the lateral SNc, our data suggest that the difference of KCNJ6 associated with FMRP is segregates to the lateral portion of the SNc. (***Figure 26.***).
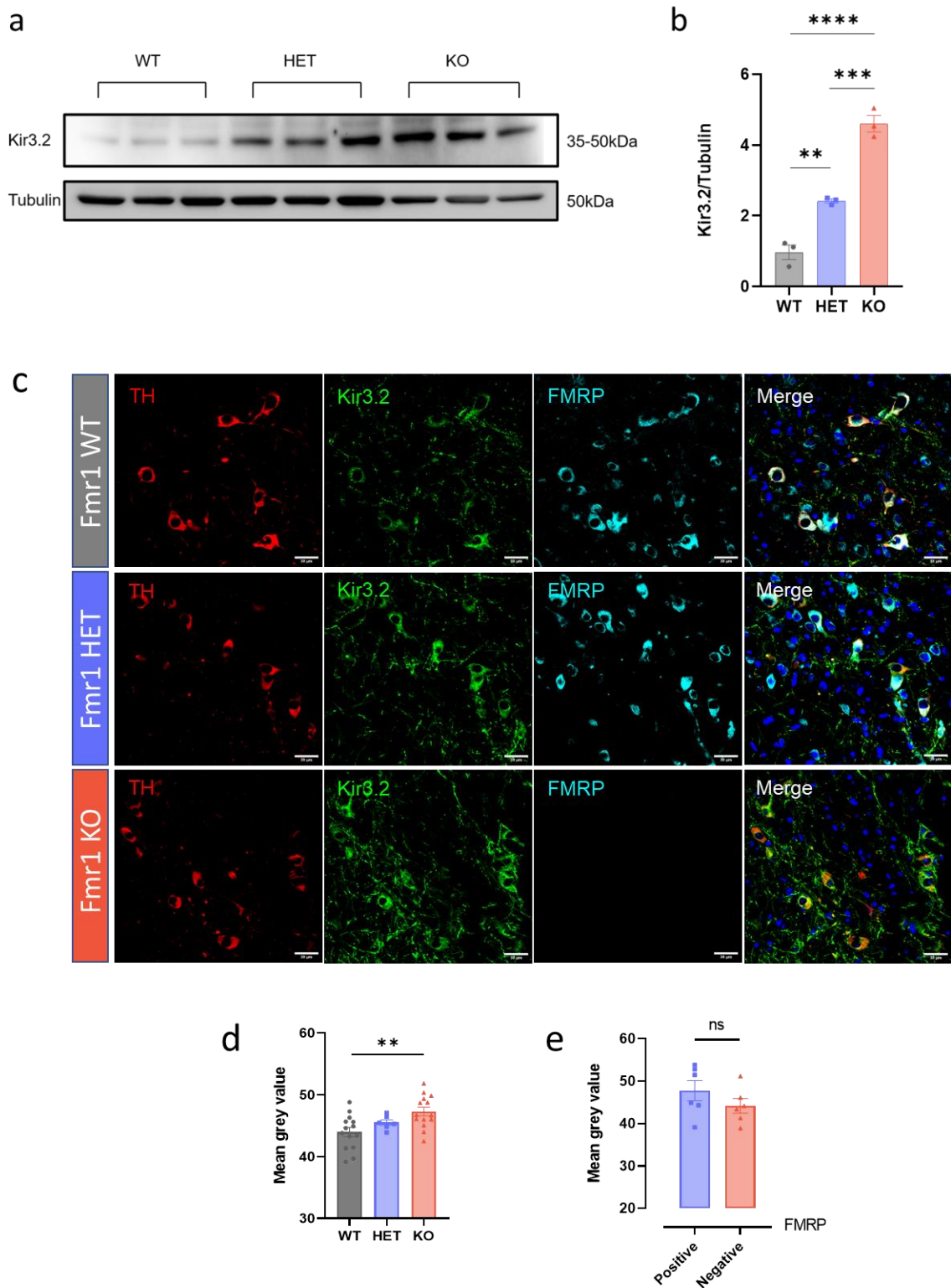
Figure 25. KCNJ6 expression is increased in the absence of FMRP. *Western blot (a), immunofluorescence (c), and bar graphs (b,d-e) illustrating the increased abundance of KCNJ6 in the striatum and in SNc DA neurons (WT vs. HET vs. KO) (n = 3 mice/group, scale bar = 30µm). For comparison of the means, one-way ANOVA with Tukey's post hoc test was used. ****P < 0.0001, ***P < 0.001, **P < 0.01. Data are shown as means ± SEM.*
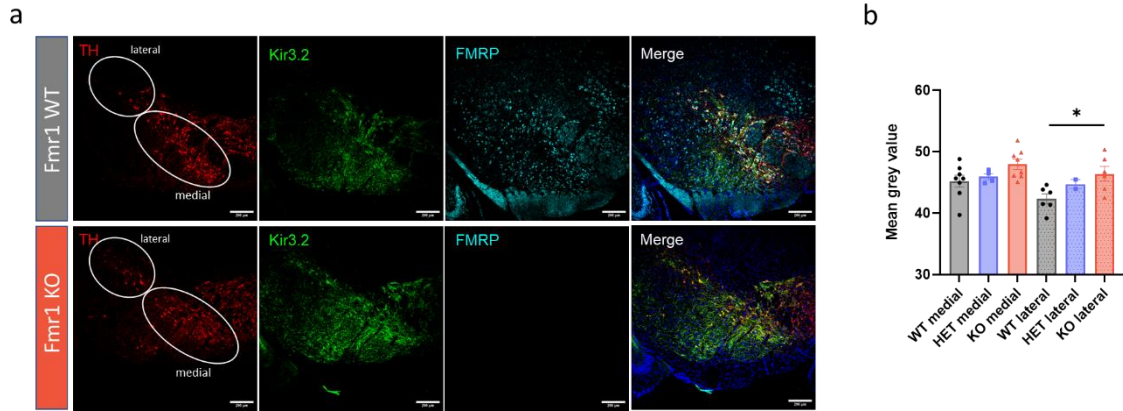
Figure 26. Differential distribution of KCNJ6 in the SNc region. *Immunofluorescence staining (a) and bar graphs (b) illustrating an increased KCNJ6-immunfluorescence in the SNc DA neurons of Fmr1 KO neurons (n = 3 mice/group, scale bar = 200µm) segregated to the lateral part (p = 0.0173). For comparison of the means, normal two-way ANOVA was used in panel b. *P < 0.05. Data are shown as means ± SEM.*

4.3 Alters in the nigrostriatal pathway related to FMRP

FMRP controls the excitability of many different types of central nervous system neurons (Contractor, Klyachko, and Portera-Cailliau 2015; Deng and Klyachko 2021). In addition, several previous reports suggest that FMRP deficiency may affect the dopamine pathway function in the brain (Wang *et al.* 2008; Chao *et al.* 2020). Given that FMRP alters the excitability of SNc DA neurons in a non-cell-autonomous manner, it would be instructive to examine whether or not FMRP alters the structural integrity of the dopamine pathway in the context of the entire nigrostriatal network.

4.3.1 Differential distribution of dopamine transporters in the striatum and SNc DA neurons

Dopamine transporter (DaT) is an integral membrane protein considered as a marker for the functional integrity of the dopamine pathway because of its role in the recycling of the neurotransmitter dopamine. We investigated DaT in brain slices containing the striatum and SNc from *Fmr1* KO and WT mice by immunhistochemistry. We found DaT density in the *Fmr1* KO group to be significantly increased in the striatum as compared to WT animals. Conversely, DaT abundance was decreased in the SNc of *Fmr1* KO group, suggesting a differential effect of FMRP on DaT abundance in the striatum vs. the SNc. (***Figure 27.***)
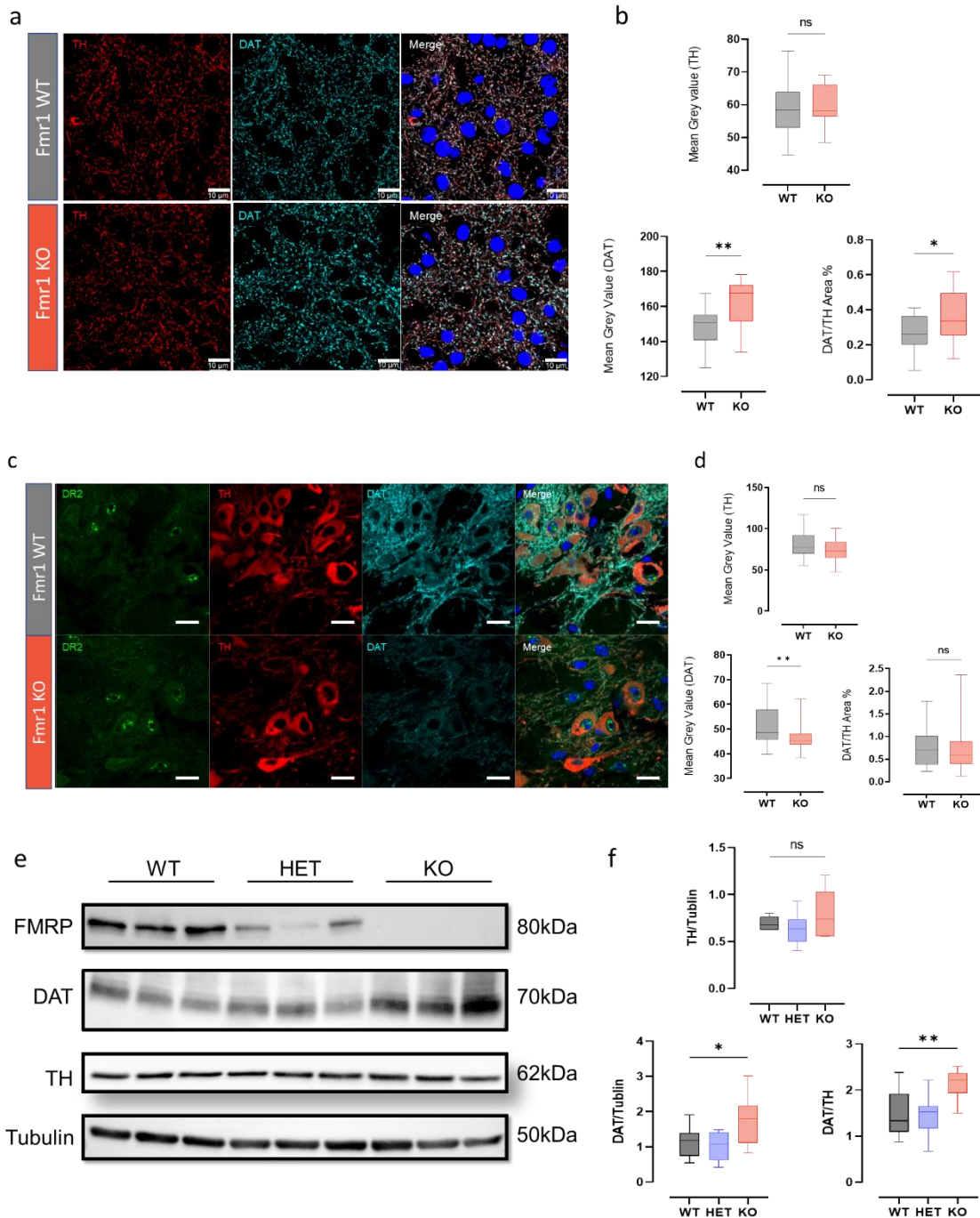
Figure 27. DaT expression level in the striatum and in SNc DA neurons. *a) Immunofluorescence staining of striatal slices with antibodies against TH and DaT (n = 18 slices out of 3 mice in each genotype, scale bar=10μm), b) Bar graphs illustrating that Fmr1 KO mice have a higher DaT signal, DaT average intensity (lower left graph, p=0.0025), and DaT density which is represented as the DaT/TH area (lower right graph, p=0.0205). c) Immunofluorescence staining of DA neurons in the SNc visualizing DR2, TH and DaT (n=36 slices out of 3 mice in each genotype, scale bar=20μm). d) DaT average intensity in Fmr1 KO is lower than in WT mice (lower left graph, p=0.0015), and DaT density seems to keep the same level (lower right, p=0.6085). e) Western blot of striatal tissue samples displaying antibody reactivity with FMRP, DaT, TH and Tubulin (n=9 samples). F) WB demonstrating an increased DaT level (p=0.0417) and DaT/TH ratio (p=0.0051) in the Fmr1 KO group. For a comparison of the means, one-way ANOVA with multiple t test was used. *P < 0.05, **P < 0.01. Data are shown as Min & Max with mean value.*

4.3.2 Dopamine receptor expression is changed in *Fmr1* KO mice

As mentioned in the introduction, the dopamine receptor (DR) is a crucial functional component of the nigrostriatal pathway, with the ratio of the two subtypes DR1/DR2 balancing the direct/indirect pathway. In addition, DR2 in the SNc DA neuron is capable of self-tuning the firing rate of DA neurons and thereby affecting dopamine release. In order to address the integrity of the DR-system in *Fmr1* KO mice, we examined the abundance of DR1 and DR2 in striatal brain slices from *Fmr1* KO and WT animals by immunohistochemistry. We found DR1 and DR2 levels in the striatum to be decreased, while the DR1/DR2 ratio remained unaffected. The decreased DR2 level with vacant DR1 signal is also found in SNc.
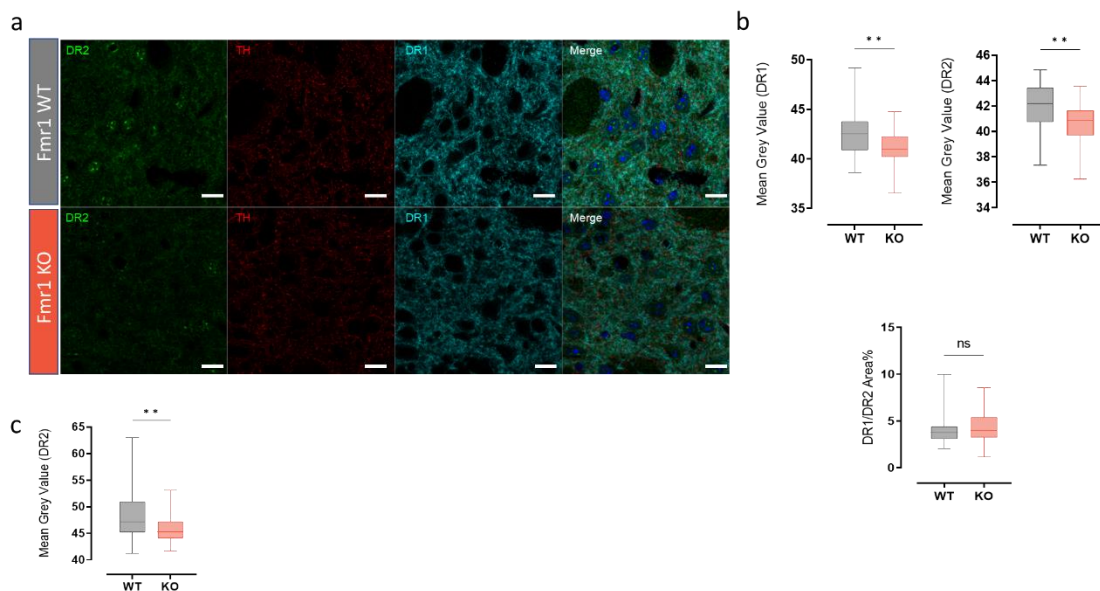
Figure 28. DR1 and DR2 expression in the striatum and SNc DA neurons. *a) Immunofluorescence staining from striatum to quantify DR1, DR2 and TH (n = 46 slices out of 3 WT mice, n = 39 slices out of 3 Fmr1 KO mice, scale bar = 10µm), b) Fmr1 KO mice exhibit a lower DR1 (upper left, p=0.0047) and DR2 signal (upper right graph, p=0.0010) compared to WT mice, whereas the DR1/DR2 ratio remained unaffected (lower center graph, p=0.4544). c) DR2 intensity was found to be lower in Fmr1 KO SNc DA neurons compared to WT neurons (p=0.008) (Representative staining picture see Fig. 27c). For comparison of the means, a student t-test was applied. **P < 0.01. Data are shown as Min & Max with mean value.*

5. Discussion

5.1 α-Synuclein overexpression results in impaired excitability of SNc DA neurons

Numerous studies found that the overexpression of wild-type or mutant α-Syn altered the excitability of DA neurons in the SNc. Studies generally concurred that α-Syn pathology could increase neuronal excitability, including higher spontaneous firing rates in vitro and increased burst firing in vivo, and thereby impose extra workload on SNc DA neurons, leading to vulnerability (Subramaniam *et al.* 2014; Deng and Klyachko 2021). However, other studies also claimed that α-Syn aggregate causes a lack of input resistance and a loss of excitability, which results in insufficient dopamine release (Hill *et al.* 2021). We advocate the former conclusion from the recapitulated phenomena that rapid outward current is impeded in SNc DA neurons with overexpression of α-Syn (***Figure 10.***). Widely divergent views on the mechanisms behind the α-Syn influence on neuronal excitability made it challenging to pinpoint the potential target to restore normal excitability. One possible theory based on the excitability alteration related to α-Syn is that α-Syn could lower the DR2 membrane enrichment, thus inhibiting the excitability suppression driven by DR2 activation (Lin *et al.* 2021; Dagra *et al.* 2021). However, since DR2 autoreceptors on DA neurons have been reported to chronically enhance pacemaker activity (Hahn *et al.* 2006), this theory would seem to be ambiguous. Additionally, the acute treatment with the DR2 antagonist, sulpiride, had no impact on the firing rate, suggesting that DR2 activity in acute brain slices may not play an important role (Dragicevic *et al.* 2014; Su *et al.* 2019). Another presumption is that oxidative overload preceded the excitability change, which interprets in detail that increased oxidative stress by α-Syn pathology leads to a redox-dependent decrease in the activity of A-type Kv4.3 channels (Subramaniam *et al.* 2014; Tozzi *et al.* 2021), albeit the peroxidative toxicity which can directly lead to neuron death happens prior to the increased excitability is counterintuitive (Roselli and Caroni 2015; Saxena and Caroni 2011). Only a few pieces of attention were drawn to the far-fetched suggestion that α-Syn may create pores on membrane and cause non-selective permeability (Mironov 2015).

Our previous research built a link between the α-Syn overexpression and the loss of FMRP in DA neurons (Tan *et al.* 2020), which shed light on a potential target to restore excitability since FMRP is an extensive neuronal excitability modulator. These results also lend credence to the hypothesis that α-Syn overexpression disrupts the A-type potassium channel, which is reported as an FMRP target (Gross *et al.* 2011; Lee *et al.* 2011; Routh, Johnston, and Brager 2013). And this finding prompts our idea to investigate the possible impact of FMRP deficiency in DA neurons on neuronal excitability. However, we didn't duplicate the α-Syn induced alterations in A-type activity in the following *Fmr1* KO mouse model (***Figure 22.***). A possible explanation is that the FMRP-regulated A-type isoform, Kv4.2, is not expressed in SNc DA neurons where Kv4.3 is abundant (Haddjeri-Hopkins *et al.* 2021; Dufour, Woodhouse, and Goaillard 2014; Liss *et al.* 2001). And whether FMRP could modify the expression or function of Kv4.3 is yet to be determined.

5.2 FMRP modulates the excitability of Substantia nigra DA neurons in a non-cell-autonomous manner

Broad-spectrum sometimes equals complexity. FMRP modulates numerous neuronal functions; therefore, its influence on neuronal excitability varies between brain regions and cell types and depends on the cellular milieu. For instance, FMRP is reported to regulate the HCN channel in a reverse way between the hippocampus and prefrontal cortex (Brandalise *et al.* 2020), and this phenomenon can also be seen in the A-type potassium channel (Darnell *et al.* 2011; Gross *et al.* 2011; Lee *et al.* 2011). On the other hand, non-cell-autonomous regulation by FMRP on neuronal function and morphology was also reported. For example, neurons pharmacologically isolated from their circuit do not exhibit INaP (persistent sodium current)-mediated abnormalities, which otherweise can be seen in a preserved circuit activity (Deng and Klyachko 2016). Dendritic spine densities of apical layer V pyramidal neurons in female *Fmr1* HET mice are significantly elevated compared to WT and KO animals (Bland *et al.* 2021). Likewise, we found that the absence of FMRP increases the excitability of DA neurons in a non-cell-autonomous manner (***Figure 23.***). *Fmr1* HET mice exhibited an increased ratio of pS6-positive neurons in FMRP-negative neurons with a higher firing rate,

indicating hyperexcitability (*Figure 13.*). However, when we compared WT and *Fmr1* KO mice, this modulation effect was not appreciated any more (*Figure 12.*) (*Figure 23.*).

Increased neuronal firing in the FXS model can be found in most brain regions like the auditory brainstem, the CA3 region of the hippocampus and the entorhinal cortex etc. (El-Hassar *et al.* 2019; Deng *et al.* 2019; Deng and Klyachko 2016), whereas decreased firing rate was also reported in other cases, like the CA1 region of the hippocampus in the adult mouse (Dwivedi, Chattarji, and Bhalla 2019). Despite these controversies, it is generally accepted that a lack of FMRP throughout the brain can lead to hyperexcitability of neuronal networks, not only in the motor pathway but also sensory system (Contractor, Klyachko, and Portera-Cailliau 2015). There are two obstacles that make it difficult to investigate how FMRP increases neuronal excitability: the first is that the control of neuronal firing rate by particular ion channels, most commonly BK channels, which have also been described as one of the targets of FMRP (Deng *et al.* 2013), are often bidirectional. BK channels contain calcium sensors on the intracellular side, which are activated in response to an increased calcium influx and serve to enhance potassium efflux. It generally shortens the AP duration, allowing the following impulse to fall into the supernormal phase and boost the firing rate. However, this channel, at the same time, mediates an enhanced potassium outward current that amplifies the magnitude and duration of the AHP (afterhyperpolarization), which may also lead to a decrease in the firing rate (Ly *et al.* 2011). Several pharmacological experiments have shown this bidirectional effect: the inhibitory effect of BK channels on the tonic firing rate observed in Purkinje neurons (Edgerton and Reinhart 2003; Swensen and Bean 2003; Womack and Khodakhah 2002) is even stronger when BK channels are ablated (Sausbier *et al.* 2004); second, the diversity of FMRP-targeted receptors can lead to controversial results (Booker *et al.* 2019; Guo *et al.* 2015). Sometimes, this comprehensive effect is really crucial for certain neurons like SNc DA neurons which involve accurate motor control, and their robust activity is a guarantee for a stable background release of dopamine in the striatum (Guzman *et al.* 2009). Our study confirms that, at least for *Fmr1* HET mice, the high excitability in FMRP-negative DA neurons is mediated by sodium currents since the change in firing rate,

threshold, fast-AHP and half-width are all related to the INaP (***Figure 16.***) (Deng and Klyachko 2016; Routh *et al.* 2017). Another supportive evidence is that the difference in half-width is way more apparent than fast-AHP between WT and *Fmr1* KO, suggesting the transient sodium current, which contributes more during depolarization than repolarization, plays a central part (***Figure 22.***). More importantly, the application of TTX is sufficient to ablate the difference between FMRP-positive DA neurons (***Figure 20.***), which is further confirmed by the application of riluzole, suggesting that the sodium component could be driven by INaP (***Figure 21.***). No specific channel should be responsible for mediating INaP because it comes from the incomplete closure of voltage-dependent sodium channels during inactivation (Wengert and Patel 2021). This background inward current drives the membrane to a slightly depolarized state, making it more sensitive and leading to a decreased threshold and hyperexcitability. The negative effect of FMRP on INaP has been revealed by Pan-Yue Deng's group, who claimed that excess INaP activity is based on exaggerated mGluR5 signaling (Deng and Klyachko 2016). The blockage effect driven by the low concentration of riluzole on INaP is not completely specific, and our riluzole application even reversed the AP duration in FMRP-negative neurons (***Figure 21.***), also proposing the possibility of INaT (transient sodium current) involvement (Routh *et al.* 2017). mGluR1/5 was found to be able to regulate both INaT and INaP (Dong and Ennis 2014; Carlier *et al.* 2006), and the activity could also be mutually modulated with FMRP (Price *et al.* 2007; Bear 2005; Antar *et al.* 2004) plus it's highly expressed in SNc DA neurons (Conn *et al.* 2005), more in-depth experiments, like micromolar TTX application companies with modified recording solutions to minimize contamination from Na^+-activated K^+ currents and other K^+ and Ca^{2+} conductances, should be carried out to isolate this background inward current to elucidate further.

Our findings that FMRP acts in a non-cell-autonomous manner to modulate the excitability of SNc DA neurons raise the important question of the mechanism of such a regulation. The application of MK-801, NBQX, and picrotoxin during recording allowed us to essentially rule out the contributions from NMDA, AMPA, and GABA-A receptors. In addition, we performed differential expression analysis of total proteins in the striatum using a proteomics strategy (***Figure 24.***). The striatum, compared to the

SNc region, can be sampled more easily and exclusively to acquire high purity without any tissue handling. As demonstrated by the dopamine release activated via electric stimuli, the axons projected from SNc DA neurons in the striatum can be preserved well (Tan *et al.* 2020). According to our findings, the KCNJ3 expression level does not shift in a way that matches the FMRP abundance. Specifically, a difference in KCNJ3 was seen between WT and *Fmr1* KO and between WT and *Fmr1* HET, but no longer existed between *Fmr1* HET and *Fmr1* KO, despite a 50% reduction in total FMRP expression in the HET group compared to the KO (***Figure 24-25.***). These results thus demonstrate that the potassium channals (KCNJ3) may highly involved in this non-cell-autonomous effect.

The presence of KCNJ6 (GIRK2/Kir3.2) is necessary for the preservation of normal function since KCNJ3 is unable to build functional homomeric channels (Kubo *et al.* 1993). KCNJ6, on the other hand, may form functional homotetramer independently (Lesage *et al.* 1995; Luscher and Slesinger 2010) and can be used as an artificial vehicle to deliver outward currents (Marcott, Mamaligas, and Ford 2014). KCNJ3/KCNJ6 heterotetramers are responsible for GIRK current conduction in the majority of neurons (Liao, Jan, and Jan 1996; Kobayashi *et al.* 1995; Karschin *et al.* 1996), while DA neurons in the SNc exclusively express KCNJ6 subunits (presumably GIRK2a/c), precisely in dendrite postsynapse area (Inanobe *et al.* 1999; Shcherbatyy *et al.* 2015). If the alteration in KCNJ3 we found in the striatum comes from the axonal compartment of DA neurons is still not clear, but it unlikely results from the medium spiny neurons (MSN) because studies reported Kir2.1/2.3 (KCNJ2/4) heterotetramers are the main GIRK channel in MSN and mediated the DR2-activated hyperpolarization (Cazorla *et al.* 2012). In accord, others also denied the GIRK1-3 expression in the caudate-putamen (Kobayashi *et al.* 1995). That is the reason why we didn't verify the KCNJ3 in striatum tissue further but switched to KCNJ6 instead. Unfortunately, we presume that the null value of KCNJ6 in our mass spect data is owing to its paucity in the striatum. As mentioned above, multiple areas of the brain have shown that KCNJ3 and KCNJ6 alterations are invariably synchronized, although to varying degrees. Knockdown of KCNJ6 decreases the amount of KCNJ3 (Signorini *et al.* 1997; Torrecilla *et al.* 2002) and vice versa (Marker, Stoffel, and Wickman 2004). The

simultaneous changes occur at the protein expression stage rather than transcription, as the mRNA content of the dependent variable may not alter (Harashima *et al.* 2006).

Our findings are in accord with the idea that SNc DA neurons express a high level of KCNJ6 and that the medial DA neurons hold a higher abundance of KCNJ6 compared to lateral (*Figure 25.*). For this reason, KCNJ6 is also reported as a marker for DA neuron vulnerability because lateral DA neurons usually degenerate more manageably than their medial counterparts (Chung *et al.* 2005; Brichta and Greengard 2014). Indeed, GIRK2-positive DA neurons were more susceptible to MPP+ toxicity, and GIRK2 overexpression enhanced PC12-Syn neurons' susceptibility to the toxin. Different voices said that the enhanced expression of GIRK2 channels as a result of electroconvulsive shock might serve as a neuroprotection against aberrant activity (Pei *et al.* 1999), and in line with this theory, activation of galanin type 2 receptors that activate GIRK channels inhibits the initiation of epileptogenesis in rats (Mazarati *et al.* 2006).

The relationship between FMRP and the expression of GIRK2 is not well addressed. Apparently, GIRK2 mRNA is not in the FMRP target list, and the same level in GIRK2 between FMRP-positive and -negative neurons in *Fmr1* HET mice (*Figure 25. e*) indicate that changes in GIRK2 between *Fmr1* KO and WT are most likely a secondary effect.

The increased expression of GIRK2 in SNc DA neurons in the *Fmr1* KO group afforded us the chance to explain the non-cell-autonomous phenomenon partially. At voltages close to the membrane resting potential, the modest outward K^+ current via GIRK channels hyperpolarize the neuron, hence lowering membrane excitability. Single-channel recordings convey that hetero- and homo-tetrameric channels have distinct biophysical qualities. While GIRK2 homotetrameric channels have rapid opening intervals (0.5 ms mean open time), homotetrameric channels are much longer (~1-2 ms mean open times) (Slesinger *et al.* 1995; Kofuji, Davidson, and Lester 1995). A lot of ligates and their receptors were reported to be able to activate the GIRK channel through the G protein, including but not limited to GABA-b receptor, dopamine

receptor 2, serotonin receptor, cannabinoids and opioids receptor (Campbell and Smrcka 2018). And due to the GIRK's PIP2 sensitivity, other potential regulators through PIP2 are also reported, like cholesterol (Mathiharan *et al.* 2021). The broad activator makes it possible that the GIRK channel is still working in an in-vitro condition, specifically in acute brain slices. Tertiapin, a specific GIRK channel blocker, administration alone is enough to suppress its negative effect on the firing rate (Arora *et al.* 2010; Llamosas, Ugedo, and Torrecilla 2017).

All in all, we hypothesized that the activation of the overexpressed GIRK channel could compensate for the INaP or INaT-induced hyperexcitability in *Fmr1* KO. GIRK channel opening decreases the excitability by threshold downward adjustment and potassium out-flow enhancement during repolarization (Luscher and Slesinger 2010), which could explain how the firing rate, fast-AHP and threshold, which are different between FMRP-negative and -positive neurons in *Fmr1* HET group (***Figure 15-16***), can be restored between *Fmr1* KO and WT, except for the half-width which is induced by fast sodium component during depolarization (***Figure 23***). Similar research was conducted that the blockage of GIRK channels could rescue the Li^+-induced abnormal excitability, including induced firing rate and latency to the threshold, but not the half-width (Dascal and Rubinstein 2017). Future studies need to perform in the presence of a GIRK channel blocker to see if the increased firing rate can be reproduced and elucidate FMRP's effect on SNc DA neuron excitability better.

5.3   FMRP and its role in the nigrostriatal dopamine pathway

Spontaneous pacemaker activities in SNc DA neurons maintain extracellular DA levels and DA receptor signals necessary for the normal network functioning of basal ganglia regions such as the striatum (Gonon and Bloch 1998). An increase in extracellular DA levels typically accompanies the enhancement of such involuntary impulses (Gonon and Bloch 1998). Although we found no differences in the firing rate of DA neurons in *Fmr1* KO versus WT, we did find that several striatal dopamine receptors, notably DaT DR1 and DR2, were altered (***Figure 27-28***). This implies that FMRP itself can shape dopamine signaling independent of neuronal excitability. Indeed Wang *et al.* were the

first to report the impact of FMRP on dopamine signaling via biomolecular interactions and highlight the critical role of FMRP in the dopamine pathway. The prefrontal cortex (PFC) DR1 function was the main area of interest. Although distinct from our findings, they did not find any changes in DR1 expression in *Fmr1* KO mice in PFC neurons, while the DR1-mediated intracellular processes are diminished, including cell surface expression and phosphorylation of the GluR1 glutamate receptor (Wang *et al.* 2008). On the identical *Fmr1* KO animal model we used, another group also did western blotting on striatum tissue and got the reverse result. It was demonstrated that DaT expression was considerably reduced in the *Fmr1* KO mice, correlating with poor dopamine recycling (Chao *et al.* 2020), which neither our WB, immunofluorescence staining, or mass spectrometry data support. The extensive role of FMRP in the control of dopamine signaling is further backed up by a large-scale proteomic analysis of DaT-KO rats showing a decreased FMRP level (Savchenko *et al.* 2022). Some researcher also claimed that DR2 may regulate DaT cell surface localization (Lee *et al.* 2007; Dickinson *et al.* 1999), our DaT staining partially support the theory that DR2 level is decreased in both DA neuron terminals and cell body (***Figure 28***) compared to a reverse change in DaT level between striatum and SNc (***Figure 27***).

Given that fragile X syndrome is not always characterized by deficits with reward-seeking and coordinated movement, there have been few studies to link altered dopamine signaling to the manifestation of this disorder. There may be an unexplored compensating component for the nigrostriatal dopamine pathway involved with locomotion, as FMRP was revealed to exhibit a non-cell-autonomous effect in regulating SNc DA neurons' excitability. Since FMRP is involved in dopamine regulation and is significantly reduced in PD cases, a conditional *Fmr1* KO in the nigrostriatal DA neurons mouse model should be used to optimally mimic the phenotype of PD in future studies.

6. Summary

By inadequately fulfilling our experiment aims, we discovered that a malfunction in the A-type potassium channel was associated with α-Syn overexpression in SNc DA neurons and not based on a decreased level of FMRP. In addition, we elaborated on the effect that FMRP has on the excitability of SNc DA neurons. We suggested that the loss of FMRP dramatically boosts the excitability of DA neurons in *Fmr1* HET mice via raised sodium influx, which was not reflected between WT and *Fmr1* KO. The unique background expression of GIRK channels was shown up to be responsible for the non-cell-autonomous effect. In addition, the profound engagement of FMRP in the nigrostriatal dopamine pathway is reflected by the differential expression of a large number of receptors linked with dopamine signaling in striatal and SNc DA neurons in animals lacking *Fmr1* gene copy number. The intricacy of FMRP's involvement in engaging in neuronal signaling pathways is reflected in this work because the regulatory role of FMRP is too wide. This applies to both the translation of proteins and the excitability of neurons. This also implies that further investigation of the impact of FMRP on certain neural processes may need the use of conditional knockout animal models.

7. References

Ahn, E. H., S. S. Kang, X. Liu, X. Cao, S. Y. Choi, L. Musazzi, P. Mehlen, and K. Ye. 2021. 'BDNF and Netrin-1 repression by C/EBPbeta in the gut triggers Parkinson's disease pathologies, associated with constipation and motor dysfunctions', *Prog Neurobiol*, 198: 101905.

Anderegg, A., J. F. Poulin, and R. Awatramani. 2015. 'Molecular heterogeneity of midbrain dopaminergic neurons--Moving toward single cell resolution', *FEBS Lett*, 589: 3714-26.

Anderson, D., G. Beecher, and F. Ba. 2017. 'Deep Brain Stimulation in Parkinson's Disease: New and Emerging Targets for Refractory Motor and Nonmotor Symptoms', *Parkinsons Dis*, 2017: 5124328.

Andressoo, J. O., and M. Saarma. 2008. 'Signalling mechanisms underlying development and maintenance of dopamine neurons', *Curr Opin Neurobiol*, 18: 297-306.

Antar, L. N., R. Afroz, J. B. Dictenberg, R. C. Carroll, and G. J. Bassell. 2004. 'Metabotropic glutamate receptor activation regulates fragile x mental retardation protein and *Fmr1* mRNA localization differentially in dendrites and at synapses', *J Neurosci*, 24: 2648-55.

Arora, D., D. M. Haluk, S. Kourrich, M. Pravetoni, L. Fernandez-Alacid, J. C. Nicolau, R. Lujan, and K. Wickman. 2010. 'Altered neurotransmission in the mesolimbic reward system of Girk mice', *J Neurochem*, 114: 1487-97.

Ascherio, A., and M. A. Schwarzschild. 2016. 'The epidemiology of Parkinson's disease: risk factors and prevention', *Lancet Neurol*, 15: 1257-72.

Barodia, S. K., R. B. Creed, and M. S. Goldberg. 2017. 'Parkin and PINK1 functions in oxidative stress and neurodegeneration', *Brain Res Bull*, 133: 51-59.

Baydyuk, M., M. T. Nguyen, and B. Xu. 2011. 'Chronic deprivation of TrkB signaling leads to selective late-onset nigrostriatal dopaminergic degeneration', *Exp Neurol*, 228: 118-25.

Bean, B. P. 2007. 'The action potential in mammalian central neurons', *Nat Rev Neurosci*, 8: 451-65.

Bear, M. F. 2005. 'Therapeutic implications of the mGluR theory of fragile X mental retardation', *Genes Brain Behav*, 4: 393-8.

Belles, B., C. O. Malecot, J. Hescheler, and W. Trautwein. 1988. '"Run-down" of the Ca current during long whole-cell recordings in guinea pig heart cells: role of phosphorylation and intracellular calcium', *Pflugers Arch*, 411: 353-60.

Benkert, J., S. Hess, S. Roy, D. Beccano-Kelly, N. Wiederspohn, J. Duda, C. Simons, K. Patil, A. Gaifullina, N. Mannal, E. Dragicevic, D. Spaich, S. Muller, J. Nemeth, H. Hollmann, N. Deuter, Y. Mousba, C. Kubisch, C. Poetschke, J. Striessnig, O. Pongs, T. Schneider, R. Wade-Martins, S. Patel, R. Parlato, T. Frank, P. Kloppenburg, and B. Liss. 2019. 'Cav2.3 channels contribute to dopaminergic neuron loss in a model of Parkinson's disease', *Nat Commun*, 10: 5094.

Betarbet, R., T. B. Sherer, G. MacKenzie, M. Garcia-Osuna, A. V. Panov, and J. T. Greenamyre. 2000. 'Chronic systemic pesticide exposure reproduces features of Parkinson's disease', *Nat Neurosci*, 3: 1301-6.

Blaess, S., G. O. Bodea, A. Kabanova, S. Chanet, E. Mugniery, A. Derouiche, D. Stephen, and A. L. Joyner. 2011. 'Temporal-spatial changes in Sonic Hedgehog expression and signaling reveal different potentials of ventral mesencephalic progenitors to populate distinct ventral midbrain nuclei', *Neural Dev*, 6: 29.

Bland, K. M., A. Aharon, E. L. Widener, M. I. Song, Z. O. Casey, Y. Zuo, and G. S. Vidal. 2021. 'FMRP regulates the subcellular distribution of cortical dendritic spine density in a non-cell-autonomous manner', *Neurobiol Dis*, 150: 105253.

Booker, S. A., A. P. F. Domanski, O. R. Dando, A. D. Jackson, J. T. R. Isaac, G. E. Hardingham, D. J. A. Wyllie, and P. C. Kind. 2019. 'Altered dendritic spine function and integration in a mouse model of fragile X syndrome', *Nat Commun*, 10: 4813.

Braak, H., K. Del Tredici, U. Rub, R. A. de Vos, E. N. Jansen Steur, and E. Braak. 2003. 'Staging of brain pathology related to sporadic Parkinson's disease', *Neurobiol Aging*, 24: 197-211.

Braak, H., U. Rub, W. P. Gai, and K. Del Tredici. 2003. 'Idiopathic Parkinson's disease: possible routes by which vulnerable neuronal types may be subject to neuroinvasion by an unknown pathogen', *J Neural Transm (Vienna)*, 110: 517-36.

Brandalise, F., B. E. Kalmbach, P. Mehta, O. Thornton, D. Johnston, B. V. Zemelman, and D. H. Brager. 2020. 'Fragile X Mental Retardation Protein Bidirectionally Controls Dendritic Ih in a Cell Type-Specific Manner between Mouse Hippocampus and Prefrontal Cortex', *J Neurosci*, 40: 5327-40.

Brichta, L., and P. Greengard. 2014. 'Molecular determinants of selective dopaminergic vulnerability in Parkinson's disease: an update', *Front Neuroanat*, 8: 152.

Brown, M. R., J. Kronengold, V. R. Gazula, Y. Chen, J. G. Strumbos, F. J. Sigworth, D. Navaratnam, and L. K. Kaczmarek. 2010. 'Fragile X mental retardation protein controls gating of the sodium-activated potassium channel Slack', *Nat Neurosci*, 13: 819-21.

Burke, R. E., and K. O'Malley. 2013. 'Axon degeneration in Parkinson's disease', *Exp Neurol*, 246: 72-83.

Cai, H., G. Liu, L. Sun, and J. Ding. 2014. 'Aldehyde Dehydrogenase 1 making molecular inroads into the differential vulnerability of nigrostriatal dopaminergic neuron subtypes in Parkinson's disease', *Transl Neurodegener*, 3: 27.

Campbell, A. P., and A. V. Smrcka. 2018. 'Targeting G protein-coupled receptor signalling by blocking G proteins', *Nat Rev Drug Discov*, 17: 789-803.

Carlier, E., V. Sourdet, S. Boudkkazi, P. Deglise, N. Ankri, L. Fronzaroli-Molinieres, and D. Debanne. 2006. 'Metabotropic glutamate receptor subtype 1 regulates sodium currents in rat neocortical pyramidal neurons', *J Physiol*, 577: 141-54.

Cazorla, M., M. Shegda, B. Ramesh, N. L. Harrison, and C. Kellendonk. 2012. 'Striatal D2 receptors regulate dendritic morphology of medium spiny neurons via Kir2 channels', *J Neurosci*, 32: 2398-409.

Chamberlain, K. A., and Z. H. Sheng. 2019. 'Mechanisms for the maintenance and regulation of axonal energy supply', *J Neurosci Res*, 97: 897-913.

Chao, O. Y., S. S. Pathak, H. Zhang, N. Dunaway, J. S. Li, C. Mattern, S. Nikolaus, J. P. Huston, and Y. M. Yang. 2020. 'Altered dopaminergic pathways and therapeutic effects of intranasal dopamine in two distinct mouse models of autism', *Mol Brain*, 13: 111.

Chen, L., S. Daniels, Y. Kim, and H. Y. Chu. 2021. 'Cell Type-Specific Decrease of the Intrinsic Excitability of Motor Cortical Pyramidal Neurons in Parkinsonism', *J Neurosci*, 41: 5553-65.

Chung, C. Y., H. Seo, K. C. Sonntag, A. Brooks, L. Lin, and O. Isacson. 2005. 'Cell type-specific gene expression of midbrain dopaminergic neurons reveals molecules involved in their vulnerability and protection', *Hum Mol Genet*, 14: 1709-25.

Collier, T. J., N. M. Kanaan, and J. H. Kordower. 2011. 'Ageing as a primary risk factor for Parkinson's disease: evidence from studies of non-human primates', *Nat Rev Neurosci*, 12: 359-66.

Conn, P. J., G. Battaglia, M. J. Marino, and F. Nicoletti. 2005. 'Metabotropic glutamate receptors in the basal ganglia motor circuit', *Nat Rev Neurosci*, 6: 787-98.

Contractor, A., V. A. Klyachko, and C. Portera-Cailliau. 2015. 'Altered Neuronal and Circuit Excitability in Fragile X Syndrome', *Neuron*, 87: 699-715.

Csordas, G., D. Weaver, and G. Hajnoczky. 2018. 'Endoplasmic Reticulum-Mitochondrial Contactology: Structure and Signaling Functions', *Trends Cell Biol*, 28: 523-40.

Dagra, A., D. R. Miller, M. Lin, A. Gopinath, F. Shaerzadeh, S. Harris, Z. A. Sorrentino, J. F. Stoier, S. Velasco, J. Azar, A. R. Alonge, J. J. Lebowitz, B. Ulm, M. Bu, C. A. Hansen, N. Urs, B. I. Giasson, and H. Khoshbouei. 2021. 'alpha-Synuclein-induced dysregulation of neuronal activity contributes to murine dopamine neuron vulnerability', *NPJ Parkinsons Dis*, 7: 76.

Darnell, J. C., S. J. Van Driesche, C. Zhang, K. Y. Hung, A. Mele, C. E. Fraser, E. F. Stone, C. Chen, J. J. Fak, S. W. Chi, D. D. Licatalosi, J. D. Richter, and R. B. Darnell. 2011. 'FMRP stalls ribosomal translocation on mRNAs linked to synaptic function and autism', *Cell*, 146: 247-61.

Dascal, N., and M. Rubinstein. 2017. 'Lithium reduces the span of G protein-activated K(+) (GIRK) channel inhibition in hippocampal neurons', *Bipolar Disord*, 19: 568-74.

de la Fuente-Fernandez, R. 2012. 'Role of DaTSCAN and clinical diagnosis in Parkinson disease', *Neurology*, 78: 696-701.

Deng, P. Y., D. Carlin, Y. M. Oh, L. K. Myrick, S. T. Warren, V. Cavalli, and V. A. Klyachko. 2019. 'Voltage-Independent SK-Channel Dysfunction Causes Neuronal Hyperexcitability in the Hippocampus of *Fmr1* Knock-Out Mice', *J Neurosci*, 39: 28-43.

Deng, P. Y., and V. A. Klyachko. 2016. 'Increased Persistent Sodium Current Causes Neuronal Hyperexcitability in the Entorhinal Cortex of *Fmr1* Knockout Mice', *Cell Rep*, 16: 3157-66.

———. 2021. 'Channelopathies in fragile X syndrome', *Nat Rev Neurosci*, 22: 275-89.

Deng, P. Y., Z. Rotman, J. A. Blundon, Y. Cho, J. Cui, V. Cavalli, S. S. Zakharenko, and V. A. Klyachko. 2013. 'FMRP regulates neurotransmitter release and synaptic information transmission by modulating action potential duration via BK channels', *Neuron*, 77: 696-711.

Diaz-Garcia, C. M., D. J. Meyer, N. Nathwani, M. Rahman, J. R. Martinez-Francois, and G. Yellen. 2021. 'The distinct roles of calcium in rapid control of neuronal glycolysis and the tricarboxylic acid cycle', *Elife*, 10.

Dickinson, S. D., J. Sabeti, G. A. Larson, K. Giardina, M. Rubinstein, M. A. Kelly, D. K. Grandy, M. J. Low, G. A. Gerhardt, and N. R. Zahniser. 1999. 'Dopamine D2 receptor-deficient mice exhibit decreased dopamine transporter function but no changes in dopamine release in dorsal striatum', *J Neurochem*, 72: 148-56.

Dolga, A. M., A. de Andrade, L. Meissner, H. G. Knaus, M. Hollerhage, P. Christophersen, H. Zischka, N. Plesnila, G. U. Hoglinger, and C. Culmsee. 2014. 'Subcellular expression and neuroprotective effects of SK channels in human dopaminergic neurons', *Cell Death Dis*, 5: e999.

Dong, H. W., and M. Ennis. 2014. 'Activation of group I metabotropic glutamate receptors enhances persistent sodium current and rhythmic bursting in main olfactory bulb external tufted cells', *J Neurophysiol*, 111: 641-7.

Dorsey, E. R., R. Constantinescu, J. P. Thompson, K. M. Biglan, R. G. Holloway, K. Kieburtz, F. J. Marshall, B. M. Ravina, G. Schifitto, A. Siderowf, and C. M. Tanner. 2007. 'Projected number of people with Parkinson disease in the most populous nations, 2005 through 2030', *Neurology*, 68: 384-6.

Dragicevic, E., C. Poetschke, J. Duda, F. Schlaudraff, S. Lammel, J. Schiemann, M. Fauler, A. Hetzel, M. Watanabe, R. Lujan, R. C. Malenka, J. Striessnig, and B. Liss. 2014. 'Cav1.3 channels control D2-autoreceptor responses via NCS-1 in substantia nigra dopamine neurons', *Brain*, 137: 2287-302.

Dragicevic, E., J. Schiemann, and B. Liss. 2015. 'Dopamine midbrain neurons in health and Parkinson's disease: emerging roles of voltage-gated calcium channels and ATP-sensitive potassium channels', *Neuroscience*, 284: 798-814.

Dufour, M. A., A. Woodhouse, and J. M. Goaillard. 2014. 'Somatodendritic ion channel expression in substantia nigra pars compacta dopaminergic neurons across postnatal development', *J Neurosci Res*, 92: 981-99.

Dwivedi, D., S. Chattarji, and U. S. Bhalla. 2019. 'Impaired Reliability and Precision of Spiking in Adults But Not Juveniles in a Mouse Model of Fragile X Syndrome', *eNeuro*, 6.

Eckert, Reiner, Dietmar Paschke, and Dieter F. Hülser. 1991. "Patch clamp techniques for the characterization of membrane channels." In.

Edgerton, J. R., and P. H. Reinhart. 2003. 'Distinct contributions of small and large conductance Ca2+-activated K+ channels to rat Purkinje neuron function', *J Physiol*, 548: 53-69.

El-Hassar, L., L. Song, W. J. T. Tan, C. H. Large, G. Alvaro, J. Santos-Sacchi, and L. K. Kaczmarek. 2019. 'Modulators of Kv3 Potassium Channels Rescue the Auditory Function of Fragile X Mice', *J Neurosci*, 39: 4797-813.

Fahn, S. 2008. 'The history of dopamine and levodopa in the treatment of Parkinson's disease', *Mov Disord*, 23 Suppl 3: S497-508.

Fay-Karmon, T., and S. Hassin-Baer. 2019. 'The spectrum of tremor among carriers of the *Fmr1* premutation with or without the fragile X-associated tremor/ataxia syndrome (FXTAS)', *Parkinsonism Relat Disord*, 65: 32-38.

Fearnley, J. M., and A. J. Lees. 1991. 'Ageing and Parkinson's disease: substantia nigra regional selectivity', *Brain*, 114 (Pt 5): 2283-301.

Ferron, L., M. Nieto-Rostro, J. S. Cassidy, and A. C. Dolphin. 2014. 'Fragile X mental retardation protein controls synaptic vesicle exocytosis by modulating N-type calcium channel density', *Nat Commun*, 5: 3628.

Frank, C. A. 2014. 'How voltage-gated calcium channels gate forms of homeostatic synaptic plasticity', *Front Cell Neurosci*, 8: 40.

Gayed, I., U. Joseph, M. Fanous, D. Wan, M. Schiess, W. Ondo, and K. S. Won. 2015. 'The impact of DaTscan in the diagnosis of Parkinson disease', *Clin Nucl Med*, 40: 390-3.

Gcwensa, N. Z., D. L. Russell, R. M. Cowell, and L. A. Volpicelli-Daley. 2021. 'Molecular Mechanisms Underlying Synaptic and Axon Degeneration in Parkinson's Disease', *Front Cell Neurosci*, 15: 626128.

Gentet, L. J., G. J. Stuart, and J. D. Clements. 2000. 'Direct measurement of specific membrane capacitance in neurons', *Biophys J*, 79: 314-20.

German, D. C., and K. F. Manaye. 1993. 'Midbrain dopaminergic neurons (nuclei A8, A9, and A10): three-dimensional reconstruction in the rat', *J Comp Neurol*, 331: 297-309.

Giguere, N., B. Delignat-Lavaud, F. Herborg, A. Voisin, Y. Li, V. Jacquemet, M. Anand-Srivastava, U. Gether, B. Giros, and L. E. Trudeau. 2019. 'Increased vulnerability of nigral dopamine neurons after expansion of their axonal arborization size through D2 dopamine receptor conditional knockout', *PLoS Genet*, 15: e1008352.

Goldberg, J. A., J. N. Guzman, C. M. Estep, E. Ilijic, J. Kondapalli, J. Sanchez-Padilla, and D. J. Surmeier. 2012. 'Calcium entry induces mitochondrial oxidant stress in vagal neurons at risk in Parkinson's disease', *Nat Neurosci*, 15: 1414-21.

Goldberg, M. S., A. Pisani, M. Haburcak, T. A. Vortherms, T. Kitada, C. Costa, Y. Tong, G. Martella, A. Tscherter, A. Martins, G. Bernardi, B. L. Roth, E. N. Pothos, P. Calabresi, and J. Shen. 2005. 'Nigrostriatal dopaminergic deficits and hypokinesia caused by inactivation of the familial Parkinsonism-linked gene DJ-1', *Neuron*, 45: 489-96.

Golovin, R. M., J. Vest, and K. Broadie. 2021. 'Neuron-Specific FMRP Roles in Experience-Dependent Remodeling of Olfactory Brain Innervation during an Early-Life Critical Period', *J Neurosci*, 41: 1218-41.

Gonon, F., and B. Bloch. 1998. 'Kinetics and geometry of the excitatory dopaminergic transmission in the rat striatum in vivo', *Adv Pharmacol*, 42: 140-4.

Grace, A. A., and S. P. Onn. 1989. 'Morphology and electrophysiological properties of immunocytochemically identified rat dopamine neurons recorded in vitro', *J Neurosci*, 9: 3463-81.

Graziane, Nicholas, and Yan Dong. 2016. 'Perforated Patch.' in, *Electrophysiological Analysis of Synaptic Transmission* (Springer New York: New York, NY).

Greco, C. M., R. F. Berman, R. M. Martin, F. Tassone, P. H. Schwartz, A. Chang, B. D. Trapp, C. Iwahashi, J. Brunberg, J. Grigsby, D. Hessl, E. J. Becker, J. Papazian, M. A. Leehey, R. J. Hagerman, and P. J. Hagerman. 2006. 'Neuropathology of fragile X-associated tremor/ataxia syndrome (FXTAS)', *Brain*, 129: 243-55.

Gross, C., X. Yao, D. L. Pong, A. Jeromin, and G. J. Bassell. 2011. 'Fragile X mental retardation protein regulates protein expression and mRNA translation of the potassium channel Kv4.2', *J Neurosci*, 31: 5693-8.

Guo, W., E. D. Polich, J. Su, Y. Gao, D. M. Christopher, A. M. Allan, M. Wang, F. Wang, G. Wang, and X. Zhao. 2015. 'Fragile X Proteins FMRP and FXR2P Control Synaptic GluA1 Expression and Neuronal Maturation via Distinct Mechanisms', *Cell Rep*, 11: 1651-66.

Guzman, J. N., E. Ilijic, B. Yang, J. Sanchez-Padilla, D. Wokosin, D. Galtieri, J. Kondapalli, P. T. Schumacker, and D. J. Surmeier. 2018. 'Systemic isradipine treatment diminishes calcium-dependent mitochondrial oxidant stress', *J Clin Invest*, 128: 2266-80.

Guzman, J. N., J. Sanchez-Padilla, C. S. Chan, and D. J. Surmeier. 2009. 'Robust pacemaking in substantia nigra dopaminergic neurons', *J Neurosci*, 29: 11011-9.

Haddjeri-Hopkins, A., M. Tapia, J. Ramirez-Franco, F. Tell, B. Marqueze-Pouey, M. Amalric, and J. M. Goaillard. 2021. 'Refining the Identity and Role of Kv4 Channels in Mouse Substantia Nigra Dopaminergic Neurons', *eNeuro*, 8.

Hagerman, R. J., E. Berry-Kravis, H. C. Hazlett, D. B. Bailey, Jr., H. Moine, R. F. Kooy, F. Tassone, I. Gantois, N. Sonenberg, J. L. Mandel, and P. J. Hagerman. 2017. 'Fragile X syndrome', *Nat Rev Dis Primers*, 3: 17065.

Haghdoost-Yazdi, H., A. Faraji, N. Fraidouni, M. Movahedi, E. Hadibeygi, and F. Vaezi. 2011. 'Significant effects of 4-aminopyridine and tetraethylammonium in the treatment of 6-hydroxydopamine-induced Parkinson's disease', *Behav Brain Res*, 223: 70-4.

Hahn, J., P. H. Kullmann, J. P. Horn, and E. S. Levitan. 2006. 'D2 autoreceptors chronically enhance dopamine neuron pacemaker activity', *J Neurosci*, 26: 5240-7.

Hall, D. A., D. Jennings, J. Seibyl, F. Tassone, and K. Marek. 2010. '*Fmr1* gene expansion and scans without evidence of dopaminergic deficits in parkinsonism patients', *Parkinsonism Relat Disord*, 16: 608-11.

Harashima, C., D. M. Jacobowitz, J. Witta, R. C. Borke, T. K. Best, R. J. Siarey, and Z. Galdzicki. 2006. 'Abnormal expression of the G-protein-activated inwardly rectifying potassium channel 2 (GIRK2) in hippocampus, frontal cortex, and substantia nigra of Ts65Dn mouse: a model of Down syndrome', *J Comp Neurol*, 494: 815-33.

Hardenberg, M. C., T. Sinnige, S. Casford, S. T. Dada, C. Poudel, E. A. Robinson, M. Fuxreiter, C. F. Kaminksi, G. S. Kaminski Schierle, E. A. A. Nollen, C. M. Dobson, and M. Vendruscolo. 2021. 'Observation of an alpha-synuclein liquid droplet state and its maturation into Lewy body-like assemblies', *J Mol Cell Biol*, 13: 282-94.

Herrmann, S., S. Schnorr, and A. Ludwig. 2015. 'HCN channels--modulators of cardiac and neuronal excitability', *Int J Mol Sci*, 16: 1429-47.

Hill, E., R. Gowers, M. J. E. Richardson, and M. J. Wall. 2021. 'alpha-Synuclein Aggregates Increase the Conductance of Substantia Nigra Dopamine Neurons, an Effect Partly Reversed by the KATP Channel Inhibitor Glibenclamide', *eNeuro*, 8.

Inanobe, A., Y. Yoshimoto, Y. Horio, K. I. Morishige, H. Hibino, S. Matsumoto, Y. Tokunaga, T. Maeda, Y. Hata, Y. Takai, and Y. Kurachi. 1999. 'Characterization of G-protein-gated K+ channels composed of Kir3.2 subunits in dopaminergic neurons of the substantia nigra', *J Neurosci*, 19: 1006-17.

Ishimoto, T., and H. Yamakado. 2021. 'Membranes and Organelle in Lewy Bodies: The Mastermind or the Bystander?', *Mov Disord*, 36: 2026.

Jasmin, M., E. H. Ahn, M. H. Voutilainen, J. Fombonne, C. Guix, T. Viljakainen, S. S. Kang, L. Y. Yu, M. Saarma, P. Mehlen, and K. Ye. 2021. 'Netrin-1 and its receptor DCC modulate survival and death of dopamine neurons and Parkinson's disease features', *EMBO J*, 40: e105537.

Kadkhodaei, B., T. Ito, E. Joodmardi, B. Mattsson, C. Rouillard, M. Carta, S. Muramatsu, C. Sumi-Ichinose, T. Nomura, D. Metzger, P. Chambon, E. Lindqvist, N. G. Larsson, L. Olson, A. Bjorklund, H. Ichinose, and T. Perlmann. 2009. 'Nurr1 is required for maintenance of maturing and adult midbrain dopamine neurons', *J Neurosci*, 29: 15923-32.

Kanaan, N. M., C. Hamel, T. Grabinski, and B. Combs. 2020. 'Liquid-liquid phase separation induces pathogenic tau conformations in vitro', *Nat Commun*, 11: 2809.

Karadottir, R., and D. Attwell. 2006. 'Combining patch clamping of cells in brain slices with immunocytochemical labeling to define cell type and developmental stage', *Nat Protoc*, 1: 1977-86.

Karschin, C., E. Dissmann, W. Stuhmer, and A. Karschin. 1996. 'IRK(1-3) and GIRK(1-4) inwardly rectifying K+ channel mRNAs are differentially expressed in the adult rat brain', *J Neurosci*, 16: 3559-70.

Kitada, T., A. Pisani, D. R. Porter, H. Yamaguchi, A. Tscherter, G. Martella, P. Bonsi, C. Zhang, E. N. Pothos, and J. Shen. 2007. 'Impaired dopamine release and synaptic plasticity in the striatum of PINK1-deficient mice', *Proc Natl Acad Sci U S A*, 104: 11441-6.

Knight, Z. A., K. Tan, K. Birsoy, S. Schmidt, J. L. Garrison, R. W. Wysocki, A. Emiliano, M. I. Ekstrand, and J. M. Friedman. 2012. 'Molecular profiling of activated neurons by phosphorylated ribosome capture', *Cell*, 151: 1126-37.

Kobayashi, T., K. Ikeda, T. Ichikawa, S. Abe, S. Togashi, and T. Kumanishi. 1995. 'Molecular cloning of a mouse G-protein-activated K+ channel (mGIRK1) and distinct distributions of three GIRK (GIRK1, 2 and 3) mRNAs in mouse brain', *Biochem Biophys Res Commun*, 208: 1166-73.

Kofuji, P., N. Davidson, and H. A. Lester. 1995. 'Evidence that neuronal G-protein-gated inwardly rectifying K+ channels are activated by G beta gamma subunits and function as heteromultimers', *Proc Natl Acad Sci U S A*, 92: 6542-6.

Kordower, J. H., C. W. Olanow, H. B. Dodiya, Y. Chu, T. G. Beach, C. H. Adler, G. M. Halliday, and R. T. Bartus. 2013. 'Disease duration and the integrity of the nigrostriatal system in Parkinson's disease', *Brain*, 136: 2419-31.

Krashia, P., A. Martini, A. Nobili, D. Aversa, M. D'Amelio, N. Berretta, E. Guatteo, and N. B. Mercuri. 2017. 'On the properties of identified dopaminergic neurons in the mouse substantia nigra and ventral tegmental area', *Eur J Neurosci*, 45: 92-105.

Kshatri, A., A. Cerrada, R. Gimeno, D. Bartolome-Martin, P. Rojas, and T. Giraldez. 2020. 'Differential regulation of BK channels by fragile X mental retardation protein', *J Gen Physiol*, 152.

Kubo, Y., E. Reuveny, P. A. Slesinger, Y. N. Jan, and L. Y. Jan. 1993. 'Primary structure and functional expression of a rat G-protein-coupled muscarinic potassium channel', *Nature*, 364: 802-6.

Lacey, M. G., N. B. Mercuri, and R. A. North. 1989. 'Two cell types in rat substantia nigra zona compacta distinguished by membrane properties and the actions of dopamine and opioids', *J Neurosci*, 9: 1233-41.

Lammel, S., A. Hetzel, O. Hackel, I. Jones, B. Liss, and J. Roeper. 2008. 'Unique properties of mesoprefrontal neurons within a dual mesocorticolimbic dopamine system', *Neuron*, 57: 760-73.

Lanciego, J. L., N. Luquin, and J. A. Obeso. 2012. 'Functional neuroanatomy of the basal ganglia', *Cold Spring Harb Perspect Med*, 2: a009621.

Lang, A. E., and A. M. Lozano. 1998. 'Parkinson's disease. Second of two parts', *N Engl J Med*, 339: 1130-43.

Lee, F. J., L. Pei, A. Moszczynska, B. Vukusic, P. J. Fletcher, and F. Liu. 2007. 'Dopamine transporter cell surface localization facilitated by a direct interaction with the dopamine D2 receptor', *EMBO J*, 26: 2127-36.

Lee, H. Y., W. P. Ge, W. Huang, Y. He, G. X. Wang, A. Rowson-Baldwin, S. J. Smith, Y. N. Jan, and L. Y. Jan. 2011. 'Bidirectional regulation of dendritic voltage-gated potassium channels by the fragile X mental retardation protein', *Neuron*, 72: 630-42.

Lees, A. J. 2007. 'Unresolved issues relating to the shaking palsy on the celebration of James Parkinson's 250th birthday', *Mov Disord*, 22 Suppl 17: S327-34.

Lerner, T. N., C. Shilyansky, T. J. Davidson, K. E. Evans, K. T. Beier, K. A. Zalocusky, A. K. Crow, R. C. Malenka, L. Luo, R. Tomer, and K. Deisseroth. 2015. 'Intact-Brain Analyses Reveal Distinct Information Carried by SNc Dopamine Subcircuits', *Cell*, 162: 635-47.

Lesage, F., E. Guillemare, M. Fink, F. Duprat, C. Heurteaux, M. Fosset, G. Romey, J. Barhanin, and M. Lazdunski. 1995. 'Molecular properties of neuronal G-protein-activated inwardly rectifying K+ channels', *J Biol Chem*, 270: 28660-7.

Li, G., J. Ma, S. Cui, Y. He, Q. Xiao, J. Liu, and S. Chen. 2019. 'Parkinson's disease in China: a forty-year growing track of bedside work', *Transl Neurodegener*, 8: 22.

Li, M., J. Shin, R. D. Risgaard, M. J. Parries, J. Wang, D. Chasman, S. Liu, S. Roy, A. Bhattacharyya, and X. Zhao. 2020. 'Identification of *Fmr1*-regulated molecular networks in human neurodevelopment', *Genome Res*, 30: 361-74.

Liang, C. L., C. M. Sinton, P. K. Sonsalla, and D. C. German. 1996. 'Midbrain dopaminergic neurons in the mouse that contain calbindin-D28k exhibit reduced vulnerability to MPTP-induced neurodegeneration', *Neurodegeneration*, 5: 313-8.

Liao, Y. J., Y. N. Jan, and L. Y. Jan. 1996. 'Heteromultimerization of G-protein-gated inwardly rectifying K+ channel proteins GIRK1 and GIRK2 and their altered expression in weaver brain', *J Neurosci*, 16: 7137-50.

Lin, M., P. M. Mackie, F. Shaerzadeh, J. Gamble-George, D. R. Miller, C. J. Martyniuk, and H. Khoshbouei. 2021. 'In Parkinson's patient-derived dopamine neurons, the triplication of alpha-synuclein locus induces distinctive firing pattern by impeding D2 receptor autoinhibition', *Acta Neuropathol Commun*, 9: 107.

Lippiat, J. D. 2008. 'Whole-cell recording using the perforated patch clamp technique', *Methods Mol Biol*, 491: 141-9.

Liss, B., O. Franz, S. Sewing, R. Bruns, H. Neuhoff, and J. Roeper. 2001. 'Tuning pacemaker frequency of individual dopaminergic neurons by Kv4.3L and KChip3.1 transcription', *EMBO J*, 20: 5715-24.

Liss, B., A. Neu, and J. Roeper. 1999. 'The weaver mouse gain-of-function phenotype of dopaminergic midbrain neurons is determined by coactivation of wvGirk2 and K-ATP channels', *J Neurosci*, 19: 8839-48.

Liu, G., J. Yu, J. Ding, C. Xie, L. Sun, I. Rudenko, W. Zheng, N. Sastry, J. Luo, G. Rudow, J. C. Troncoso, and H. Cai. 2014. 'Aldehyde dehydrogenase 1 defines and protects a nigrostriatal dopaminergic neuron subpopulation', *J Clin Invest*, 124: 3032-46.

Llamosas, N., L. Ugedo, and M. Torrecilla. 2017. 'Inactivation of GIRK channels weakens the pre- and postsynaptic inhibitory activity in dorsal raphe neurons', *Physiol Rep*, 5.

Lo, P. S., V. V. Rymar, T. E. Kennedy, and A. F. Sadikot. 2022. 'The netrin-1 receptor DCC promotes the survival of a subpopulation of midbrain dopaminergic neurons: Relevance for ageing and Parkinson's disease', *J Neurochem*.

Loesch, D. Z., F. Tassone, G. D. Mellick, M. Horne, J. P. Rubio, M. Q. Bui, D. Francis, and E. Storey. 2018. 'Evidence for the role of *Fmr1* gray zone alleles as a risk factor for parkinsonism in females', *Mov Disord*, 33: 1178-81.

Luk, K. C., V. Kehm, J. Carroll, B. Zhang, P. O'Brien, J. Q. Trojanowski, and V. M. Lee. 2012. 'Pathological alpha-synuclein transmission initiates Parkinson-like neurodegeneration in nontransgenic mice', *Science*, 338: 949-53.

Luscher, C., and P. A. Slesinger. 2010. 'Emerging roles for G protein-gated inwardly rectifying potassium (GIRK) channels in health and disease', *Nat Rev Neurosci*, 11: 301-15.

Ly, C., T. Melman, A. L. Barth, and G. B. Ermentrout. 2011. 'Phase-resetting curve determines how BK currents affect neuronal firing', *J Comput Neurosci*, 30: 211-23.

Madeo, G., F. Alemseged, B. Di Pietro, O. Schillaci, and A. Pisani. 2013. 'Early abnormalities in 123I-ioflupane (DaTSCAN) imaging in the fragile X-associated tremor ataxia syndrome (FXTAS): a case report', *Neurol Sci*, 34: 1475-7.

Maiti, B., and J. S. Perlmutter. 2020. 'A Clinical Trial of Isradipine: What Went Wrong?', *Ann Intern Med*, 172: 625-26.

Marcott, P. F., A. A. Mamaligas, and C. P. Ford. 2014. 'Phasic dopamine release drives rapid activation of striatal D2-receptors', *Neuron*, 84: 164-76.

Marker, C. L., M. Stoffel, and K. Wickman. 2004. 'Spinal G-protein-gated K+ channels formed by GIRK1 and GIRK2 subunits modulate thermal nociception and contribute to morphine analgesia', *J Neurosci*, 24: 2806-12.

Mathiharan, Y. K., I. W. Glaaser, Y. Zhao, M. J. Robertson, G. Skiniotis, and P. A. Slesinger. 2021. 'Structural insights into GIRK2 channel modulation by cholesterol and PIP2', *Cell Rep*, 36: 109619.

Mattson, M. P. 2003. 'Excitotoxic and excitoprotective mechanisms: abundant targets for the prevention and treatment of neurodegenerative disorders', *Neuromolecular Med*, 3: 65-94.

Mazarati, A., L. Lundstrom, U. Sollenberg, D. Shin, U. Langel, and R. Sankar. 2006. 'Regulation of kindling epileptogenesis by hippocampal galanin type 1 and type 2 receptors: The effects of subtype-selective agonists and the role of G-protein-mediated signaling', *J Pharmacol Exp Ther*, 318: 700-8.

McGregor, M. M., and A. B. Nelson. 2019. 'Circuit Mechanisms of Parkinson's Disease', *Neuron*, 101: 1042-56.

McRitchie, D. A., and G. M. Halliday. 1995. 'Calbindin D28k-containing neurons are restricted to the medial substantia nigra in humans', *Neuroscience*, 65: 87-91.

Mendez, I., R. Sanchez-Pernaute, O. Cooper, A. Vinuela, D. Ferrari, L. Bjorklund, A. Dagher, and O. Isacson. 2005. 'Cell type analysis of functional fetal dopamine cell suspension transplants in the striatum and substantia nigra of patients with Parkinson's disease', *Brain*, 128: 1498-510.

Milber, J. M., J. V. Noorigian, J. F. Morley, H. Petrovitch, L. White, G. W. Ross, and J. E. Duda. 2012. 'Lewy pathology is not the first sign of degeneration in vulnerable neurons in Parkinson disease', *Neurology*, 79: 2307-14.

Mironov, S. L. 2015. 'alpha-Synuclein forms non-selective cation channels and stimulates ATP-sensitive potassium channels in hippocampal neurons', *J Physiol*, 593: 145-59.

Murakami, T., S. Qamar, J. Q. Lin, G. S. Schierle, E. Rees, A. Miyashita, A. R. Costa, R. B. Dodd, F. T. Chan, C. H. Michel, D. Kronenberg-Versteeg, Y. Li, S. P. Yang, Y. Wakutani, W. Meadows, R. R. Ferry, L. Dong, G. G. Tartaglia, G. Favrin, W. L. Lin, D. W. Dickson, M. Zhen, D. Ron, G. Schmitt-Ulms, P. E. Fraser, N. A. Shneider, C. Holt, M. Vendruscolo, C. F. Kaminski, and P. St George-Hyslop. 2015. 'ALS/FTD Mutation-Induced Phase Transition of FUS Liquid Droplets and Reversible Hydrogels into Irreversible Hydrogels Impairs RNP Granule Function', *Neuron*, 88: 678-90.

Nandhagopal, R., L. Kuramoto, M. Schulzer, E. Mak, J. Cragg, J. McKenzie, S. McCormick, T. J. Ruth, V. Sossi, R. de la Fuente-Fernandez, and A. J. Stoessl. 2011. 'Longitudinal evolution of compensatory changes in striatal dopamine processing in Parkinson's disease', *Brain*, 134: 3290-8.

Okamura, H., C. Yokoyama, and Y. Ibata. 1995. 'Lateromedial gradient of the susceptibility of midbrain dopaminergic neurons to neonatal 6-hydroxydopamine toxicity', *Exp Neurol*, 136: 136-42.

Pacheco, C. R., C. N. Morales, A. E. Ramirez, F. J. Munoz, S. S. Gallegos, P. A. Caviedes, L. G. Aguayo, and C. M. Opazo. 2015. 'Extracellular alpha-synuclein alters synaptic transmission in brain neurons by perforating the neuronal plasma membrane', *J Neurochem*, 132: 731-41.

Parker, J. G., J. D. Marshall, B. Ahanonu, Y. W. Wu, T. H. Kim, B. F. Grewe, Y. Zhang, J. Z. Li, J. B. Ding, M. D. Ehlers, and M. J. Schnitzer. 2018. 'Diametric neural ensemble dynamics in parkinsonian and dyskinetic states', *Nature*, 557: 177-82.

Parker, P. R., A. L. Lalive, and A. C. Kreitzer. 2016. 'Pathway-Specific Remodeling of Thalamostriatal Synapses in Parkinsonian Mice', *Neuron*, 89: 734-40.

Parkinson, J. 2002. 'An essay on the shaking palsy. 1817', *J Neuropsychiatry Clin Neurosci*, 14: 223-36; discussion 22.

Parkkinen, L., S. S. O'Sullivan, C. Collins, A. Petrie, J. L. Holton, T. Revesz, and A. J. Lees. 2011. 'Disentangling the relationship between lewy bodies and nigral neuronal loss in Parkinson's disease', *J Parkinsons Dis*, 1: 277-86.

Patel, A. B., K. W. Loerwald, K. M. Huber, and J. R. Gibson. 2014. 'Postsynaptic FMRP promotes the pruning of cell-to-cell connections among pyramidal neurons in the L5A neocortical network', *J Neurosci*, 34: 3413-8.

Paul, R., A. Dutta, B. C. Phukan, M. K. Mazumder, A. Justin-Thenmozhi, T. Manivasagam, P. Bhattacharya, and A. Borah. 2018. 'Accumulation of Cholesterol and Homocysteine in the Nigrostriatal Pathway of Brain Contributes to the Dopaminergic Neurodegeneration in Mice', *Neuroscience*, 388: 347-56.

Pei, Q., L. Lewis, D. G. Grahame-Smith, and T. S. Zetterstrom. 1999. 'Alteration in expression of G-protein-activated inward rectifier K+-channel subunits GIRK1 and GIRK2 in the rat brain following electroconvulsive shock', *Neuroscience*, 90: 621-7.

Pelzer, E. A., C. Melzer, A. Schonberger, M. Hess, L. Timmermann, C. Eggers, and M. Tittgemeyer. 2019. 'Axonal degeneration in Parkinson's disease - Basal ganglia circuitry and D2 receptor availability', *Neuroimage Clin*, 23: 101906.

Pereira Luppi, M., M. Azcorra, G. Caronia-Brown, J. F. Poulin, Z. Gaertner, S. Gatica, O. A. Moreno-Ramos, N. Nouri, M. Dubois, Y. C. Ma, C. Ramakrishnan, L. Fenno, Y. S. Kim, K. Deisseroth, F. Cicchetti, D. A. Dombeck, and R. Awatramani. 2021. 'Sox6 expression distinguishes dorsally and ventrally biased dopamine neurons in the substantia nigra with distinctive properties and embryonic origins', *Cell Rep*, 37: 109975.

Ping, H. X., and P. D. Shepard. 1996. 'Apamin-sensitive Ca(2+)-activated K+ channels regulate pacemaker activity in nigral dopamine neurons', *Neuroreport*, 7: 809-14.

Poulin, J. F., G. Caronia, C. Hofer, Q. Cui, B. Helm, C. Ramakrishnan, C. S. Chan, D. A. Dombeck, K. Deisseroth, and R. Awatramani. 2018. 'Mapping projections of molecularly defined dopamine neuron subtypes using intersectional genetic approaches', *Nat Neurosci*, 21: 1260-71.

Pretegiani, E., and L. M. Optican. 2017. 'Eye Movements in Parkinson's Disease and Inherited Parkinsonian Syndromes', *Front Neurol*, 8: 592.

Price, T. J., M. H. Rashid, M. Millecamps, R. Sanoja, J. M. Entrena, and F. Cervero. 2007. 'Decreased nociceptive sensitization in mice lacking the fragile X mental retardation protein: role of mGluR1/5 and mTOR', *J Neurosci*, 27: 13958-67.

Puopolo, M., E. Raviola, and B. P. Bean. 2007. 'Roles of subthreshold calcium current and sodium current in spontaneous firing of mouse midbrain dopamine neurons', *J Neurosci*, 27: 645-56.

Ray, S., N. Singh, R. Kumar, K. Patel, S. Pandey, D. Datta, J. Mahato, R. Panigrahi, A. Navalkar, S. Mehra, L. Gadhe, D. Chatterjee, A. S. Sawner, S. Maiti, S. Bhatia, J. A. Gerez, A. Chowdhury, A. Kumar, R. Padinhateeri, R. Riek, G. Krishnamoorthy, and S. K. Maji. 2020. 'alpha-Synuclein aggregation nucleates through liquid-liquid phase separation', *Nat Chem*, 12: 705-16.

Reetz, K., C. Gaser, C. Klein, J. Hagenah, C. Buchel, S. Gottschalk, P. P. Pramstaller, H. R. Siebner, and F. Binkofski. 2009. 'Structural findings in the basal ganglia in genetically determined and idiopathic Parkinson's disease', *Mov Disord*, 24: 99-103.

Richter, J. D., and X. Zhao. 2021. 'The molecular biology of FMRP: new insights into fragile X syndrome', *Nat Rev Neurosci*, 22: 209-22.

Rietdijk, C. D., P. Perez-Pardo, J. Garssen, R. J. van Wezel, and A. D. Kraneveld. 2017. 'Exploring Braak's Hypothesis of Parkinson's Disease', *Front Neurol*, 8: 37.

Roselli, F., and P. Caroni. 2015. 'From intrinsic firing properties to selective neuronal vulnerability in neurodegenerative diseases', *Neuron*, 85: 901-10.

Routh, B. N., D. Johnston, and D. H. Brager. 2013. 'Loss of functional A-type potassium channels in the dendrites of CA1 pyramidal neurons from a mouse model of fragile X syndrome', *J Neurosci*, 33: 19442-50.

Routh, B. N., R. K. Rathour, M. E. Baumgardner, B. E. Kalmbach, D. Johnston, and D. H. Brager. 2017. 'Increased transient Na(+) conductance and action potential output in layer 2/3 prefrontal cortex neurons of the *Fmr1*(-/y) mouse', *J Physiol*, 595: 4431-48.

Sacino, A. N., S. Prokop, M. A. Walsh, J. Adamson, S. H. Subramony, A. Krans, P. K. Todd, B. I. Giasson, and A. T. Yachnis. 2019. 'Fragile X-associated tremor ataxia syndrome with co-occurrent progressive supranuclear palsy-like neuropathology', *Acta Neuropathol Commun*, 7: 158.

Salcedo-Arellano, M. J., M. W. Wolf-Ochoa, T. Hong, S. Amina, F. Tassone, M. Lechpammer, R. Hagerman, and V. Martinez-Cerdeno. 2020. 'Parkinsonism Versus Concomitant Parkinson's Disease in Fragile X-Associated Tremor/Ataxia Syndrome', *Mov Disord Clin Pract*, 7: 413-18.

Sanchez-Padilla, J., J. N. Guzman, E. Ilijic, J. Kondapalli, D. J. Galtieri, B. Yang, S. Schieber, W. Oertel, D. Wokosin, P. T. Schumacker, and D. J. Surmeier. 2014. 'Mitochondrial oxidant stress in locus coeruleus is regulated by activity and nitric oxide synthase', *Nat Neurosci*, 17: 832-40.

Sausbier, M., H. Hu, C. Arntz, S. Feil, S. Kamm, H. Adelsberger, U. Sausbier, C. A. Sailer, R. Feil, F. Hofmann, M. Korth, M. J. Shipston, H. G. Knaus, D. P. Wolfer, C. M. Pedroarena, J. F. Storm, and

P. Ruth. 2004. 'Cerebellar ataxia and Purkinje cell dysfunction caused by Ca2+-activated K+ channel deficiency', *Proc Natl Acad Sci U S A*, 101: 9474-8.

Savchenko, A., C. Muller, J. Lubec, D. Leo, V. Korz, L. Afjehi-Sadat, J. Malikovic, F. J. Sialana, G. Lubec, and I. Sukhanov. 2022. 'The Lack of Dopamine Transporter Is Associated With Conditional Associative Learning Impairments and Striatal Proteomic Changes', *Front Psychiatry*, 13: 799433.

Saxena, S., and P. Caroni. 2011. 'Selective neuronal vulnerability in neurodegenerative diseases: from stressor thresholds to degeneration', *Neuron*, 71: 35-48.

Schiemann, J., F. Schlaudraff, V. Klose, M. Bingmer, S. Seino, P. J. Magill, K. A. Zaghloul, G. Schneider, B. Liss, and J. Roeper. 2012. 'K-ATP channels in dopamine substantia nigra neurons control bursting and novelty-induced exploration', *Nat Neurosci*, 15: 1272-80.

Sharott, A., F. Vinciati, K. C. Nakamura, and P. J. Magill. 2017. 'A Population of Indirect Pathway Striatal Projection Neurons Is Selectively Entrained to Parkinsonian Beta Oscillations', *J Neurosci*, 37: 9977-98.

Shcherbatyy, V., J. Carson, M. Yaylaoglu, K. Jackle, F. Grabbe, M. Brockmeyer, H. Yavuz, and G. Eichele. 2015. 'A digital atlas of ion channel expression patterns in the two-week-old rat brain', *Neuroinformatics*, 13: 111-25.

Shendelman, S., A. Jonason, C. Martinat, T. Leete, and A. Abeliovich. 2004. 'DJ-1 is a redox-dependent molecular chaperone that inhibits alpha-synuclein aggregate formation', *PLoS Biol*, 2: e362.

Shibu, M. A., M. Bharath, and B. K. Velmurugan. 2021. 'Regulating Inflammation Associated Ferroptosis - A Treatment Strategy for Parkinson Disease', *Curr Med Chem*, 28: 6895-914.

Signorini, S., Y. J. Liao, S. A. Duncan, L. Y. Jan, and M. Stoffel. 1997. 'Normal cerebellar development but susceptibility to seizures in mice lacking G protein-coupled, inwardly rectifying K+ channel GIRK2', *Proc Natl Acad Sci U S A*, 94: 923-7.

Slesinger, P. A., E. Reuveny, Y. N. Jan, and L. Y. Jan. 1995. 'Identification of structural elements involved in G protein gating of the GIRK1 potassium channel', *Neuron*, 15: 1145-56.

Stefani, A., A. M. Lozano, A. Peppe, P. Stanzione, S. Galati, D. Tropepi, M. Pierantozzi, L. Brusa, E. Scarnati, and P. Mazzone. 2007. 'Bilateral deep brain stimulation of the pedunculopontine and subthalamic nuclei in severe Parkinson's disease', *Brain*, 130: 1596-607.

Su, M., L. Li, J. Wang, H. Sun, L. Zhang, C. Zhao, Y. Xie, N. Gamper, X. Du, and H. Zhang. 2019. 'Kv7.4 Channel Contribute to Projection-Specific Auto-Inhibition of Dopamine Neurons in the Ventral Tegmental Area', *Front Cell Neurosci*, 13: 557.

Subramaniam, M., D. Althof, S. Gispert, J. Schwenk, G. Auburger, A. Kulik, B. Fakler, and J. Roeper. 2014. 'Mutant alpha-synuclein enhances firing frequencies in dopamine substantia nigra neurons by oxidative impairment of A-type potassium channels', *J Neurosci*, 34: 13586-99.

Sun, S., F. Li, X. Gao, Y. Zhu, J. Chen, X. Zhu, H. Yuan, and D. Gao. 2011. 'Calbindin-D28K inhibits apoptosis in dopaminergic neurons by activation of the PI3-kinase-Akt signaling pathway', *Neuroscience*, 199: 359-67.

Surmeier, D. J., J. A. Obeso, and G. M. Halliday. 2017. 'Selective neuronal vulnerability in Parkinson disease', *Nat Rev Neurosci*, 18: 101-13.

Swensen, A. M., and B. P. Bean. 2003. 'Ionic mechanisms of burst firing in dissociated Purkinje neurons', *J Neurosci*, 23: 9650-63.

Tan, Y., C. Sgobio, T. Arzberger, F. Machleid, Q. Tang, E. Findeis, J. Tost, T. Chakroun, P. Gao, M. Hollerhage, K. Botzel, J. Herms, G. Hoglinger, and T. Koeglsperger. 2020. 'Loss of fragile X mental retardation protein precedes Lewy pathology in Parkinson's disease', *Acta Neuropathol*, 139: 319-45.

Tassone, F., R. J. Hagerman, A. K. Taylor, J. B. Mills, S. W. Harris, L. W. Gane, and P. J. Hagerman. 2000. 'Clinical involvement and protein expression in individuals with the *Fmr1* premutation', *Am J Med Genet*, 91: 144-52.

Torrecilla, M., C. L. Marker, S. C. Cintora, M. Stoffel, J. T. Williams, and K. Wickman. 2002. 'G-protein-gated potassium channels containing Kir3.2 and Kir3.3 subunits mediate the acute inhibitory effects of opioids on locus ceruleus neurons', *J Neurosci*, 22: 4328-34.

Tozzi, A., M. Sciaccaluga, V. Loffredo, A. Megaro, A. Ledonne, A. Cardinale, M. Federici, L. Bellingacci, S. Paciotti, E. Ferrari, A. La Rocca, A. Martini, N. B. Mercuri, F. Gardoni, B. Picconi, V. Ghiglieri, E. De Leonibus, and P. Calabresi. 2021. 'Dopamine-dependent early synaptic and motor dysfunctions induced by alpha-synuclein in the nigrostriatal circuit', *Brain*, 144: 3477-91.

Tran, S. S., H. I. Jun, J. H. Bahn, A. Azghadi, G. Ramaswami, E. L. Van Nostrand, T. B. Nguyen, Y. E. Hsiao, C. Lee, G. A. Pratt, V. Martinez-Cerdeno, R. J. Hagerman, G. W. Yeo, D. H. Geschwind, and X. Xiao. 2019. 'Widespread RNA editing dysregulation in brains from autistic individuals', *Nat Neurosci*, 22: 25-36.

Trinkaus, V. A., I. Riera-Tur, A. Martinez-Sanchez, F. J. B. Bauerlein, Q. Guo, T. Arzberger, W. Baumeister, I. Dudanova, M. S. Hipp, F. U. Hartl, and R. Fernandez-Busnadiego. 2021. 'In situ architecture of neuronal alpha-Synuclein inclusions', *Nat Commun*, 12: 2110.

Valldeoriola, F., E. Munoz, J. Rumia, P. Roldan, A. Camara, Y. Compta, M. J. Marti, and E. Tolosa. 2019. 'Simultaneous low-frequency deep brain stimulation of the substantia nigra pars reticulata and high-frequency stimulation of the subthalamic nucleus to treat levodopa unresponsive freezing of gait in Parkinson's disease: A pilot study', *Parkinsonism Relat Disord*, 60: 153-57.

Venderova, K., and D. S. Park. 2012. 'Programmed cell death in Parkinson's disease', *Cold Spring Harb Perspect Med*, 2.

Wallen, P., B. Robertson, L. Cangiano, P. Low, A. Bhattacharjee, L. K. Kaczmarek, and S. Grillner. 2007. 'Sodium-dependent potassium channels of a Slack-like subtype contribute to the slow afterhyperpolarization in lamprey spinal neurons', *J Physiol*, 585: 75-90.

Wang, H., L. J. Wu, S. S. Kim, F. J. Lee, B. Gong, H. Toyoda, M. Ren, Y. Z. Shang, H. Xu, F. Liu, M. G. Zhao, and M. Zhuo. 2008. 'FMRP acts as a key messenger for dopamine modulation in the forebrain', *Neuron*, 59: 634-47.

Wengert, E. R., and M. K. Patel. 2021. 'The Role of the Persistent Sodium Current in Epilepsy', *Epilepsy Curr*, 21: 40-47.

Wilson, C. J., and J. A. Goldberg. 2006. 'Origin of the slow afterhyperpolarization and slow rhythmic bursting in striatal cholinergic interneurons', *J Neurophysiol*, 95: 196-204.

Wolfart, J., H. Neuhoff, O. Franz, and J. Roeper. 2001. 'Differential expression of the small-conductance, calcium-activated potassium channel SK3 is critical for pacemaker control in dopaminergic midbrain neurons', *J Neurosci*, 21: 3443-56.

Womack, M., and K. Khodakhah. 2002. 'Active contribution of dendrites to the tonic and trimodal patterns of activity in cerebellar Purkinje neurons', *J Neurosci*, 22: 10603-12.

Wu, J., J. Kung, J. Dong, L. Chang, C. Xie, A. Habib, S. Hawes, N. Yang, V. Chen, Z. Liu, R. Evans, B. Liang, L. Sun, J. Ding, J. Yu, S. Saez-Atienzar, B. Tang, Z. Khaliq, D. T. Lin, W. Le, and H. Cai. 2019. 'Distinct Connectivity and Functionality of Aldehyde Dehydrogenase 1a1-Positive Nigrostriatal Dopaminergic Neurons in Motor Learning', *Cell Rep*, 28: 1167-81 e7.

Yang, F., L. Feng, F. Zheng, S. W. Johnson, J. Du, L. Shen, C. P. Wu, and B. Lu. 2001. 'GDNF acutely modulates excitability and A-type K(+) channels in midbrain dopaminergic neurons', *Nat Neurosci*, 4: 1071-8.

Yang, J., Y. Xiao, L. Li, Q. He, M. Li, and Y. Shu. 2019. 'Biophysical Properties of Somatic and Axonal Voltage-Gated Sodium Channels in Midbrain Dopaminergic Neurons', *Front Cell Neurosci*, 13: 317.

8. Acknowledgment

First and foremost, I would like to express my appreciation to Prof. Dr. Günter U. Hoglinger and Dr. med. Thomas Koglsperger for providing me with the chance to pursue my degree in Munich. Being exposed to this high-quality research environment has been a very beneficial experience for me. My time spent studying here has been quite enjoyable and beneficial because of the supportive staff, the conducive surroundings, and the attentiveness with which the group is cared for.

I'd like to express my gratitude to Prof. Dr. Günter U. Höglinger, head of the Department of Translational Neurodegeneration at DZNE, for his invaluable assistance and feedback on my thesis, as well as for fostering a welcoming, supportive, and challenging academic environment for me throughout my time here.

To Dr. med. Thomas Köglsperger, to whom I am indebted for his fantastic guidance, my deepest gratitude. He has been tremendously supportive monetarily, motivating intellectually, and inclusive unconditionally. He pushed me to develop my own ideas and backed me up to do anything I wanted to. The thesis would not have been done successfully without his guiding hand and incessant motivation. I count myself lucky to be under his supervision.

I owe a great debt of gratitude to Prof. Dr. Jochen Herms and his lab for providing me with an excellent place to work and showing me so much about the cutting-edge techs of neuroscience, which allowed me to broaden my horizons. Say many thanks to Prof. Dr. Gerhard Rammes; I grew from knowing nothing about patch clamp to knowing almost everything after training in his lab.

Special thanks to Dr. Lars Paeger, Dr. Paul Feyen, Dr. Yi Tan, and Dr. Rohit Kumar for their attentive instruction and insightful conversations on experimental techniques; My colleague Svenja-Lotta Rumpf's technical assistance on my research is very appreciated, our conversations are always interesting. Thanks to Dr. Qilin Tang, Dr. Diana Mahlstedt, Dr. Yuan Shi, Mochen Cui, Juan Zu, Dr. Katharina Ochs, Weilin Chen, Carolin Klaus and Yiyang Wu for their valuable help and support.

Prof. Dr. Stefan Lichtenthaler, Dr. Xiao Feng, and Dr. Pieter Giesbertz are to be acknowledged for providing us with the platform of proteomics and for their comprehensive assistance and interaction. In addition, I would like to thank the China Scholarship Council (CSC) for financing

me during my MD studies, as well as the Technical University of Munich Medical School for the courses and outdoor activities that helped me gain knowledge. Lastly, I would want to express my gratitude to my family for their continuous love, inspiration, and unwavering support. Specifically, I would want to thank my wife, Dr. Sicheng Tang, who has always been at my side with faith and love and who has taken care of me in every manner so that I may focus on my study.